Wave Energy Extraction from Buoys

by

Xavier Garnaud

Submitted to the Department of Aeronautics and Astronautics
in partial fulfillment of the requirements for the degree of

Master of Science in Aeronautics and Astronautics

at the

MASSACHUSETTS INSTITUTE OF TECHNOLOGY

February 2009

Author .....
Department of Aeronautics and Astronautics
December 19, 2008

Certified by .....
Prof. Chiang C. Mei
Ford Professor of Engineering
Department of Civil and Environmental Engineering
Thesis Supervisor

Accepted by .....
Prof. David L. Darmofal
Associate Department Head
Chair, Committee on Graduate Students

Wave Energy Extraction from Buoys

by

Xavier Garnaud

Submitted to the Department of Aeronautics and Astronautics
on December 19, 2008, in partial fulfillment of the
requirements for the degree of
Master of Science in Aeronautics and Astronautics

Abstract

Different types of Wave Energy Converters currently tested or under development are using the vertical movement of floating bodies to generate electricity. For commercial applications, arrays have to be considered in order to produce a significant power. In this thesis, we investigate the interaction between floating buoys from an hydrodynamic point of view. The objective is to derive general features of energy extraction without resorting to direct numerical simulation by applying the method of homogenization.

After reviewing characteristic aspects of power extraction from a single oscillating body, we study a first configuration where many small buoys are placed close to each other. We show that a collection of point absorbers extract more energy than a single big buoy and that the bandwidth is wider.

We also show that multiple scales analysis allows to treat radiation problems, and that if the incoming wave length is a multiple of the spacing between buoys, energy extraction can be reduced in a very significant way due to a very strong reflection, which prevents the wave from traveling inside the array.

Thesis Supervisor: Prof. Chiang C. Mei
Title: Ford Professor of Engineering
Department of Civil and Environmental Engineering

Acknowledgments

This research has been supported by a grant from MASDAR Institute of Science and Technology in the program of MIT-Abu Dhabi Alliance, directed by Professor F. Moavenzadeh.

I am grateful to Professor Chiang C. Mei for his guidance and availability throughout the realization of this thesis.

Contents

List of Figures

List of Tables

Chapter 1

Introduction

Interest in wave power extraction is not new. Although the first studies about this date back to the end of the nineteenth century, it really started developing in the seventies (See Evans (1981), Falnes (2007), McCormick. (1981), Mei et al. (2005)), but the first commercial plant just opened on the coast of Portugal. This source of renewable energy can be used to produce electricity, or can be integrated in desalinization or hydrogen production facilities (See Cruz (2008)). An efficient industrial design has not yet been found, and much attention is currently given to the power take-off system and the phase control of the device. For most of the designs currently developed, a single wave energy converter (WEC) will not produce significant energy so it is necessary to assemble many of them in a 'wave farm' (Budal and Falnes (1975)).

From the hydrodynamic point of view, one of the simplest type of WEC is a buoy for which energy is extracted from the heaving movement. This is not just a theoretical model, as it is in particular the type of device tested by the Oregon State University or developed by Ocean Power Technologies Inc. (See figure 1-1). The objective of this thesis is to study of such buoys placed in an array will interact with each other. For simplicity, we restrict ourselves to linearized equations and do not take into account viscous effects. We also keep the geometry simple by considering cylindrical buoys in order to avoid numerical computation as much as possible. Finally, we only consider time harmonic movement, but this is not much of a restriction

as we only consider linear equations.

In the first chapter, we focus on wave energy extraction from a single buoy putting together methods developed over 30 years ago (Black et al. (1971), Garrett (1971)). This will allow us to characterize the conditions for a buoy to extract as much energy as possible and will show us the limitations of such a system for practical application.

Several methods have been developed to compute the scattering and radiation by a finite number of floating bodies. In Falnes (1980, 1984), Falnes and Budal (1982), based upon the hypothesis that the interaction between buoys is weak, a simple solution method is given. Kagemoto and Yue (1986) gave an exact method to treat an arbitrary number of bodies using eigenfunction expansion and addition theorems for Bessel functions. Infinite arrays have also been treated by using multipole expansions, see ,for example, Linton and Evans (1992), Linton and McIver (1996). See Mavrakos and McIver (1997), McIver (2002) for a review of the different methods.

Our objective is to provide methods to evaluate the impact of the array while keeping numerical simulation as simple as possible. In the second chapter, motivated by the development of FO3 device in Norway (See ABB Power Systems Inc.), we consider the case of an array of small buoys located close to one another. In Falnes (1984), Falnes and Budal (1982), wave energy by an array has been studied with the assumption that waves radiated by one buoy do not interact with other bodies. This approximation is not valid when the spacing is comparable to the radii of the buoys, but the method of homogenization turns out to be useful to treat this problem and we show that grouping buoys together in a circle has potential benefits.

In the last chapter, we study wave energy extraction from an array where small buoys are located far from each other in a channel. It has been showed that in this configuration, even very small objects can lead to very strong scattering effects: Chen et al. (2004) showed that for some frequencies propagation can be impossible over an array of cylindrical steps, and Li and Mei (2007a,b) gave an analytic method to treat Braggs scattering by an array of small cylindrical piles and showed that nearly all of the energy of an incoming wave can be reflected by an array of finite width. Following these approaches, we show that Braggs resonance should be avoided in

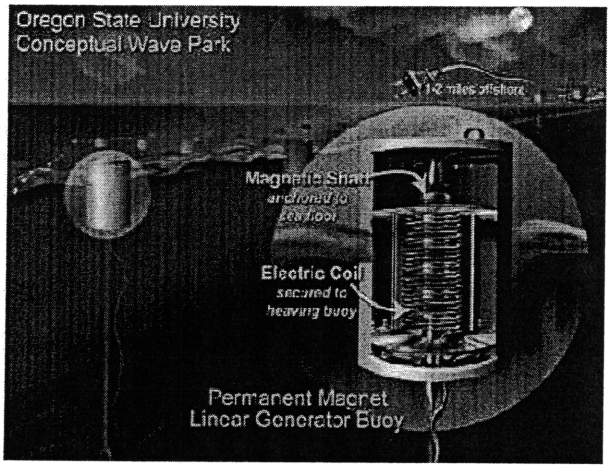

(a) Oregon State University's WEC. Image taken from Oregon State University

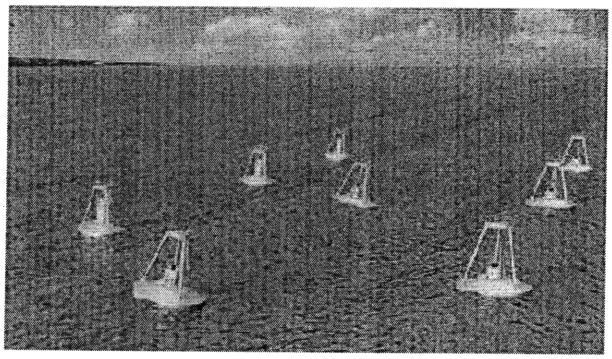

(b) Power buoy from Ocean Power Technologies Inc.. Image taken from Ocean Power Technologies Inc.

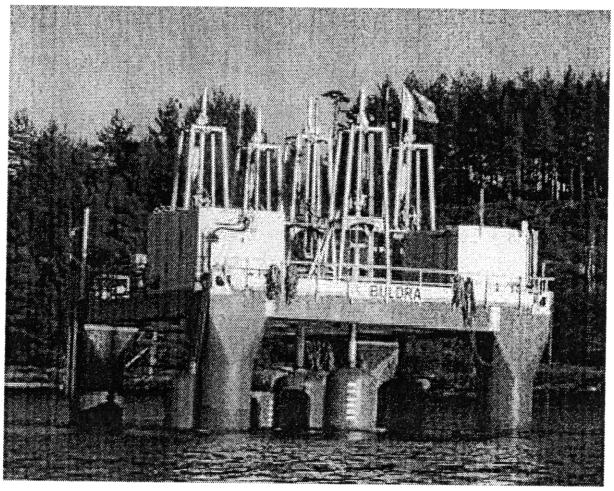

(c) Prototype for the FO3 WEC. Image taken from ABB Power Systems Inc.

Figure 1-1: Example of WECs

order to maximize the power take-off.

Chapter 2

Wave energy extraction from one buoy

In this first part, we will consider the interaction of a single buoy of arbitrary size with an incoming plane wave. In order to keep the numerical solution simple, the buoy that we consider is cylindrical, as shown in figure 2-1. Tools to treat this type of problem have been developed over 30 years ago, in particular by Black et al. (1971) and involve only limited numerical computation. More general geometries can be considered by using the methods of Hybrid Finite Elements (See e.g. Aranha et al. (1979)) or Boundary Elements Method / Fast Multipole Method (See e.g. Utsunomiya and Watanabe (2006)).

We will also restrict ourselves to a linearized study of the flow, and to the power extraction by a linear damper.

2.1 Scattering problem

It is well known (See e.g. Mei et al. (2005)) that the problem of the interaction of a wave with a floating body can be decomposed into scattering and radiation problems. We first consider the diffraction of an incoming wave by a fixed buoy.

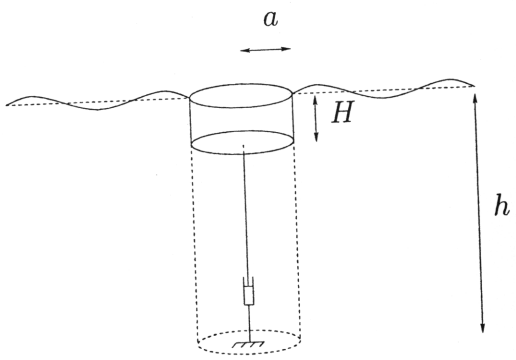

(a) Schema of the system

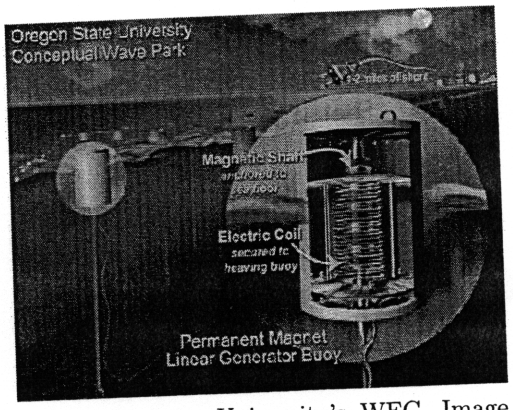

(b) Oregon State University's WEC. Image taken from Oregon State University

Figure 2-1: Point absorber

2.1.1 Equations

Flow equations in physical coordinates Let us denote all physical variables with asterisks, and introduce the following notations:

- Ω_f is the fluid domain,
- S_f is the free surface,
- S_W is the lateral surface of the buoy,
- S_B is the bottom surface of the buoy.

The equations of for the diffraction potential are known to be:

$$\Delta^* \phi^* = 0, \qquad \boldsymbol{x}^* \in \Omega_f \tag{2.1.1a}$$

$$\frac{\partial \phi^*}{\partial z^*} - \frac{\omega^{*2}}{g^*}\phi^* = 0, \qquad \boldsymbol{x}^* \in S_f \tag{2.1.1b}$$

$$\frac{\partial \phi^*}{\partial z^*} = 0, \qquad z^* = -h^* \tag{2.1.1c}$$

$$\frac{\partial \phi^*}{\partial n^*} = 0, \qquad \boldsymbol{x}^* \in S_B \cup S_W \tag{2.1.1d}$$

And the pressure is given by the linearized Bernoulli equation:

$$-\frac{p^*}{\rho^*} = g^* z^* + \frac{\partial \phi^*}{\partial t^*} = -g^* H^* - \mathrm{i}\omega^* \phi^* \tag{2.1.2}$$

We can suppose that the incoming wave is given by the following potential:[1]

$$\phi_i^*(\boldsymbol{x}^*, t^*) = \mathrm{Re}\left\{A^* Z^*(z^*) \exp(\mathrm{i}k^* x^*)\right\} \tag{2.1.3}$$

Where A^* is the amplitude of the incoming wave. In order to satisfy (2.1.6b) and (2.1.6c), Z^* should be chosen of the form

$$Z^*(z^*) = \frac{g^*}{\mathrm{i}\omega^*} \frac{\cosh(k^*(z^* + h^*))}{\cosh(k^* h^*)} \tag{2.1.4}$$

Introduction of dimensionless parameters Let us introduce normalized variables as follows,

$$\begin{aligned} &x_i^* = h^* x_i, \qquad t^* = t\sqrt{\frac{h^*}{g^*}}, \qquad \eta^* = A^*\eta, \quad p^* = \rho^* g^* A^* p, \\ &\phi^* = A^*\sqrt{g^* h^*}\phi, \quad \zeta^* = A^*\zeta \qquad k^* h^* = k \end{aligned} \tag{2.1.5}$$

and rewrite the governing equations. Equation (2.1.1) gives

$$\Delta\phi = 0, \qquad \boldsymbol{x} \in \Omega_f \tag{2.1.6a}$$

$$\frac{\partial\phi}{\partial z} - \omega^2\phi = 0, \qquad \boldsymbol{x} \in S_f \tag{2.1.6b}$$

$$\frac{\partial\phi}{\partial z} = 0, \qquad z = -1 \tag{2.1.6c}$$

$$\frac{\partial\phi}{\partial n} = 0, \qquad \boldsymbol{x} \in S_B \cup S_W \tag{2.1.6d}$$

Equation (2.1.2) becomes

$$-p = \frac{h^*}{A^*} z + \frac{\partial\phi}{\partial t} = \frac{h^*}{A^*} z - \mathrm{i}\omega\phi \tag{2.1.7}$$

and the incoming wave is now represented by

$$\phi_i(\boldsymbol{x}, t) = Z(z)\exp(\mathrm{i}kx) \tag{2.1.8}$$

[1] In everything that follows, the symbol Re will be omitted.

with

$$Z(z) = \frac{1}{\mathrm{i}\omega} \frac{\cosh(k(z+1))}{\cosh(k)} \tag{2.1.9}$$

If ϕ_s is the scattered potential so that $\phi = \phi_i + \phi_s$, it should satisfy (2.1.6a), (2.1.6b), (2.1.6c) and

$$\frac{\partial \phi_s}{\partial n} = -\frac{\partial \phi_i}{\partial n}, \quad \boldsymbol{x} \in S_B \tag{2.1.10}$$

This can be rewritten as

$$\frac{\partial \phi_s}{\partial z} = -Z'(-H)\exp(\mathrm{i}kx), \quad \boldsymbol{x} \in S_B \tag{2.1.11a}$$

and

$$\frac{\partial \phi_s}{\partial r} = -Z(z)\mathrm{i}k\cos(\theta)\exp(\mathrm{i}kr\cos(\theta)), \quad \boldsymbol{x} \in S_W \tag{2.1.11b}$$

in polar coordinates. In order to ensure the uniqueness of the solution, we also impose the radiation condition that the scattered wave should be outgoing at infinity, which can be written as

$$\lim_{r\to\infty} \sqrt{kr}\left(\frac{\partial \phi_s}{\partial r} - \mathrm{i}k\phi_s\right) = 0 \tag{2.1.12}$$

In order to take advantage of the 'cylindrical' geometry, we decompose the incoming plane wave into angular modes,[2]

$$\phi_i(\boldsymbol{x}, t) = Z(z)\sum_{m=0}^{\infty} \varepsilon_m i^m J_m(kr)\cos(m\theta) \tag{2.1.13a}$$

and we will later truncate this series after N_θ terms for the numerical analysis. This way (2.1.11a) and (2.1.11b) will be replaced by:

$$\frac{\partial \phi_s}{\partial z} = -Z'(-H)\sum_{m=0}^{\infty} \varepsilon_m i^m J_m(kr)\cos(m\theta) \tag{2.1.13b}$$

[2] $\varepsilon_0 = 1$ and $\varepsilon_n = 2\,\forall n \geq 1$

for $r \leq a, z = -H$, and

$$\frac{\partial \phi_s}{\partial r} = -Z(z)k \sum_{m=0}^{\infty} \varepsilon_m i^m J'_m(kr)\cos(m\theta) \equiv -\sum_m U_m^W \cos(m\theta) \tag{2.1.13c}$$

for $r = a, -H \leq z \leq 0$. Similarly, we can decompose our solution into angular modes using Fourier series: [3]

$$\phi_s = \sum_m \phi_m \cos(m\theta)$$

The method of solution that follows can be applied to any angular mode m.

2.1.2 Solution

Decomposition

Let us follow the approach of Black et al. (1971): in order to find the form of possible solutions to the problem, we proceed by separation of variables. and we decompose the fluid domain into two sub-domains:

Outer domain This domain is defined in polar coordinates by $r \geq a$ and $-1 \leq z \leq 0$. Given (2.1.6a), (2.1.6c), (2.1.6b) and (2.1.12), we find that the solution should be of the form:

$$\phi_m = \sum_{n=0}^{\infty} b_{n,m} f_n(z) \psi_{n,m}(r) \tag{2.1.14}$$

with

$$f_0(z) = \frac{\sqrt{2}\cosh(k(z+1))}{\sqrt{(1+\sinh^2(k)/\omega^2)}} \equiv c_0 \cosh(k(z+1)), \quad k\tanh(k) = \omega^2 \tag{2.1.15a}$$

$$f_n(z) = \frac{\sqrt{2}\cos(k_n(z+1))}{\sqrt{(1-\sin^2(k_n)/\omega^2)}} \equiv c_n \cos(k_n(z+1)), \quad k_n\tan(k_n) = -\omega^2 \tag{2.1.15b}$$

$$\psi_{m,0}(r) = H_m^{(1)}(kr) \tag{2.1.15c}$$

$$\psi_{n,m}(r) = K_m(k_n r) \tag{2.1.15d}$$

[3] Given the symmetry $\theta \leftrightarrow -\theta$ all terms proportional to $\sin(m\theta)$ must be excluded.

and

$$(n - 1/2)\pi \leq k_n \leq n\pi \quad \forall n \geq 1 \tag{2.1.15e}$$

Inner domain This domain is defined in polar coordinates by $r \leq a$ and $-1 \leq z \leq -H$. For the potential to remain finite for $r \to 0$, we find that the solution of (2.1.6a), (2.1.6c) and (2.1.11a) should be of the form:

$$\Phi_m = \Phi_m^p + \sum_{n=0}^{\infty} B_{n,m} F_n(z) \Psi_{n,m}(r) \tag{2.1.16}$$

where the first term of the RHS, Φ_m^p, is a particular solution that solves

$$\Delta \Phi_m^p = 0, \qquad -1 \leq z \leq -H \text{ and } r \leq a \tag{2.1.17a}$$

$$\frac{\partial \Phi_m^p}{\partial z} = 0, \qquad z = -1 \text{ and } r \leq a \tag{2.1.17b}$$

$$\frac{\partial \Phi_m^p}{\partial z} = -\varepsilon_m \mathrm{i}^m J_m(kr) \left.\frac{\mathrm{d}Z}{\mathrm{d}z}\right|_{-H}, \qquad z = -1 \text{ and } r \leq a \tag{2.1.17c}$$

A solution to this problem is

$$\Phi_m^p = -Z(z) \varepsilon_m \mathrm{i}^m J_m(kr) \tag{2.1.18}$$

where ϕ_i is the potential associated with the incoming wave, as defined in (2.1.8). The second (series) term in (2.1.16) solves the homogeneous problem. The eigenfunctions in the inner domain are given by:

$$F_0(z) = \frac{1}{\sqrt{1 - H}} \tag{2.1.19a}$$

$$F_n(z) = \frac{\sqrt{2}\cos(K_n(z+1))}{\sqrt{1 - H}} \qquad K_n = \frac{n\pi}{1 - H} \tag{2.1.19b}$$

$$\Psi_{0,m}(r) = r^m \tag{2.1.19c}$$

$$\Psi_{n,m}(r) = I_m(K_n r) \tag{2.1.19d}$$

Matching both domains: the Fredholm equation

We know that the normal velocity and the pressure must be continuous across any surface, so we need to match the value of the potential (pressure) and its normal derivative (velocity) at the interface between the two regions. Let us introduce the velocity U_m corresponding to the series in (2.1.14):

$$U_m = \sum_{n=0}^{\infty} B_{n,m} F_n(z) \Psi'_{n,m}(a) \tag{2.1.20}$$

Continuity of the velocity: We know that we should have:

$$\sum_n b_{n,m} \psi'_{n,m}(a) f_n(z) = \begin{cases} U_m^W \equiv -\varepsilon_m \mathrm{i}^m J_m(ka) f(z) & -H \le z \le 0 \\ U_m + \dfrac{\partial \Phi_m^p}{\partial r} & -1 \le z \le -H \end{cases} \tag{2.1.21}$$

For simplicity, let us introduce

$$U_m^p \equiv \left. \frac{\partial \Phi_m^p}{\partial r} \right|_{r=a}$$

Using (2.1.20) and (2.1.21), let us express the coefficients $\{b_n\}$ and $\{B_n\}$ as a function of U_m. Using the fact that $\{f_n\}$ and $\{F_n\}$ define orthonormal bases, we can take the dot product of (2.1.21) with f_n and we find that [4]

$$b_{n,m} \psi'_{n,m}(a) = \langle U_m^W, f_n \rangle_{-H,0} + \langle U_m + U_m^p, f_n \rangle_{-1,-H} \tag{2.1.22a}$$

Similarly, taking the dot product of (2.1.20) with F_n we find

$$B_{n,m} \Psi'_{n,m}(a) = \langle U_m, F_n \rangle_{-1,-H} \tag{2.1.22b}$$

[4] We denote the scalar product by

$$\langle F, G \rangle_{a,b} = \int_a^b F(z) G(z \, \mathrm{d}z$$

When the subscripts are omitted, the integration bounds are -1 and $-H$.

Continuity of the pressure: We can now replace the expressions obtained in (2.1.22) in (2.1.16) and (2.1.14). In order to make notations lighter, let us introduce

$$\alpha_{n,m} = \frac{\psi_{n,m}(a)}{\psi'_{n,m}(a)}$$

$$\beta_{n,m} = \begin{cases} 0 & \text{if } m = n = 0 \\ \dfrac{\Psi_{n,m}(a)}{\Psi'_{n,m}(a)} & \text{else} \end{cases}$$

Equaling the potentials for $r = a$ and $-1 \leq z \leq -H$, we find

$$\sum_{n=0}^{\infty} \alpha_{n,m}\langle U_m, f_n\rangle f_n(z) - \beta_{n,m}\langle U_m, F_n\rangle F_n(z)$$

$$= -\Phi^p_m - \sum_{n=0}^{\infty} \alpha_{n,m}\left[\langle U^W_m, f_n\rangle_{-H,0} + \langle U^p_m, f_n\rangle\right] f_n(z)$$

which can be rewritten as

$$\mathcal{L}_m U_m \equiv \int_{-1}^{-H} G_m(z,\zeta) U_m(\zeta)\,\mathrm{d}\zeta = \gamma_m(z) \tag{2.1.23}$$

This defines $\mathcal{L}_m$, with

$$G_m(z,\zeta) \equiv \sum_{n=0}^{\infty} \alpha_{n,m} f_n(z) f_n(\zeta) - \beta_{n,m} F_n(z) F_n(\zeta)$$

$$\gamma_m(z) \equiv \Phi^p_m(z) - \sum_{n=0}^{\infty} \alpha_{n,m} f_n(z)\left(\langle U^p_m, f_n\rangle_{-1,-H} + \langle U^W_m, f_n\rangle_{-H,0}\right)$$

when $m \neq 0$. For $m = 0$ (2.1.22b) does not allow us to express $B_{0,0}$ in terms of W_0 as $\Psi'_{0,0}(a) = 0$, but we can still replace the other coefficients in terms of U_0. We get

$$\mathcal{L}_0 U_0 \equiv \int_{-1}^{-H} G_0(z,\zeta) U_0(\zeta)\,\mathrm{d}\zeta = \gamma_0(z) + B_{0,0}.F_0(z) \tag{2.1.24}$$

with

$$G_0(z,\zeta) = \sum_{n=0}^{\infty} \alpha_{n,0} f_n(z) f_n(\zeta) - \sum_{n=1}^{\infty} \beta_{n,0} F_n(z) F_n(\zeta)$$

The problem (2.1.24) has one extra unknown compared to (2.1.23), $B_{0,0}$, so we need an extra equation to solve this problem. We now have to solve it for U_0 and $B_{0,0}$. Note that U_0 is the radial flux associated with an isotropic potential f that solves:

$$\begin{aligned}
\Delta f &= 0 && \boldsymbol{x} \in \Omega_f,\ r \leq a \\
\frac{\partial f}{\partial z} &= 0 && \boldsymbol{x} \in S_B \\
\frac{\partial f}{\partial z} &= 0 && z = -1,\ r \leq a \\
\frac{\partial f}{\partial \theta} &= 0 && \boldsymbol{x} \in \Omega_f,\ r \leq a \text{ (as } m = 0)
\end{aligned}$$

therefore

$$0 = -\iiint_{\Omega_f} \Delta f \, \mathrm{d}V = \int_0^{2\pi} \int_{-1}^{-H} \left.\frac{\partial f}{\partial n}\right|_{r=a} \mathrm{d}S = 2\pi \int_{-1}^{-H} U_0(z) \, \mathrm{d}z \tag{2.1.25}$$

Physically, this extra equation expresses the mass conservation for an incompressible fluid. The system of equations defined by the problem (2.1.24) and (2.1.25) can now be solved for U_0 and $B_{0,0}$.

Solution of the Fredholm equation

We expand U_m on the base of $\{F_n\}$:

$$U_m(z) = \sum_{n=0}^{\infty} u_{n,m} F_n(z) \tag{2.1.26}$$

When this expression is inserted into (2.1.23), we get, for each m:[5]

$$\langle \mathcal{L} U_m, F_q \rangle = \sum_{k=0}^{\infty} \left(\sum_{n=0}^{\infty} \alpha_{n,m} \langle f_n, F_q \rangle \langle f_n, F_k \rangle - \beta_{k,m} \delta_{k,q} \right) u_{k,m} \equiv \mathcal{L}_{qk,m} u_{k,m} \tag{2.1.27}$$

and

$$\langle \gamma_m, F_q \rangle = \langle \phi_p^m, F_q \rangle + \sum_{n=0}^{\infty} \alpha_{n,m} \langle f_n, F_q \rangle \left(\langle f_n, U_p^m \rangle + \langle f_n, U_W^m \rangle_{-H,0} \right) \equiv \gamma_{q,m} \tag{2.1.28}$$

[5] $\delta_{i,j}$ is the Kronecker symbol

So (2.1.23) gives us an 'infinite' linear system,

$$\sum_{k=0}^{\infty} \mathcal{L}_{qk,m} u_{k,m} = \gamma_{q,m}, \quad \forall q \in \mathbb{N}$$

which will be solved numerically by truncating the series after the N^{th} term.

As we mentioned earlier, the problem is slightly different for $m = 0$. As we know that $w_{0,0} = 0$, then

$$U_0(z) = \sum_{n=1}^{\infty} u_{n,0} F_n(z) \tag{2.1.29}$$

We can take the projection of (2.1.24) onto the base $\{F_n\}$, and we get

$$\langle \mathcal{L}U_0, F_q \rangle = \sum_{k=1}^{\infty} \left(\sum_{n=0}^{\infty} \alpha_{n,0} \langle f_n, F_q \rangle \langle f_n, F_k \rangle - \beta_{k,0} \delta_{k,q} \right) u_{k,0} \equiv \mathcal{L}_{qk,0} u_{k,0} \tag{2.1.30}$$

and

$$\langle \gamma_0, F_q \rangle = \langle \phi_p^0, F_q \rangle + \sum_{n=0}^{\infty} \alpha_{n,0} \langle f_n, F_q \rangle \left(\langle f_n, U_p^0 \rangle + \langle f_n, U_W^0 \rangle_{-H,0} \right) \equiv \gamma_{q,0} - B_{0,0} \delta_{q,0} \tag{2.1.31}$$

for any q. Imposing conservation of mass finally requires

$$\sum_{n=1}^{\infty} u_{n,0} \int_{-1}^{-H} F_n(z)\, \mathrm{d}z = 0 \tag{2.1.32}$$

and (2.1.30), (2.1.31) and (2.1.32) form a linear system of equation for the unknown $(-B_{0,0}, u_{1,0}, \dots)^T$

$$\sum_{k=1}^{\infty} \mathcal{L}_{qk,0} u_{k,0} = \gamma_{q,0} - B_{0,0} \delta_{q,0}, \qquad \forall q \in \mathbb{N}$$

$$\sum_{k=1}^{\infty} u_{k,0} a_k = 0$$

where

$$a_n \equiv \int_{-1}^{-H} F_n(z)\, \mathrm{d}z$$

Analytical expressions for all the coefficients appearing in these equations are given in Appendix A.1.

2.2 Radiation by a heaving buoy

The radiation problem consists of finding the flow induced by a vertical movement of the buoy. As this flow is imposed by the movement of the buoy, it will be linear in $\dot{\zeta}$, the velovity of the buoy. As a consequence we look for ϕ_r such that $\phi = \phi_r \dot{\zeta}$. This means that the radiation potential should be normalized by:

$$\phi_r^* = h^* \phi_r$$

The governing set of equation for this flow is:

$$\Delta \phi_r = 0, \qquad \boldsymbol{x} \in \Omega_f \tag{2.2.1a}$$

$$\frac{\partial \phi_r}{\partial z} - \omega^2 \phi = 0, \qquad \boldsymbol{x} \in S_f \tag{2.2.1b}$$

$$\frac{\partial \phi_r}{\partial z} = 0, \qquad z = -1 \tag{2.2.1c}$$

$$\frac{\partial \phi_r}{\partial z} = 1, \qquad \boldsymbol{x} \in S_B \tag{2.2.1d}$$

$$\frac{\partial \phi_r}{\partial r} = 0, \qquad \boldsymbol{x} \in S_W \tag{2.2.1e}$$

with the radiation condition at infinity. The main difference between this problem and the scattering one is that the forcing term is not due to the incoming wave but to the movement of the buoy. Note also that the radiated wave has only an isotropic mode. We still decompose the fluid domain into two regions. In the outer domain, $R \geq a$, we look for $\{b_n^r\}$ such that:

$$\phi_r = \phi_0^r = \sum_{n=0} b_n^r \psi_{n,0}(r) f_n(z), \quad r > a \text{ and } -1 < z < 0 \tag{2.2.2}$$

where the f_n and $\psi_{n,0}$ are given in (2.1.15). In the inner domain, we will have:

$$\phi_r = \Phi_r^P + \sum_{n=0} B_n^r F_n(z) \Psi_{n,0}(r), \quad r > a \text{ and } -1 < z < -H \tag{2.2.3}$$

where F_n and $\Psi_{n,0}$ are defined in (2.1.19).

In order to find a particular solution for the inner domain that satisfies (2.2.1) we seek a solution of the form:

$$P(r,z) = \frac{(z+1)^2}{2(1-H)} + g(r)$$

then we have $\left.\frac{\partial P}{\partial z}\right|_{-H} = 1$ and $\left.\frac{\partial P}{\partial z}\right|_{-h} = 0$. The Laplace equation gives:

$$r^2 g''(r) + r g'(r) + \frac{r^2}{(1-H)} = 0$$

a solution of this equation is given by:

$$g(r) = -\frac{r^2}{4(1-H)}$$

Let us therefore define

$$\Phi_r^p(r,z) \equiv P = \frac{1}{2(1-H)}\left((z+1)^2 - \frac{r^2}{2}\right) \tag{2.2.4}$$

and the radial velocity introduced by this potential:

$$U_r^p(z) \equiv \left.\frac{\partial P}{\partial r}\right|_a = \frac{-a}{2(1-H)} \tag{2.2.5}$$

With these definitions, we can perform the same analysis as in §2.1 in order get a Fredholm equation and to solve it. Analytical values of the coefficients associated to the radiation problem are given in Appendix A.1.

2.3 Validation of the numerical results

2.3.1 Case $H \approx 1$

In this case the buoy is a vertical cylinder standing on the sea bed. The well known analytical solution (See (Mei et al., 2005, p.369)) is given by:

$$\phi_s = -Z(z) \sum_{m=0}^{\infty} \varepsilon_m \mathrm{i}^m \frac{J'_m(ka)}{H_m^{(1)'}(ka)} H_m^{(1)}(ka) \cos(m\theta) \tag{2.3.1}$$

Our numerical solution is in very good agreement with this analytic expression in the limit of $H \approx 1$.

2.3.2 Discontinuity of the velocity at the bottom of the buoy.

Order of magnitude.

We notice numerically a discontinuity of the velocity at the bottom of the buoy. In order to evaluate its order of magnitude , let us consider the flow in the neighborhood of the corner. The time scale is ω^{-1}, but the length scale is much smaller than a or any other length in the problem, therefore we can neglect the time derivatives compared to the spatial derivatives, and we can approximate the flow in the neighborhood by a two dimensional steady flow around a corner. Let us notice that if the potential is of the form (See Huerre (1998))

$$\varphi(\zeta) = \frac{\zeta^{m+1}}{m+1} \tag{2.3.2a}$$

with a plane cut for $\zeta \in \mathbb{R}_+$, then the complex velocity $W = u - \mathrm{i}v$ is given by

$$W(\zeta) = \zeta^m \tag{2.3.2b}$$

The velocity will be parallel to the real axis for $\zeta = x + \mathrm{i}\varepsilon$ when $\varepsilon \longrightarrow 0^+$, and will be parallel to ζ for

$$m\theta_0 = -\theta_0 + 2\pi \tag{2.3.3}$$

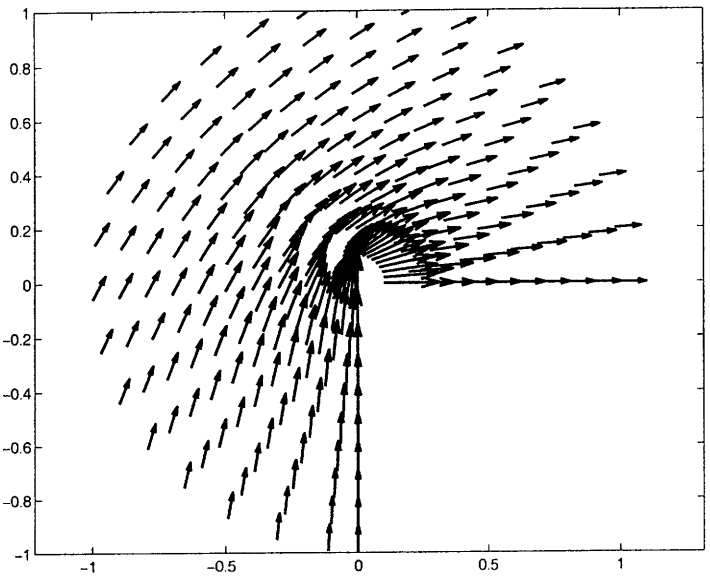

Figure 2-2: Potential flow around a corner

therefore by choosing $m = -1/3$ we will get the flow around a right angle. Figure 2-2 shows this flow, which goes to infinity for $y \to 0^-$ as $y^{-1/3}$.

Truncation error

It is well known that convergence of a Fourier series towards a discontinuous function is not uniform, and that truncated series will oscillate near the points of discontinuity (This is called Gibbs phenomenon.). Following Porter and Evans (1995), an idea to get a better convergence would therefore be to introduce a new base of functions, that will also have the same type of singularity as our solution:

$$G_n(z) = F_n(z)(z+H)^{-1/3} \tag{2.3.4}$$

We can apply the same method as in (2.1.27) and (2.1.28) except we compute the scalar product with function G_n instead of F_n. For the mode $m = 0$ we should be more careful as

$$\int_{-1}^{-H} G_0(z)\,\mathrm{d}z \neq 0$$

so we have to take the term $n = 0$ into account and add an equation on $\{w_i\}$ stating that the average should be 0. In this we have to compute numerically:

- The scalar products $\langle f_n, G_m \rangle$ and $\langle \phi^p, G_m \rangle$.
- The averages $\int_{-1}^{-H} G_n(z)\,\mathrm{d}z$ in order to impose $\int_{-1}^{-H} W(z)\,\mathrm{d}z = 0$.

In order to compute these integrals, one should be careful that the functions are singular and have fast oscillations. The use of the modified base gives better results even if we need to compute all coefficients numerically. If we were interested only in the inner flow, and we had memory limitations, this would be a good solution. We did not use this method for two reasons:

- Numerical integration is very time consuming.
- If we are also interested in the outer flow, all the gain will be lost as we will have to project our result onto the base $\{f_n\}$ which does not have the singularity.

We notice numerically (See Appendix A.2.1) that solutions in the inner and outer domains are matched properly and that boundary conditions are enforced, but that 'artificial' oscillation occur for the velocity field near the bottom of the buoy due to the truncation error. Unlike this, the pressure, which is continuous, is approximated in a much better way. Let us now show, in the following sections and in Appendix A.2.2 that despite the imprecision in the determination of the velocity, our results in terms of forces and energy are valid.

2.3.3 Optical theorem

The far field amplitude $\mathcal{A}(\theta)$ is defined by

$$\phi = \phi_i + \phi_s \approx \frac{1}{\mathrm{i}\omega} \frac{\cosh(k(z+1))}{\cosh(k)} \left(\mathrm{e}^{\mathrm{i}kx} + \mathcal{A}(\theta) \sqrt{\frac{2}{\pi kr}} \mathrm{e}^{i(kr-\pi/4)} \right) \tag{2.3.5}$$

for large kr. Therefore, given the asymptotic expansion of the Hankel functions, we have:

$$\mathcal{A}(\theta) = \sum_m \mathrm{i}\omega c_0 \cosh(k) b_{0m} \mathrm{i}^{-m} \tag{2.3.6}$$

It is known (See (Mei et al., 2005, p.381)) that $\mathcal{A}(\theta)$ should satisfy the optical theorem:

$$\frac{1}{\pi}\int_0^{2\pi} |\mathcal{A}(\theta)|^2 \,\mathrm{d}\theta = -2\mathrm{Re}(\mathcal{A}(0)) \tag{2.3.7}$$

This relation expresses the conservation of energy for the scattering problem, We have checked numerically that this result is satisfied with a very good precision, as the relative error is smaller than 10^{-4}.

2.3.4 Vertical exciting force: Haskind relation

In physical coordinates, the exiting force due to diffraction

$$F_z^{D*} = \mathrm{i}\rho^*\omega^* \int_0^{a^*} \left(\phi^*_{s,0}(r^*, -H^*) + Z^*(-H^*)J_0(k^*r^*)\right) r^* \,\mathrm{d}r^* \tag{2.3.8}$$

so in dimentionless form

$$F_z^{D} = \mathrm{i}\omega \int_0^{a} \left(\phi_{s,0}(r, -H) + Z(-H)J_0(kr)\right) r \,\mathrm{d}r \tag{2.3.9}$$

with

$$F_z^{D*} = \rho^* g^* h^{*2} A^* F_z^D$$

According to Haskind's theorem, it is related to the far-field amplitude of the radiated wave $\mathcal{A}_z$ by the relation:

$$F_z^D = -\frac{4C_g}{k}\mathcal{A}_z(\pi) \tag{2.3.10}$$

Replacing the expansion (2.1.14) in (2.3.9), we get:

$$\boxed{F_z^D = \mathrm{i}\omega \sum_{n=0}^{\infty} B_{n,0} f_n(-H)\gamma_n} \tag{2.3.11}$$

with

$$\gamma_0 = \frac{a^2}{2} \tag{2.3.12}$$

$$\gamma_j = \frac{a}{K_n} I_1(K_n a) \quad \forall j \geq 1 \tag{2.3.13}$$

Using the computed coefficients $B_{n,0}$, this relation is verified numerically with a good precision (the relative error is smaller than 10^{-4}), and the result we obtain are in good agreement with the graphs given in Garrett (1971) (See figures 2-3(a) and 2-3(b).)

2.3.5 Horizontal exciting force

Using (2.1.7), the horizontal force due to scattering is given by

$$\begin{aligned} F_x^D &\equiv -\mathrm{i}\omega \int_0^{2\pi} \int_{-H}^{0} \phi_D(a,\theta,z) a \left(-\cos(\theta)\right) \, \mathrm{d}\theta \, \mathrm{d}z \\ &= \mathrm{i}\pi\omega a \int_{-H}^{0} \left(2\mathrm{i} J_1(ka) Z(z) + \phi_1(a,0,z)\right) \, \mathrm{d}z \end{aligned}$$

using the same normalization as before. We still have good agreement with the results given in Garrett (1971) (See figures 2-3(c) and 2-3(d)).

2.3.6 Vertical restoring force: Relation (8.6.13) from Mei et al. (2005)

The force due to radiation [6]

$$F_{zz} = 2\mathrm{i}\pi\omega \int_0^a \phi_{r,0}(r,-H) r \, \mathrm{d}r$$

is related to the far-field amplitude of the radiated wave $\mathcal{A}_z$ by the relation

$$\lambda_{zz} = -\mathrm{Re}(F_{zz}) = \frac{4C_g}{k} |\mathcal{A}_z|^2 \tag{2.3.14}$$

[6] F_{zz}^* itself is not the force, $-\mathrm{i}\omega^*\zeta^* F_{zz}^*$ is, so it should be normalized by $\rho^* h^{*5/2} g^{*-1/2}$.

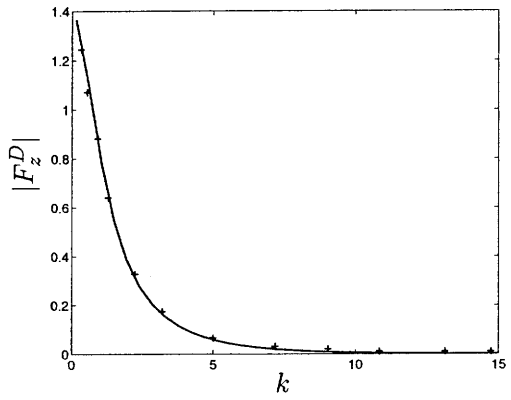

(a) Vertical force, amplitude

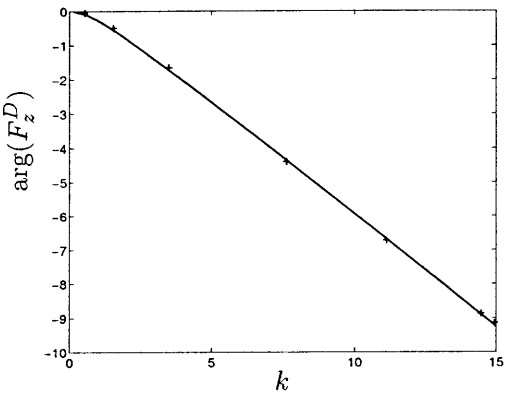

(b) Vertical force, phase

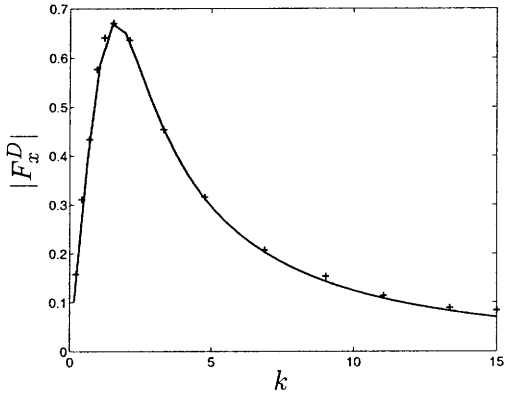

(c) Horizontal force, amplitude

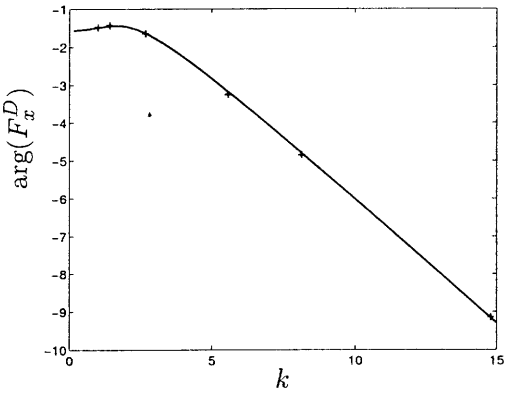

(d) Horizontal force, phase

Figure 2-3: Scattering forces on the buoy ($N = 100$, $a = 2/3 = 2H$). The crosses correspond to the values given in Garrett (1971)

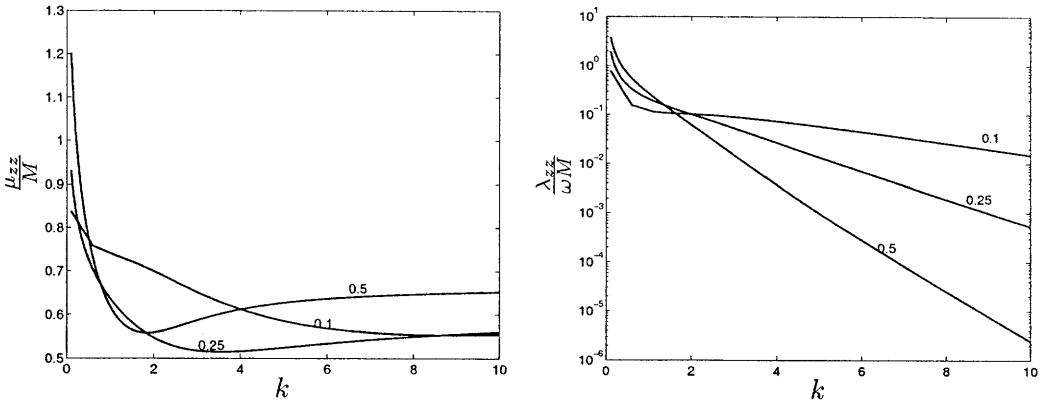

(a) Added mass (b) Radiation damping

Figure 2-4: Added mass and radiation damping for different geometries. The value of $a = H$ is indicated next to the curves.

As we did for the exciting force, we get:

$$\boxed{F_{zz} = 2i\pi\omega \left(\sum_{n=0}^{\infty} B_{n,r} F_n(-H)\gamma_n + \frac{1}{2(1-H)} \left(\frac{(1-H)^2 a^2}{2} - \frac{a^4}{8} \right) \right)}$$

In the simulations, (2.3.14) is verified numerically with a good precision (the relative error is smaller than 10^{-10})

2.4 Buoy dynamics and energy extraction

2.4.1 Equations of movement

If we assume that the buoy vertical displacement is given by $\zeta(t) = \zeta e^{-i\omega t}$, then the hydrodynamic force is given by:

$$F_{hydro} = F_z^D - i\omega\zeta F_{zz} + \pi a^2 \zeta \tag{2.4.1}$$

in dimensionless coordinates. The first term is due to scattering, the second one to radiation and the last one to the dynamic pressure. The static pressure is not present as it is balanced by the weight of the buoy. If we decompose the restoring force into $F_{zz} = -\lambda_{zz} + i\omega\mu_{zz}$, the equation of movement is:

$$-M\omega^2\zeta = F_z^D - \omega^2\mu_{zz}\zeta - i\omega\zeta(\lambda_{zz} + \lambda_g) + \pi a^2\zeta \tag{2.4.2}$$

where the force applied by the power extraction device is assumed to be of the form

$$F_{gen} = -\lambda_g\dot{\zeta} = i\omega\lambda_g\zeta$$

From (2.4.2), we get

$$\zeta = \frac{F_z^D}{\pi a^2 - \omega^2(M + \mu_{zz}) - i\omega(\lambda_g + \lambda_{zz})} \tag{2.4.3}$$

For two geometries, this displacement is plotted in figures 2-7(a) and 2-7(b).

2.4.2 Energy extraction

Once ζ is known, one can get the extracted power which is given by:

$$\begin{aligned}\overline{\dot{E}} &= \frac{1}{2}\lambda_g\omega^2|\zeta|^2 \\ &= \frac{1}{2}\frac{\lambda_g\omega^2|F_z^D|^2}{(\pi a^2 - \omega^2(M + \mu_{zz}))^2 + \omega^2(\lambda_g + \lambda_{zz})^2}\end{aligned}$$

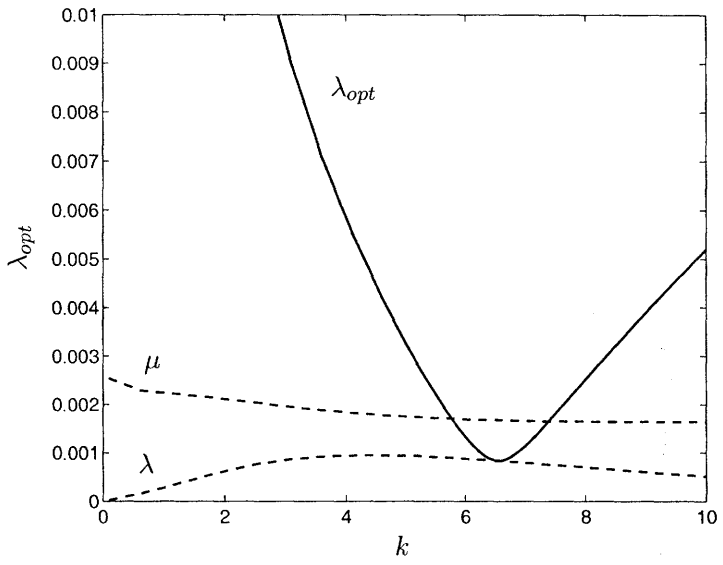

Figure 2-5: Optimal value λ_{opt} of the energy extraction rate. ($a = H = 0.1$)

Note that in physical coordinates, the extracted power would be

$$\overline{\dot{E}}^* = \rho^* h^{*5/2} g^{*-1/2} \frac{g^*}{h^*} A^{*2} \overline{\dot{E}} = \rho^* h^{*3/2} g^{*1/2} A^{*2} \overline{\dot{E}}$$

It is maximum for

$$\lambda_g = \lambda_{opt} \equiv \sqrt{\left(\frac{\pi a^2 - (M + \mu_{zz})\omega^2}{\omega} \right)^2 + \lambda_{zz}^2}$$

This optimal value of the extraction rate depends on the frequency, as shown in figure 2-5. An analytical study shows that the maximum power that one can extract from a buoy with only one degree of freedom in heaving is equal to the energy incoming on one wave length (See (Mei et al., 2005, §(8.9.3))):

$$\overline{\dot{E}}_{max} = \frac{C_g}{2k} \tag{2.4.4}$$

so we can define the capture width by:

$$k\mathcal{W} \equiv \frac{\overline{\dot{E}}_{opt}}{\overline{\dot{E}}_{max}} = \frac{k}{C_g} \frac{\lambda_g \omega^2 |\widetilde{F_z^D}|^2}{\omega^2(\lambda_{zz} + \lambda_g)^2 + (\pi a^2 - \omega^2 (\pi a^2 H + \mu))^2} \tag{2.4.5}$$

2.5 Conclusion

Energy extraction is represented in figure 2-7(c). We first note that, as expected, the optimal $k\mathcal{W}$ is 1 for any geometry, but that this maximum is obtained only at resonance, and that the bandwidth is limited. Figure 2-7(a) shown the amplitude of the buoy displacement. We see that, in agreement with general features derived in Mei et al. (2005), the amplitude of the buoy displacement at resonance increases as the size of the buoy diminishes. What is maybe more significant for energy extraction is that resonance occurs at higher frequencies as the size of the buoy decreases. Let us recall that in usual conditions $k^*h^* \sim 1$, so resonance is possible only for large buoys. For such large buoys, we see that the bandwidth is very limited.

***Remark* 2.5.1** (Analytic estimation of the bandwidth). *We see in figure 2-4 that (at least near the resonant peaks) we have $\mu \sim M/2$ and $\lambda \ll \omega M$, so we can approximate $k\mathcal{W}$ as*

$$k\mathcal{W} \propto \frac{s}{(\pi a^2 - 3sM/2)^2}$$

with $s = \omega^2$, which gives a bandwidth

$$\delta = \frac{8}{9} \frac{\sqrt{1 + 3\,a^5\pi^2}}{\pi^2 a^6}$$

in terms of s. We see that it goes to ∞ as $a \to 0$ and to 0 as $a \to \infty$.

In addition to the damper, we could have considered that the buoy was also linked to a spring of dimensionless stiffness κ. Everything would be similar, except that the dynamic pressure term $\pi a^2 \zeta$, which already acts like a spring, would be replaced by $(\pi a^2 + \kappa)\,\zeta$. If $\kappa > 0$, which is the case for a spring, this would result in increasing the resonant frequency, which is not something we are looking for. Note that the resonant frequency decreases as the mass of the buoy increases, so in order to have better performance, we may want to increase the mass while keeping the hydrodynamic forces constant. A solution for that is to add mass to the buoy deep into the water, where hydrodynamic effects are weak, as shown in figure 2-6.

An idea to improve the power output would be to be able to adapt the damping

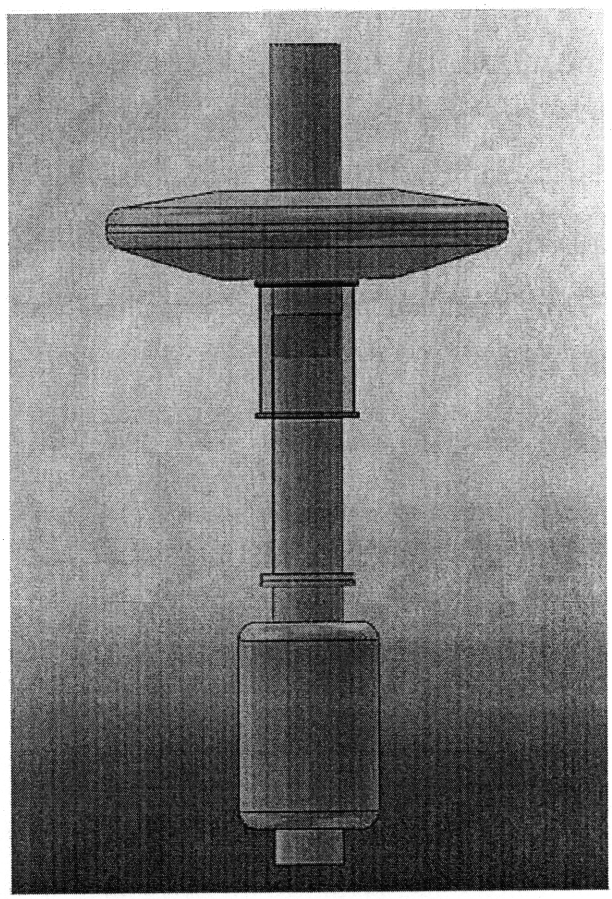

Figure 2-6: Buoy design from the Oregon State University. Image taken from Oregon State University

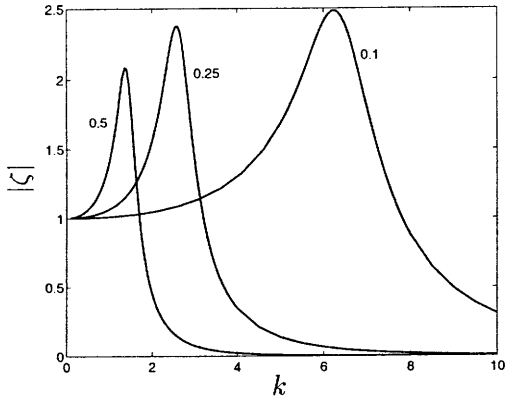

(a) Amplitude of the buoy displacement

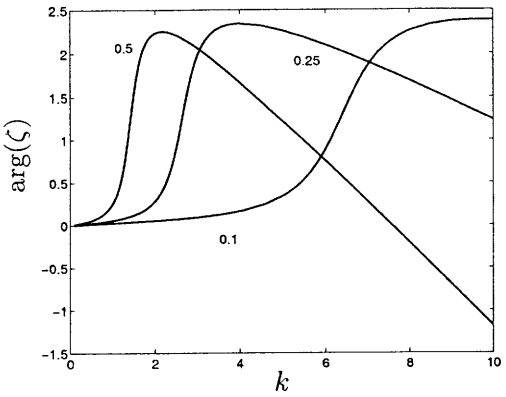

(b) Phase of the buoy displacement

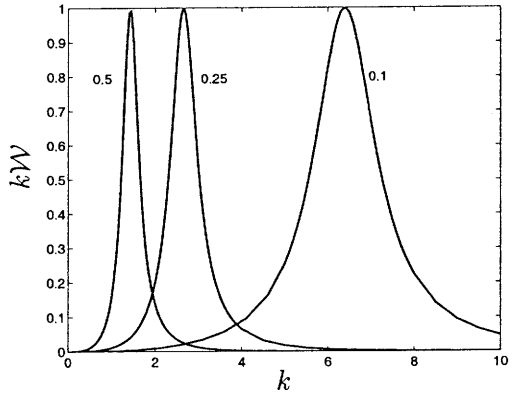

(c) Capture width

Figure 2-7: Energy extraction and buoy movement for three different sizes of buoys. The energy extraction rate λ_g is constant and chosen such that the energy extraction is maximum at resonance, and the value of $a = H$ is indicated next to the curves.

rate in order to maximize the power output for any frequency. Figure 2-7(c) shows the energy extraction when λ_g is varied with the frequency. If instead we have an energy extraction device with fixed properties, then we would have a lower capture width, as shown in figure 2-8. More complex phase control strategies have been developed (See e.g. Falcão (2008), Falnes (2002b)), and take into account different types of wave power extractor. Note finally that we only studied monochromatic waves, but any linear wave could be treated in this way using superposition (See for example Eriksson et al. (2005)).

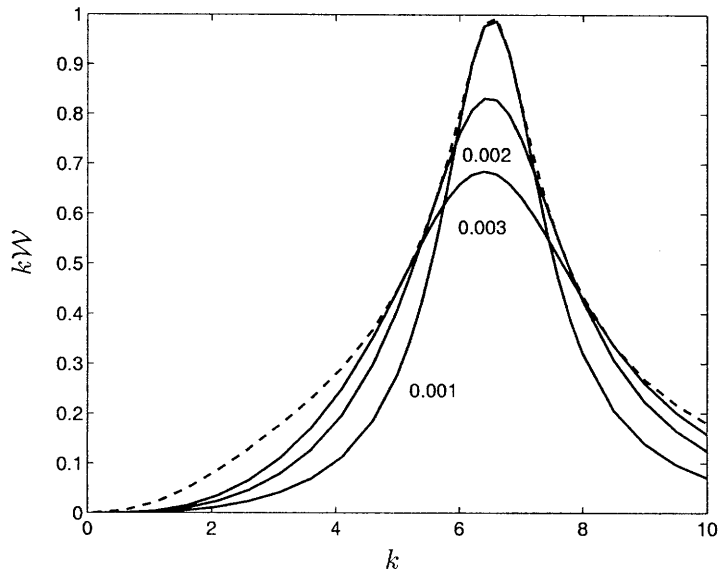

Figure 2-8: Capture width with an energy extraction device of fixed damping rate, as indicated next to the curve. ($a = H = 0.1$)

Chapter 3

Wave-Power Extraction by a Compact Array of Buoys

3.1 Introduction

Recently Fred Olsen and ABB Power Systems Inc. in Norway have designed a system called FO3 which consists of a rig with many small floating cylinders hanging underneath it, as shown in figure 3-1(b). Energy is absorbed from the waves as they set the cylinders into vertical motion which then activates a hydraulic system driving a generator to produce electricity. Currently being tested is a 1:3-scale research model which measures 12 by 12 meters and is 8 meters high. It is estimated that the full-scale model can produce 2.52 MW from 6-meter high waves with a period of 9 seconds, which is comparable to the capacity of a wind turbine. Eventually a large array of many rigs can be installed over a large sea surface area and produce much more electricity.

In order to investigate wave energy extraction from such a device, we consider a square array of small and identical buoys floating on the surface of the sea of constant mean depth h^*, as shown in figure 3-1(a). Each buoy is a vertical cylinder of circular cross section of radius a^* and draft H^*, spaced at the distance d^* from centre to centre. Assuming monochromatic waves of frequency ω^*, the wave number k^* of the

incident waves is given by the real root of the dispersion relation

$$\omega^{*2} = g^* k^* \tanh k^* h^* \tag{3.1.1}$$

In this chapter, we shall consider the incoming wave length and the sea depth to be comparable but both are much greater than the buoy radius a^*, the draft H^* and the separation distance d^*. i.e.,

$$\frac{a^*}{h^*} \equiv \mu \ll 1, \quad O(a^*) = O(H^*) = O(d^*), \quad k^* h^* = O(1) \tag{3.1.2}$$

Wave energy is extracted from the heaving oscillation of each buoy through an absorbing device anchored to the seabed or attached to a fixed supporting structure.

3.2 Linearized governing equations

As we did in the Chapter 2, we employ the following symbols for physical domains: Ω_f is the fluid domain, S_f is the free surface, S_W is the lateral surface of the buoys, and S_B is the bottom surface of the buoys. Let us denote all physical variables with asterisks. For infinitesimal waves the velocity potential in water, is governed by Laplace's equation

$$\Delta^* \Phi^* = \frac{\partial^2 \Phi^*}{\partial x^{*2}} + \frac{\partial^2 \Phi^*}{\partial y^{*2}} + \frac{\partial^2 \Phi^*}{\partial z^{*2}} = 0, \quad \boldsymbol{x}^* \in \Omega_f \tag{3.2.1}$$

Assuming constant atmospheric pressure on the sea surface, the total pressure inside water is given by Bernoulli's equation:

$$p^* = -\rho^* \frac{\partial \Phi^*}{\partial t^*} - \rho^* g^* z^* \tag{3.2.2}$$

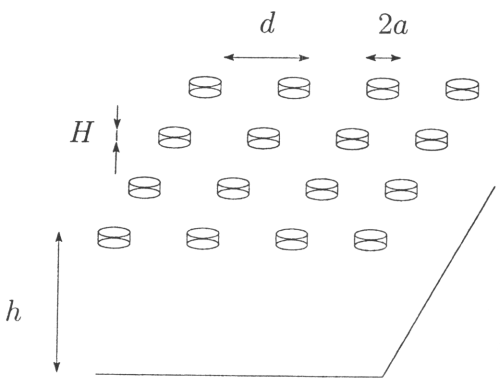

(a) A periodic array of buoys

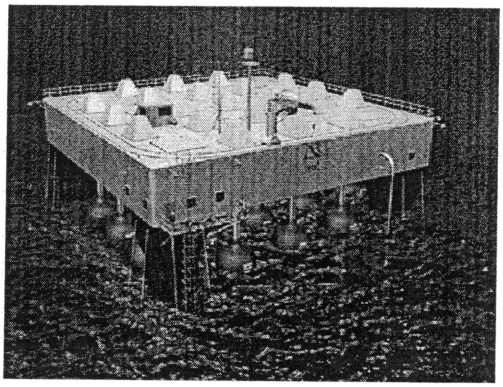

(b) WEC platform concept FO3. Image taken from ABB Power Systems Inc.

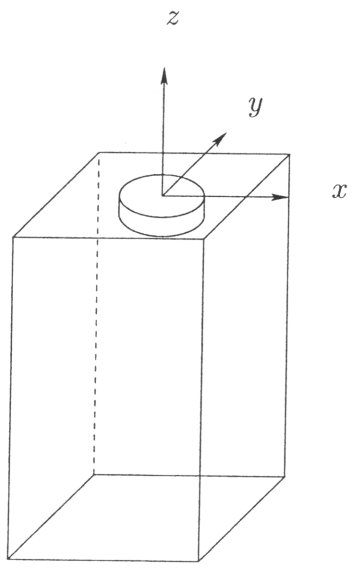

(c) Cell geometry

Figure 3-1: Geometry of the array of buoys.

On the free surface $z^* = \eta^*(x^*, y^*, t^*)$, the kinematic boundary condition is

$$\frac{\partial \Phi^*}{\partial z^*} = \frac{\partial \eta^*}{\partial t^*}, \quad \boldsymbol{x}^* \in S_F \tag{3.2.3}$$

and the dynamic boundary condition is

$$g^* \eta^* + \frac{\partial \Phi^*}{\partial t^*} = 0, \quad \boldsymbol{x}^* \in S_F \tag{3.2.4}$$

On the sea bed the vertical velocity vanishes, which gives

$$\frac{\partial \Phi^*}{\partial z^*} = 0, \quad z^* = -h^* \tag{3.2.5}$$

On the side wall of the buoy, there is no normal velocity:

$$\frac{\partial \Phi^*}{\partial r^*} = 0, \quad \boldsymbol{x}^* \in S_W \tag{3.2.6}$$

where r^* is the local radial coordinate from the axis of a cylindrical buoy. On the flat bottom of the buoy the kinematic condition is

$$\frac{\partial \Phi^*}{\partial z^*} = \frac{\partial \zeta^*}{\partial t^*}, \quad \boldsymbol{x}^* \in S_B \tag{3.2.7}$$

where $\zeta^*(t^*)$ is the unknown vertical displacement of the buoy. We model the action of the energy extraction device on the buoy by a damping force

$$F^*_{extr} = -\lambda^*_g \frac{\partial \zeta^*}{\partial t^*} \tag{3.2.8}$$

The conservation law of vertical momentum of the buoy serves as the dynamic condition

$$M^* \frac{\partial^2 \zeta^*}{\partial t^{*2}} + \lambda^*_g \frac{\partial \zeta^*}{\partial t^*} + \pi a^{*2} \rho^* g^* \zeta^* = -\rho^* \iint_{S_B} \frac{\partial \Phi^*}{\partial t^*} \, \mathrm{d}S^* \tag{3.2.9}$$

where $M^* = \rho \pi a^{*2} H^*$ is the buoy mass and H^* its draft.

Let us introduce normalized variables as follows,

$$x_i^* = a^* x_i', \quad t^* = t' \sqrt{\frac{h^*}{g^*}}, \quad \eta^* = A^* \eta', \quad \Phi^* = A^* \sqrt{g^* h^*} \Phi, \quad \zeta^* = A^* \zeta' \tag{3.2.10}$$

and rewrite the governing equations. Note that the length scale is the small radius of the buoy (the micro-scale). In normalized form, Laplace's equation (3.2.1) is unchanged. The free surface conditions (3.2.3) becomes

$$\mu \frac{\partial \eta}{\partial t'} = \frac{\partial \Phi}{\partial z'}, \quad \boldsymbol{x}' \in S_F \tag{3.2.11}$$

where

$$\mu = \frac{a^*}{h^*} \ll 1 \tag{3.2.12}$$

is the key parameter in this study and

$$\eta' + \frac{\partial \Phi}{\partial t'} = 0, \quad \boldsymbol{x}' \in S_F \tag{3.2.13}$$

Equations (3.2.11) and (3.2.13) can be combined to give

$$\frac{\partial \Phi}{\partial z'} + \mu \frac{\partial^2 \Phi}{\partial t'^2} = 0, \quad \boldsymbol{x}' \in S_F \tag{3.2.14}$$

and the condition on the seabed now reads

$$\frac{\partial \Phi}{\partial z'} = 0, \quad z' = -\frac{h^*}{a^*} = -\frac{1}{\mu} \sim -\infty \tag{3.2.15}$$

On the buoy, the kinematic conditions are

$$\frac{\partial \Phi}{\partial r'} = 0', \quad \boldsymbol{x}' \in S_W \tag{3.2.16}$$

and

$$\frac{\partial \Phi}{\partial z'} = \mu \frac{\partial \zeta'}{\partial t'}, \quad \boldsymbol{x}' \in S_B \tag{3.2.17}$$

The dynamic condition (3.2.9) now reads

$$\frac{H^*}{a^*}\frac{\partial^2\zeta'}{\partial t'^2}+\frac{\lambda_g^*\sqrt{g^*/h^*}}{\rho^* g^*\pi a'^2}\frac{\partial\zeta'}{\partial t'}+\zeta'=-\iint_{S_B}\frac{\partial\Phi}{\partial t'}\frac{\mathrm{d}S'}{\pi} \tag{3.2.18}$$

Defining

$$H'=\frac{H^*}{a^*}=O(1), \qquad \lambda_g=\frac{\lambda_g^*\sqrt{g^*/h^*}}{\rho^* g^*\pi a^{*2}}=O(1) \tag{3.2.19}$$

we can write

$$\mu H'\frac{\partial^2\zeta'}{\partial t'^2}+\lambda_g\frac{\partial\zeta'}{\partial t'}+\zeta'=-\frac{1}{\pi}\iint_{S_B}\frac{\partial\Phi}{\partial t'}\,\mathrm{d}S' \tag{3.2.20}$$

which can be combined with the kinematic condition (3.2.17) to give,

$$\left(\mu H'\frac{\partial^2}{\partial t'^2}+\lambda_g\frac{\partial}{\partial t'}+1\right)\frac{\partial\Phi}{\partial z'}=-\frac{\mu}{\pi}\iint_{S_B}\frac{\partial^2\Phi}{\partial t'^2}\,\mathrm{d}S' \tag{3.2.21}$$

3.3 Multiple-scale Approximation

We now invoke the assumption of small buoys. Since the problem has two contrasting length scales, a' and $h'=\mu^{-1}$, we seek an asymptotic approximation by the method of multiple scales. With the small parameter $\mu=a^*/h^*$, we define the slow (macro-scale) coordinates without primes

$$x_i=\mu x_i', \quad i=1,2,3. \tag{3.3.1}$$

We next introduce the expansions

$$\Phi=\mathrm{e}^{-\mathrm{i}\omega t'}\left[\phi_0(x_i',x_i;t')+\mu\phi_1(x_i',x_i;t')+\mu^2\phi_2\,(x_i',x_i;t')+\ldots\right] \tag{3.3.2}$$

where ω is the dimensionless frequency normalized according to

$$\omega=\omega^*\sqrt{\frac{h^*}{g^*}} \tag{3.3.3}$$

For later use we expand

$$\frac{1}{1-\mathrm{i}\lambda\omega-\mu H'\omega^2}=\sum_{j=0}\mu^j\mathcal{F}_j(\omega) \tag{3.3.4}$$

where

$$\mathcal{F}_0(\omega)=\frac{1}{1-\mathrm{i}\lambda\omega},\quad \mathcal{F}_1(\omega)=-\frac{H'\omega^2}{1-\mathrm{i}\lambda\omega^2},\quad \text{etc.} \tag{3.3.5}$$

Referring to the dimensionless governing equations in §3.1, we get from Laplace's equation,

$$\left(\Delta'+2\mu\boldsymbol{\nabla}.'\boldsymbol{\nabla}+\mu^2\Delta\right)(\phi_0+\mu\phi_1+...)=0,\quad \boldsymbol{x}'\in\Omega_f \tag{3.3.6}$$

The combined free surface condition becomes

$$\left(\frac{\partial}{\partial z'}+\mu\frac{\partial}{\partial z}-\mu\omega^2\right)(\phi_0+\mu\phi_1+...)=0,\quad \boldsymbol{x}'\in S_F \tag{3.3.7}$$

while the kinematic condition is

$$\left(\frac{\partial}{\partial z'}+\mu\frac{\partial}{\partial z}+\cdots\right)(\phi_0+\mu\phi_1+\mu^2\phi_2+\cdots)=-\mathrm{i}\mu\omega(\eta_0'+\mu\eta_1'+\cdots),\quad \boldsymbol{x}'\in S_F \tag{3.3.8}$$

On the side wall of the buoy we have

$$\left(\frac{\partial}{\partial r'}+\mu\frac{\partial}{\partial r}\right)(\phi_0+\mu\phi_1+...)=0,\quad \boldsymbol{x}'\in S_W \tag{3.3.9}$$

and on the sea bed

$$\left(\frac{\partial}{\partial z'}+\mu\frac{\partial}{\partial z}\right)(\phi_0+\mu\phi_1+...)=0,\quad z'=-\frac{1}{\mu}\sim-\infty \tag{3.3.10}$$

At the bottom of the buoy, the kinematic condition (3.2.17) gives

$$\left(\frac{\partial}{\partial z'}+\mu\frac{\partial}{\partial z}\right)(\phi_0+\mu\phi_1+\phi_2+\cdots)=-\mathrm{i}\mu\omega(\zeta_0'+\mu\zeta_1'+\cdots),\quad z'=-H' \tag{3.3.11}$$

and the dynamic condition

$$\left(-\mu\omega^2 H - \mathrm{i}\lambda\omega + 1\right)\left(\zeta_0' + \mu\zeta_1' + \mu^2\zeta_2' + \cdots\right) = \frac{\mathrm{i}\omega}{\pi}\iint_{S_B}\left(\phi_0 + \mu\phi_1 + \mu^2\phi_2 + \cdots\right)\mathrm{d}S' \quad (3.3.12)$$

Finally from the combined buoy condition,

$$\left(-\mu\omega^2 H' - \mathrm{i}\lambda\omega + 1\right)\left[\frac{\partial\phi_0}{\partial z'} + \mu\left(\frac{\partial\phi_0}{\partial z} + \frac{\partial\phi_1}{\partial z'}\right) + \mu^2\left(\frac{\partial\phi_1}{\partial z} + \frac{\partial\phi_2}{\partial z'}\right) + \cdots\right] - \mu\frac{\omega^2}{\pi}\iint_{S_B}\left(\phi_0 + \mu\phi_1 + \mu^2\phi_2 + \cdots\right)\mathrm{d}S' = 0 \quad (3.3.13)$$

Separating the orders we obtain the perturbation boundary value problems at the orders $O(1), O(\mu)$ and $O(\mu^2)$. For later use we expand

$$\frac{1}{1 - \mathrm{i}\lambda\omega - \mu H'\omega^2} = \sum_{j=0}\mu^j\mathcal{F}_j(\omega) \quad (3.3.14)$$

where

$$\mathcal{F}_0(\omega) = \frac{1}{1 - \mathrm{i}\lambda\omega}, \quad \mathcal{F}_1(\omega) = -\frac{H'\omega^2}{1 - \mathrm{i}\lambda\omega^2}, \quad \text{etc.} \quad (3.3.15)$$

3.3.1 Leading order $O(1)$

The governing conditions on the short scale are homogeneous

$$\Delta'\phi_0 = 0, \qquad \boldsymbol{x}' \in \Omega \quad (3.3.16a)$$

$$\frac{\partial\phi_0}{\partial n'} = 0, \qquad \boldsymbol{x}' \in S \quad (3.3.16b)$$

with $S \equiv S_F \cup S_W \cup S_B \cup (z' = -\mu^{-1})$. Let us define an unit cell of the array as shown in figure 3-1, and impose further the condition of periodicity on the cell boundaries:

$$\phi_0(x', y', z', \boldsymbol{x}; t) = \phi_0(x' + d', y', z', \boldsymbol{x}; t), \quad (3.3.17a)$$

$$\phi_0(x', y', z', \boldsymbol{x}; t) = \phi_0(x', y' + d', z', \boldsymbol{x}; t) \quad (3.3.17b)$$

with

$$d' \equiv d^*/a^* \tag{3.3.18}$$

being the center-to-center distance between adjacent buoys.

The leading-order solution is clearly independent of the micro-scale,

$$\phi_0 = \phi_0(\boldsymbol{x}; t) \tag{3.3.19}$$

where the dependence on the macro-scale is yet to be found. It follows from (3.3.12) that

$$\zeta_0' = \mathrm{i}\omega \mathcal{F}_0(\omega)\ \phi_0|_0\,, \quad \boldsymbol{x}' \in S_B. \tag{3.3.20}$$

3.3.2 First Order ($O(\mu)$)

Using (3.3.19), we get from (3.3.6) that

$$\Delta' \phi_1 = 0, \quad \boldsymbol{x}' \in \Omega_f \tag{3.3.21a}$$

and from (3.3.7) that

$$\frac{\partial \phi_1}{\partial z'} = -\left(\frac{\partial \phi_0}{\partial z} - \omega^2 \phi_0\right), \quad \boldsymbol{x}' \in S_F \tag{3.3.21b}$$

Equation (3.3.13) becomes

$$\frac{\partial \phi_1}{\partial z'} = -\left(\frac{\partial \phi_0}{\partial z} - \omega^2 \mathcal{F}_0 \phi_0\right), \quad \boldsymbol{x} \in S_B \tag{3.3.21c}$$

We also have on the side wall of the buoy,

$$\frac{\partial \phi_1}{\partial r'} = -\frac{\partial \phi_0}{\partial r} = -n_i \frac{\partial \phi_0}{\partial x_i}, \quad \boldsymbol{x}' \in S_W \tag{3.3.21d}$$

where $\boldsymbol{n} = (n_1, n_2) = (\cos\theta, \sin\theta)$ denotes the unit vector normal to the side wall, and

$$\frac{\partial \phi_1}{\partial z'} = -\frac{\partial \phi_0}{\partial z}, \quad z' = -\frac{1}{\mu} \ll -1 \tag{3.3.21e}$$

on the seabed. In addition we impose the periodicity condition on the cell boundaries. Once ϕ_1 is found, ζ_1 follows from (3.3.12). As it is usual in homogenization analysis, the macro-scale physics at the leading order is found by requiring the solvability of the inhomogeneous micro-scale problem at a higher order. The micro-scale cell problem for ϕ_1 is inhomogeneous. By applying Gauss' theorem (or, equivalently applying Green's formula to ϕ_0 and ϕ_1 over a unit cell) ϕ_1 over the cell volume, we get

$$\iint_{\partial\Omega} \frac{\partial \phi_1}{\partial n'} \, \mathrm{d}S' = 0 \tag{3.3.22}$$

where $\partial\Omega$ is the boundary of the cell. This is just the condition of solvability for the inhomogeneous problem of ϕ_1. Since

$$\iint_{S_W} \frac{\partial \phi_1}{\partial r'} \, \mathrm{d}S' = -\mu \iint_{S_W} \frac{\partial \phi_0}{\partial r} \, \mathrm{d}S' = -\mu \boldsymbol{\nabla}\phi_0 \cdot \iint_{S_W} \boldsymbol{e}_r \, \mathrm{d}S' = 0 \tag{3.3.23}$$

we must have

$$\iint_{S_B} \frac{\partial \phi_1}{\partial z'} \, \mathrm{d}S' = - \iint_{S_f} \frac{\partial \phi_1}{\partial z'} \, \mathrm{d}S'$$

which gives at the leading order:

$$(1-f)\left(\frac{\partial \phi_0}{\partial z} - \omega^2 \phi_0\right) + f\left(\frac{\partial \phi_0}{\partial z} - \omega^2 \mathcal{F}_0 \phi_0\right) = 0, \quad z = 0 \tag{3.3.24}$$

where for circular buoys

$$f \equiv \frac{\pi a^{*2}}{d^{*2}} = \frac{\pi}{d'^2}, \quad \text{with} \quad 0 < f < \frac{\pi}{4} \tag{3.3.25}$$

is the area fraction of solid, or the *packing ratio*. Hence we have

$$\left(\frac{\partial \phi_0}{\partial z} - \omega^2 \left[1 + f(\mathcal{F}_0 - 1)\right] \phi_0\right)\Big|_{z=0} = 0 \tag{3.3.26}$$

which is a macro-scale boundary condition at $z = 0$. In the open water with no buoy,

$f = 0$, so (3.3.26) reduces to the familiar condition on the free surface:

$$\frac{\partial \phi_0}{\partial z} - \omega^2 \phi_0 = 0, \quad \boldsymbol{x}' \in S_F \tag{3.3.27}$$

Because of (3.3.26), (3.3.21b) and (3.3.21c) can be rewritten as

$$\frac{\partial \phi_1}{\partial z'} = -\frac{\partial \phi_0}{\partial z}\left(1 - \frac{1}{1 - f(\mathcal{F}_0 - 1)}\right) \equiv -\beta \frac{\partial \phi_0}{\partial z}, \quad \boldsymbol{x} \in S_F \tag{3.3.28}$$

and

$$\frac{\partial \phi_1}{\partial z'} = -\frac{\partial \phi_0}{\partial z}\left(1 - \frac{\mathcal{F}_0}{1 + f(\mathcal{F}_0 - 1)}\right) \equiv -\beta' \frac{\partial \phi_0}{\partial z}, \quad \boldsymbol{x} \in S_B \tag{3.3.29}$$

In view of the forms of the boundary conditions, the solution of the micro-scale problem for ϕ_1 in a unit cell can be sought in the form

$$\phi_1(\boldsymbol{x}', \boldsymbol{x}) = -\sum_{j=1}^{3} S_j(\boldsymbol{x}') \frac{\partial \phi_0}{\partial x_j} \tag{3.3.30}$$

Then the horizontal components S_j, $j = 1, 2$ are governed by the following boundary value problems in the unit cell,

$$\Delta' S_j = 0, \qquad \boldsymbol{x}' \in \Omega_f \tag{3.3.31a}$$

$$\frac{\partial S_j}{\partial z'} = 0, \qquad \boldsymbol{x}' \in S_F, \ \ S_B \text{ and } z' \to -\infty; \tag{3.3.31b}$$

$$\frac{\partial S_j}{\partial r'} = n_j, \qquad \boldsymbol{x}' \in S_W \tag{3.3.31c}$$

The vertical component S_3 is governed by

$$\Delta' S_3 = 0, \qquad \boldsymbol{x}' \in \Omega_f \tag{3.3.32a}$$

$$\frac{\partial S_3}{\partial z'} = \beta, \qquad \boldsymbol{x}' \in S_F \tag{3.3.32b}$$

$$\frac{\partial S_3}{\partial z'} = 0, \qquad z' \sim -\infty \tag{3.3.32c}$$

$$\frac{\partial S_3}{\partial z'} = \beta', \qquad \boldsymbol{x}' \in S_B \tag{3.3.32d}$$

$$\frac{\partial S_3}{\partial r'} = 0, \qquad \boldsymbol{x}' \in S_W \tag{3.3.32e}$$

The solutions are made unique by adding the constraint

$$\iiint_{\Omega_f} S_j(x)\, \mathrm{d}V' = 0, \quad j = 1, 2 \tag{3.3.33}$$

and $S_3 = 0$ at a point $\boldsymbol{x} = \boldsymbol{x}_b$ on the seabed. These elliptic cell problems with Neumann boundary conditions can be solved numerically. Being periodic in (x', y'), the harmonic functions $S_j(\boldsymbol{x}')$ are expected to diminish exponentially in z'. For confirmation we have performed a numerical simulation using Finite Elements. The results, given in figure C-4, Appendix C.3, show indeed that the solutions S_i are localized near the buoy. In view of (3.3.30), a consequence is that,

$$\frac{\partial \phi_1}{\partial z'} \to 0 \quad \text{as } z' \sim -\infty \tag{3.3.34}$$

which in turn implies

$$\frac{\partial \phi_0}{\partial z} = 0, \quad z = -1 \tag{3.3.35}$$

because of (3.3.21e).

3.3.3 Second Order and the Macro-scale problem

At the second order the micro-scale problem for ϕ_2 is again inhomogeneous,

$$\Delta'\phi_2 = -2\boldsymbol{\nabla}.'\boldsymbol{\nabla}\phi_1 - \Delta\phi_0, \qquad \boldsymbol{x}' \in \Omega_f \tag{3.3.36a}$$

$$\frac{\partial\phi_2}{\partial z'} = -\left(\frac{\partial\phi_1}{\partial z} + \omega^2\phi_1\right), \qquad \boldsymbol{x}' \in S_F \tag{3.3.36b}$$

$$\frac{\partial\phi_2}{\partial z'} = -\left(\frac{\partial\phi_1}{\partial z} - \omega^2\mathcal{F}_0\phi_1 - \omega^2\mathcal{F}_1\phi_0\right), \qquad \boldsymbol{x}' \in S_B \tag{3.3.36c}$$

$$\frac{\partial\phi_2}{\partial z'} = -\frac{\partial\phi_1}{\partial z}, \qquad z' \sim -\infty \tag{3.3.36d}$$

$$\frac{\partial\phi_2}{\partial r'} = -\frac{\partial\phi_1}{\partial r}, \qquad \boldsymbol{x}' \in S_W \tag{3.3.36e}$$

As $S_i \to 0$ for $z' \to -\infty$, (3.3.36d) reduces to :

$$\frac{\partial\phi_2}{\partial z'} \to 0, \qquad z' \sim -\infty \tag{3.3.37}$$

We can apply Green's formula for ϕ_0 and ϕ_2 in the unit cell and invoke their governing conditions on the micro-scale to get

$$\begin{aligned}\iiint_{\Omega_f} (\Delta\phi_0 + 2\boldsymbol{\nabla}.'\boldsymbol{\nabla}\phi_1)\,\mathrm{d}V' = \iint_{S_f}\left(\frac{\partial\phi_1}{\partial z} - \omega^2\phi_1\right)\mathrm{d}S' \\ + \iint_{S_B}\left(\frac{\partial\phi_1}{\partial z} - \omega^2\mathcal{F}_0\phi_1 - \omega^2\mathcal{F}_1\phi_0\right)\mathrm{d}S' - \iint_{S_W}\frac{\partial\phi_1}{\partial r}\,\mathrm{d}S'\end{aligned} \tag{3.3.38}$$

Using the fact ϕ_1 vanishes with S_i outside the vertical distance of $O(1)$ from $z = 0$, and that the cell volume $|\Omega_f| = O(1/\mu)$ is much greater than unity, we conclude that:

$$\iiint_{\Omega_f} \Delta\phi_0\,\mathrm{d}V' = 0$$

but we can not take the term $\Delta\phi_0$ out of the integral as it is usually done in homogenization, as the variations of this term over the depth are significant. We can however conclude that

$$\Delta\phi_0 = 0, \qquad -1 < z < 0 \tag{3.3.39}$$

by remarking that we can replace Ω_f in (3.3.38) by

$$\Omega_{\mathcal{H}'} = \begin{cases} \Omega_f \cap \{-\mu^{-1} \leq z' \leq -\mathcal{H}'\} & \text{for } 1 \ll \mathcal{H}' \leq \mu^{-1}/2 \\ \Omega_f \cap \{-\mathcal{H}' \leq z' \leq 0\} & \text{for } \mathcal{H}' \geq \mu^{-1}/2 \end{cases}$$

and conclude that $\forall \mathcal{H}'$

$$\iiint_{\Omega_{\mathcal{H}'}} \Delta\phi_0 \, \mathrm{d}V' = 0$$

We can finally take the derivative with respect to $\mathcal{H}'$, and make use of the fact that $\Delta\phi_0$ is constant on and horizontal cross section of the cell to conclude that ϕ_0 must satisfy Laplace's equation on the long scale.

In summary, in the region with buoys, the macro-scale variation of $\phi_0(\boldsymbol{x})$ is governed by (3.3.39) in the fluid region, subject to the boundary condition (3.3.26) on $z = 0$, and (3.3.35) on the seabed. In the open water without buoys, condition (3.3.26) must be replaced by (3.3.27), while (3.3.39) and (3.3.35) still apply. Note that due to the small draft H of buoys, buoyancy and resonance are unimportant.

We shall next apply these equations to examine wave power extraction from one- and two-dimensional arrays in response to a plane incident wave train arriving from $x \sim -\infty$.

Finally we remark that the present theory can be extended in principle to periodic buoys of any shape.

3.4 Vertical eigenfunctions

As it is well known, the general solution in the open water region where $f = 0$ can be expressed as a series of the form

$$\phi_0(\boldsymbol{x}) = \sum_{n=0} \psi_n(x, y) f_n(z), \quad n = 0, 1, 2, 3, \ldots \tag{3.4.1}$$

where

$$f_0 = c_0 \cosh\left(k_0(z+1)\right), \quad f_n = c_n \cos\left(\kappa_n(z+1)\right) \tag{3.4.2}$$

are real orthogonal eigenfunctions in $-1 < z < 0$, and $(k_0, k_1, k_2 \dots)$ are the eigenvalues of the dispersion relation,

$$\omega^2 = k_n \tanh(k_n), \quad n = 0, 1, 2, \dots \tag{3.4.3}$$

In particular k_0 is the positive real root and $k_n \equiv \mathrm{i}\kappa_n$ is the n-th imaginary root i.e.,

$$\omega^2 = k_0 \tanh(k_0), \quad \omega^2 = -\kappa_n \tan(\kappa_n), \quad n = 1, 2, 3, \dots \tag{3.4.4}$$

With the choice of

$$c_0 = \sqrt{\frac{2}{1 + \omega^{-2} \sinh^2 k_0}}, \qquad c_n = \sqrt{\frac{2}{1 - \omega^{-2} \sin^2(\kappa_n)}} \tag{3.4.5}$$

the vertical eigenfunctions are orthonormal,

$$\langle f_n | f_m \rangle \equiv \int_{-1}^{0} f_n(z) f_m(z) \, \mathrm{d}z = \delta_{nm} \tag{3.4.6}$$

Note that these functions are the same as in Chapter 2. Furthermore the horizontal factors ψ_n must satisfy Helmholtz equations in the horizontal plane

$$\left(\frac{\partial^2}{\partial x^2} + \frac{\partial^2}{\partial y^2} + k_0^2 \right) \psi_0 = 0, \quad \left(\frac{\partial^2}{\partial x^2} + \frac{\partial^2}{\partial y^2} - \kappa_n^2 \right) \psi_n = 0, \quad n = 1, 2, 3, \dots \tag{3.4.7}$$

In the region of wave absorbing buoys we also assume

$$\phi_0(\boldsymbol{x}) = \sum_{n=0} \Psi_n(x, y) F_n(z) \tag{3.4.8}$$

It can be shown that the eigenfunctions $\{F_n\}$, $n = 0, 1, 2, 3, \dots$ are the solutions of the boundary value problem

$$\begin{aligned} F_n''(z) - K_n^2 F_n(z) &= 0 \qquad -1 < z < 0 \\ \left(F_n' - \sigma^2 F_n \right) &= 0 \qquad z = 0 \\ F_n' &= 0, \qquad z = -1, \end{aligned} \tag{3.4.9}$$

with

$$\sigma^2 \equiv \omega^2[f\mathcal{F}_0(\omega) + (1-f)] \tag{3.4.10}$$

Note that σ is complex due to energy extraction. Therefore the eigenfunctions F_n are complex

$$F_n = C_n \cosh K_n(z+1) \tag{3.4.11}$$

The eigenvalue K_n is the $n-$th complex root of the relation

$$\sigma^2 = K_n \tanh K_n \tag{3.4.12}$$

It is straightforward to show that the set $\{F_n\}$ is orthogonal. By choosing the coefficients $\{C_n\}$ to be

$$C_n = \sqrt{\frac{2}{\sigma^{-2}\sinh^2(K_n)+1}} \tag{3.4.13}$$

the eigenfunctions $\{F_n\}$ are also orthonormal,

$$\langle F_n|F_m\rangle \equiv \int_{-1}^{0} F_n(z)F_m(z)dz = \delta_{nm} \tag{3.4.14}$$

Since K_n is complex, the square root above is defined such that if the complex radical is $z = re^{i\theta}$, its phase is limited to the range $-\pi < \theta \leq \pi$.

For a given frequency ω, packing ratio f and damping rate λ_g, σ is first defined. K_n and F_n are then found numerically. Before employing an usual algorithm to solve the complex transcendental equation, a good initial guess of the solution is needed. The numerical procedure we employed for this purpose is described in Appendix B.1. Sample F_n's are shown in figure 3-2, and sample eigenvalues are given in Table 3.1.

Note that for $f = 0$, k is purely real and $k_n = i\kappa_n, n = 1,2,3...$ are purely imaginary. For $f \ll 1$, K_0 is almost real and $K_n, n = 1,2,3,...$ are almost imaginary. Perturbation solutions of (3.4.12) have been used to confirm the values in Table 3.1 where $f = 0.2$.

We now apply these results to examine two simple arrays.

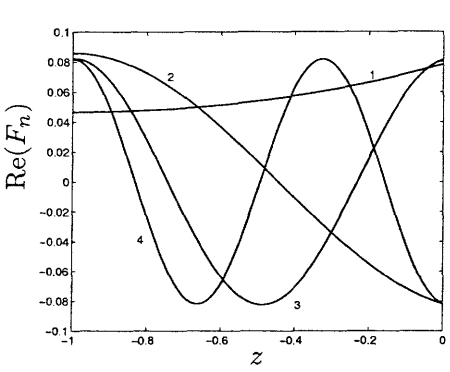

(a) Real part of eigenfunction. The value of n is indicated next to the curves. ($\omega = 1$)

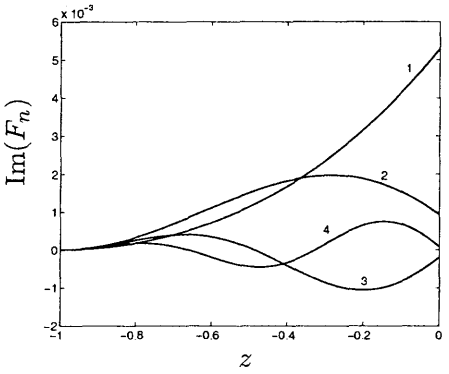

(b) Imaginary part of eigenfunction. The value of n is indicated next to the curves and ($\omega = 1$).

Figure 3-2: First solutions of the eigenvalue problem (3.4.9). $\lambda_g = 1$ and $f = 0.2$

K_n	$\omega = 0.5$	$\omega = 1$	$\omega = 2$
K_1	0.5107 + 0.0230i	1.1165 + 0.0835i	3.3669 + 0.3159i
K_2	0.0067 + 3.0634i	0.0357 + 2.8342i	0.0545 + 2.1332i
K_3	0.0032 + 6.2448i	0.0163 + 6.1376i	0.0449 + 5.7538i
K_4	0.0021 + 9.3992i	0.0107 + 9.3286i	0.0322 + 9.0697i
K_5	0.0016 +12.5472i	0.0080 +12.4945i	0.0247 +12.2996i
K_6	0.0013 +15.6927i	0.0064 +15.6505i	0.0200 +15.4944i
K_7	0.0011 +18.8368i	0.0053 +18.8017i	0.0168 +18.6715i
K_8	0.0009 +21.9802i	0.0046 +21.9502i	0.0144 +21.8385i
K_9	0.0008 +25.1232i	0.0040 +25.0969i	0.0126 +24.9991i
K_{10}	0.0007 +28.2658i	0.0035 +28.2425i	0.0113 +28.1555i

Table 3.1: First ten eigenvalues for (3.4.9) for $\lambda_g = 1$ and $f = 0.2$.

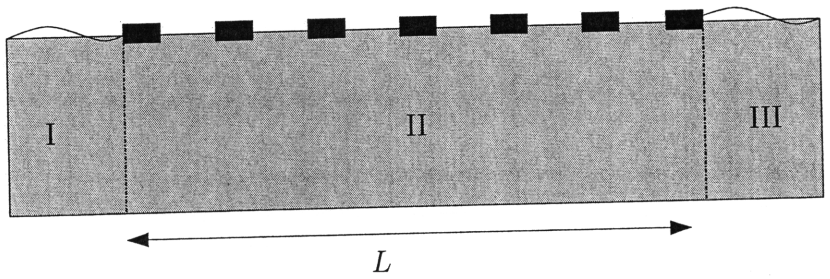

Figure 3-3: Cross section of an infinitely long array.

3.5 A long array of energy-absorbing buoys

Referring to figure 3-3, let us first consider a long array of width L with its edges parallel to the crests of incoming plane waves. Assuming an incoming wave of unit amplitude, the velocity potential in the open water on the incidence side (zone I) is

$$\phi_I(x,z) = \frac{1}{\mathrm{i}\omega f_0(0)} \left(\mathrm{e}^{\mathrm{i}k_0 x} f_0(z) + \sum_{n=0}^{\infty} R_n \mathrm{e}^{-\mathrm{i}k_n x} f_n(z) \right), \quad -\infty < x < 0 \qquad (3.5.1)$$

where k_0 is real and $k_n = \mathrm{i}\kappa_n, n = 1, 2, 3, \ldots$ are imaginary roots of the dispersion relation. In zone II of the buoys, the potential is

$$\phi_{II}(x,z) = \frac{1}{\mathrm{i}\omega f_0(0)} \sum_{n=0}^{\infty} \left(B_n \mathrm{e}^{\mathrm{i}K_n x} + B'_n \mathrm{e}^{-\mathrm{i}K_n x} \right) F_n(z), \quad 0 < x < L \qquad (3.5.2)$$

and in the open water on the transmission side (zone III) we have

$$\phi_{III}(x,z) = \frac{1}{\mathrm{i}\omega f_0(0)} \sum_{n=0}^{\infty} T_n \mathrm{e}^{\mathrm{i}k_n x} f_n(z), \quad L < x < \infty \qquad (3.5.3)$$

The eigenvalues (k_n, K_n) and eigenfunctions (f_n, F_n) have been defined in §3.4. Let us introduce

$$U(z) = \frac{\partial \phi_0}{\partial x}(0,z), \qquad U'(z) = \frac{\partial \phi_0}{\partial x}(L,z) \qquad (3.5.4)$$

as the horizontal velocities at $x = 0$ and $x = L$ respectively. Requiring flux continuity and using the orthogonality of eigenfunctions, we find

$$R_0 = 1 - \frac{\langle U|f_0\rangle}{\mathrm{i}k_0} \qquad R_n = -\frac{\langle U|f_n\rangle}{\mathrm{i}k_n} \tag{3.5.5a}$$

$$B_n = -\frac{\langle (U' - \mathrm{e}^{-\mathrm{i}K_nL}U)|F_n\rangle}{2K_n \sin(K_nL)} \qquad B'_n = -\frac{\langle (U' - \mathrm{e}^{\mathrm{i}K_nL}U)|F_n\rangle}{2K_n \sin(K_nL)} \tag{3.5.5b}$$

$$T_n = \frac{\langle U'|f_n\rangle}{\mathrm{i}k_n \mathrm{e}^{\mathrm{i}k_nL}} \tag{3.5.5c}$$

We further require continuity of pressure (i.e., of potentials) at $x = 0$

$$\begin{aligned} f_0(z) + \left(1 - \frac{\langle U|f_0\rangle}{\mathrm{i}k_0}\right) f_0(z) - \sum_{n\geq 1} \frac{\langle U|f_n\rangle}{\mathrm{i}k_n} f_n(z) \\ = -\sum_{n\geq 0} \frac{\langle (U' - \cos(K_nL)U)|F_n\rangle}{K_n \sin(K_nL)} F_n(z) \end{aligned} \tag{3.5.6}$$

and at $x = L$

$$-\sum_{n\geq 0} \frac{\langle (U'\cos(K_nL) - U)|F_n\rangle}{K_n \sin(K_nL)} F_n(z) = \sum_{n\geq 0} \frac{\langle U'|f_n\rangle}{\mathrm{i}k_n} f_n(z) \tag{3.5.7}$$

These are a pair of integral equations for $U(z)$ and $U'(z)$ in $-1 < z < 0$. Let their solutions be the following orthonormal expansions

$$U = \sum_m U_m F_m, \quad U' = \sum_m U'_m F_m, \quad -1 < z < 0 \tag{3.5.8}$$

with unknown coefficients, and let

$$f_n = \sum_m M_{nm} F_m \quad \text{where} \quad \langle f_n|F_m\rangle = M_{nm} \tag{3.5.9}$$

where the matrix elements M_{nm} can be obtained explicitly,

$$M_{nm} = \omega^2 f(1 - \mathcal{F}) \frac{c_n \cosh(k_n) C_m \cosh(K_m)}{(k_n^2 - K_m^2)} \tag{3.5.10}$$

Equations (3.5.6) and (3.5.7) become

$$2f_0(z)\sum_{n,q} M_{nq}U_q\frac{1}{\mathrm{i}k_n}f_n(z) = \sum_n \left(-\frac{U_n'}{K_n\sin(K_nL)} + \frac{U_n}{K_n\tan(K_nL)}\right)F_n(z) \quad (3.5.11)$$

$$\sum_{n,q} M_{nq}U_q'\frac{1}{\mathrm{i}k_n}f_n(z) = \sum_n \left(-\frac{U_n'}{K_n\tan(K_nL)} + \frac{U_n}{K_n\sin(K_nL)}\right)F_n(z) \quad (3.5.12)$$

By taking the scalar product with F_p for $p = 0, 1, 2, 3, ...$ in turn we obtain from (3.5.11) and (3.5.12)

$$\begin{aligned} 2M_{0p} - \sum_{n,q} M_{nq}U_q\frac{1}{\mathrm{i}k_n}M_{np} &= \left(-\frac{1}{K_p\sin(K_pL)}U_n' + \frac{1}{K_p\tan(K_pL)}U_p\right) \\ \sum_{n,q} M_{nq}U_q'\frac{1}{\mathrm{i}k_n}M_{np} &= \left(-\frac{1}{K_p\tan(K_pL)}U_p' + \frac{1}{K_p\sin(K_pL)}U_p\right) \end{aligned} \quad (3.5.13)$$

The expansion coefficients U_n, U_q' are solved numerically after truncation. Details of the convergence are given in Appendix B.2.1. Afterwards we get the buoy displacement ζ_0 from the expression of ϕ_{II}. The transmission and reflection coefficients follow from (3.5.5c) and (3.5.5a) :

$$T \equiv T_0 = \frac{M_{0q}U_q'}{\mathrm{i}k_0\mathrm{e}^{\mathrm{i}k_0L}} \quad (3.5.14)$$

and

$$R \equiv R_0 = 1 - \frac{\langle U|f_0\rangle}{\mathrm{i}k_0} \quad (3.5.15)$$

The dimensionless power-extraction efficiency is

$$\mathcal{E} = 1 - |T|^2 - |R|^2. \quad (3.5.16)$$

Figure 3-4 and figure 3-5 show the amplitude of the free surface elevation and the buoy displacement in and outside of arrays of length $L = 1$ and $L = 5$. Note first that there is no resonance. There is a slight phase difference between the movements of the free surface and the buoys, in agreement with (3.3.12).

For a fixed array width L, the reflection coefficient R increases with the extraction rate λ_g, as shown in figure 3-6. Both the transmission coefficient T and the extraction

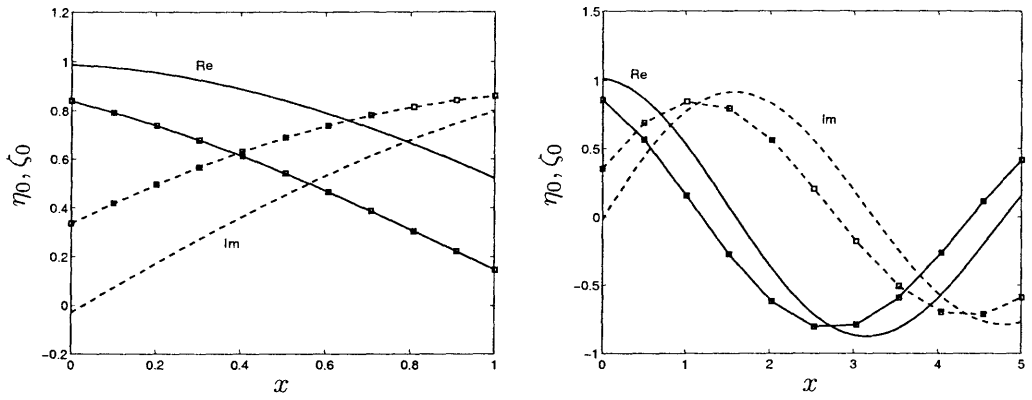

(a) $L = 1$ (b) $L = 5$

Figure 3-4: Real and imaginary parts of amplitude of the free surface elevation η_0 and buoy displacement ζ_0 (squares) for different array length $L = 1, 5$, and for the same $f = 0.2$, $\lambda_g = 0.5$ and $k_0 = 1$. The buoys are in $0 < x < L$.

efficiency $\mathcal{E}$ are the largest for some intermediate extraction rate around $\lambda_g = 0.5$ as shown in figure 3-8(a). The precise optimal value is around 0.5 and can be determined numerically.

For a fixed extraction rate, the effects of array width L on the transmission and reflection coefficients are shown in figure 3-7(b). The corresponding extraction efficiency is shown in figure 3-8(b). The oscillatory variation of the reflection coefficient shown in figures 3-6(b) and 3-7(b) is due to interference, similar to the case of a finite shelf (See Mei, Stiassnie, and Yue (2005), p. 149). In the transmission coefficient, this oscillatory behavior is less prominent due to energy extraction. In the limit of extremely high damping rate, $\lambda_g \gg 1$, the buoys no longer move, interference effects are recovered, see figure 3-7(c).

While it is not surprising that a larger L gives a higher efficiency, as shown in figure 3-8(b), it is nevertheless interesting that the gain of energy extraction with a wider array is more significant at low frequency. In practical situations $k_0 = k_0^* h^*$ will likely be between 0 and 3. Our predictions can help the designer to choose the proper width by considering both efficiency and construction economy.

In general scattering is significant, hence the maximum efficiency of energy extraction is somewhat lower than that a large beam-sea device such as a Salter's duck (See Mynett et al. (1979)).

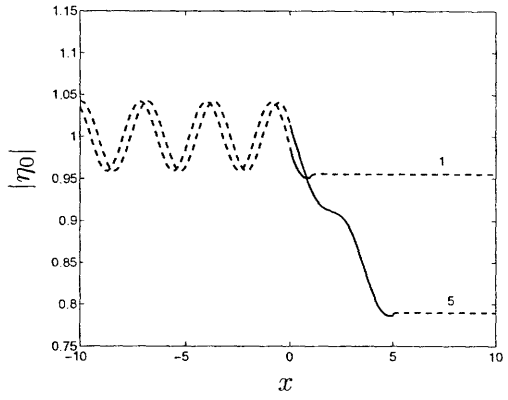

Figure 3-5: Amplitude of free surface near the array of two lengths $L = 1$ and 5, showing wave attenuation, for the same $f = 0.2$, $\lambda_g = 0.5$ and $k_0 = 1$. The buoys are in $0 < x < L$.

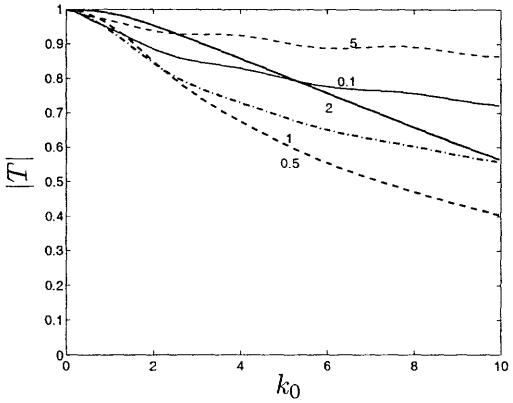

(a) Transmission coefficient for $L = 1$, and different λ_g.

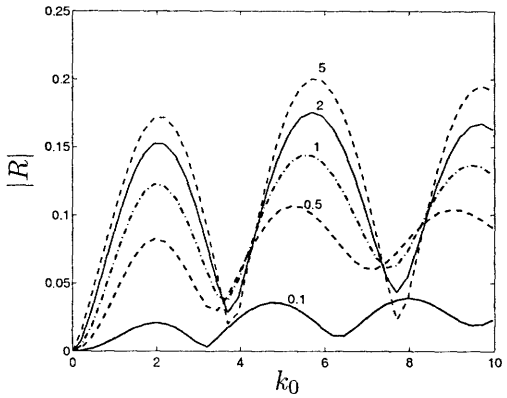

(b) Reflection coefficient for $L = 1$, and different λ_g.

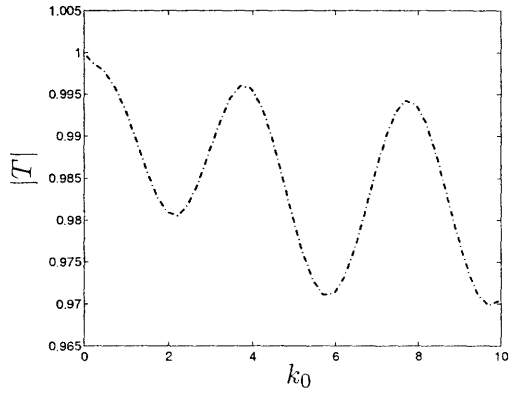

(c) Transmission coefficient of a nearly fixed buoy-array with $\lambda_g = 100$. .

Figure 3-6: Transmission and reflection coefficients for an array of buoys with various extraction rates λ_g, as indicated by numbers next to each curve. The packing ratio is $f = 0.2$.

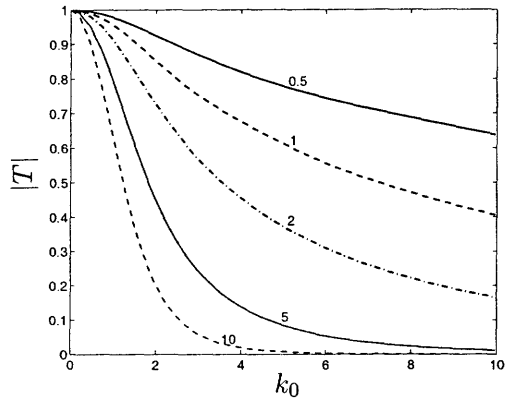

(a) Transmission coefficient for $\lambda_g = .5$, and different L.

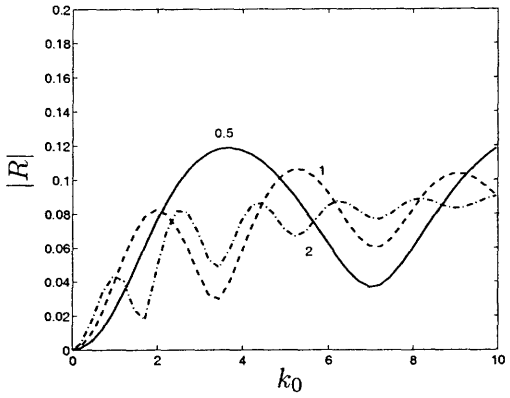

(b) Reflection coefficient for $\lambda_g = 0.5$, and different L.

Figure 3-7: Transmission and reflection coefficients for a buoy array with various array width L, as indicated next to each curve. The packing ratio is $f = 0.2$.

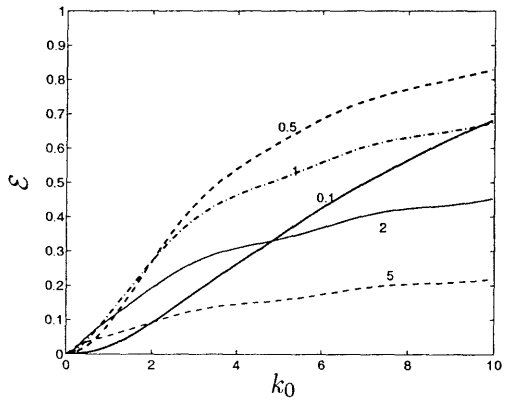

(a) Effects of extraction rate for $L = 1$.

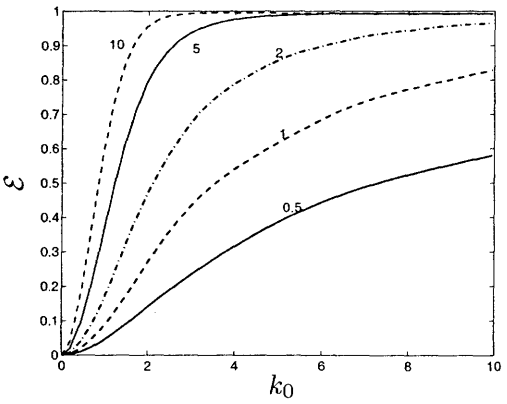

(b) Effects of total array width for $\lambda_g = 0.5$.

Figure 3-8: Extraction efficiency as influenced by λ_g for a given L (a) , or by L for a given λ_g (b). Values of the varying parameter are indicated by numbers next to each curve. The packing ratio is $f = 0.2$.

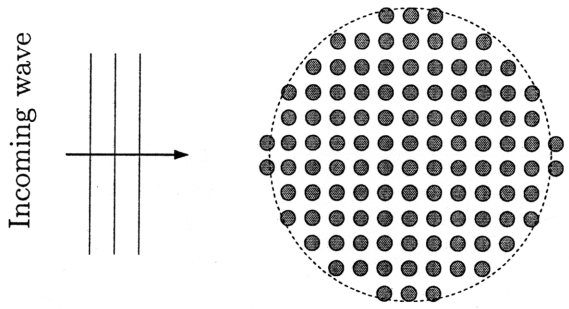

Figure 3-9: A circular array of energy-absorbing buoys.

3.6 A circular array

3.6.1 The solution

Now let many buoys be gathered inside a circular array of radius R. In order to solve this problem, let us follow the same approach as in Chapter 2. First, it is well known that the incident plane wave in the direction of x can be expanded as a sum of partial waves (see e.g. Abramowitz and Stegun, 1964)

$$\phi_i(\mathbf{x}) = \frac{1}{\mathrm{i}\omega f_0(0)} f_0(z) \mathrm{e}^{\mathrm{i}k_0 x} = \frac{1}{\mathrm{i}\omega f_0(0)} f_0(z) \sum_{m=0}^{\infty} \varepsilon_m \mathrm{i}^m J_m(k_0 r) \cos(m\theta)$$

where $\varepsilon_0 = 1$ and $\varepsilon_n = 2$ for $n = 1, 2, 3, \ldots$. Let us express the total solution as

$$\phi = \sum_m \phi_m(r, z) \cos(m\theta) \tag{3.6.1}$$

In the open water, the $m - th$ mode potential ϕ_m can be written as

$$\phi_m = \frac{1}{\mathrm{i}\omega f_0(0)} \left(\varepsilon_m \mathrm{i}^m J_m(k_0 r) f_0(z) + \sum_{n=0}^{\infty} a_{n,m} \psi_{n,m}(r) f_n(z) \right), \quad r > R \tag{3.6.2}$$

with

$$\psi_{n,m}(r) = \begin{cases} H_m^{(1)}(k_0 r) & \text{for } n = 0 \\ K_m(\kappa_n r) = H_m^{(1)}(\mathrm{i}\kappa_n r) & \text{for } n = 1, 2, \ldots \end{cases} \tag{3.6.3}$$

The first term in (3.6.2) corresponds to the incident wave and the series to the scattered/radiated waves. In the circular region of buoys, $0 < r < R$, we can expand the potential as:

$$\phi_m = \frac{1}{\mathrm{i}\omega f_0(0)} \sum_{n=0}^{\infty} b_{n,m} \Psi_{n,m}(r) F_n(z), \quad 0 < r < R, \tag{3.6.4}$$

with

$$\Psi_{n,m}(r) = J_m(K_n r)$$

where (f_n, k_n) and (F_n, K_n) are the same as before. Let us denote the common radial flux along $r = R$ by

$$U_m(\theta, z) = \frac{\partial \phi_m}{\partial r}, \quad r = R. \tag{3.6.5}$$

The expansion coefficients are found in terms of U_m by orthogonality:

$$a_{0,m} = \frac{\langle U_m | f_0 \rangle - \varepsilon_m \mathrm{i}^m k_0 J'_m(k_0 R)}{\psi'_{0,m}(R)} \tag{3.6.6}$$

$$a_{n,m} = \frac{\langle U_m | f_n \rangle}{\psi'_{n,m}(R)} \tag{3.6.7}$$

$$b_{n,m} = \frac{\langle U_m | F_n \rangle}{\Psi'_{n,m}(R)} \tag{3.6.8}$$

which assures the continuity of radial flux. Continuity of pressure (i.e., potential) at $r = R$ requires that

$$\varepsilon_m \mathrm{i}^m \left(J_m(k_0 R) - \frac{k_0 J'_m(k_0 R)}{\psi'_{0,m}(R)} \psi_{0,m}(R) \right) f_0(z) + \sum_{n=0}^{\infty} \frac{\langle U_m | f_n \rangle}{\psi'_{n,m}(R)} \psi_{n,m}(R) f_n(z)$$
$$= \sum_{n=0}^{\infty} \frac{\langle U_m | \phi_n \rangle}{\Psi'_{n,m}(R)} \Psi_{n,m}(R) F_n(z) \tag{3.6.9}$$

Introducing the expansions

$$f_i = \sum_j M_{ij} F_j, \quad U_m = \sum_j U_{j,m} F_j \tag{3.6.10}$$

We get

$$\left(J_m(k_0R) - \frac{k_0J'_m(k_0R)}{\psi'_{0,m}(R)}\psi_{0,m}(R)\right)\sum_j M_{0j}F_j(z) + \sum_{i,j,k}\frac{\psi_{k,m}(R)}{\psi'_{k,m}(R)}M_{ki}U_{i,m}M_{kj}F_j(z) = \sum_n \frac{\Psi_{n,m}(R)}{\Psi'_{n,m}(R)}U_{n,m}F_n(z) \quad (3.6.11)$$

for $m = 0, 1, 2, 3, \ldots$. By taking the scalar product with F_p, we finally obtain for any value of m

$$\sum_j \left[\left(\sum_k M_{kp}\frac{\psi_{k,m}(R)}{\psi'_{k,m}(R)}M_{kj}\right) - \frac{\Psi_{p,m}(R)}{\Psi'_{p,m}(R)}\delta_{p,j}\right]U_{j,m} = -\varepsilon_m \mathrm{i}^m\left(J_m(k_0R) - \frac{k_0J'_m(k_0R)}{\psi'_{0,m}(R)}\psi_{0m}(R)\right)M_{0p} \quad (3.6.12)$$

which is a matrix equation for the unknown vector $U_{j,m}$ for every m. Numerical computations can be carried out after truncation of the series, details are given in Appendix B.2.2. After solving for $U_{j,m}$, the velocity U_m hence ϕ_m are found. Combining (3.6.2) and (3.3.20), we get the displacement of the buoys

$$\zeta_0(r,\theta) = \mathcal{F}_0(\omega)\sum_{m=0}^{\infty}\sum_{n=0}^{\infty} b_{n,m}\Psi_{n,m}(r)\frac{F_n(0)}{f_0(0)}\cos(m\theta) \quad (3.6.13)$$

Figure 3-10 displays the computed free surface displacement around the array, and Figure 3-11 gives the computed buoys displacement. For the smaller array of radius 1 the amplitude of displacement is relatively uniform and less than 1. For a large array, with $R = 5$, the amplitude of buoy displacement can vary significantly and be slightly larger than the amplitude of the incoming wave.

3.6.2 Energy absorbtion

One can evaluate the extracted energy by calculating the total energy flux into a large circular cylindrical surface of radius $r \gg R$. In physical variables the power output

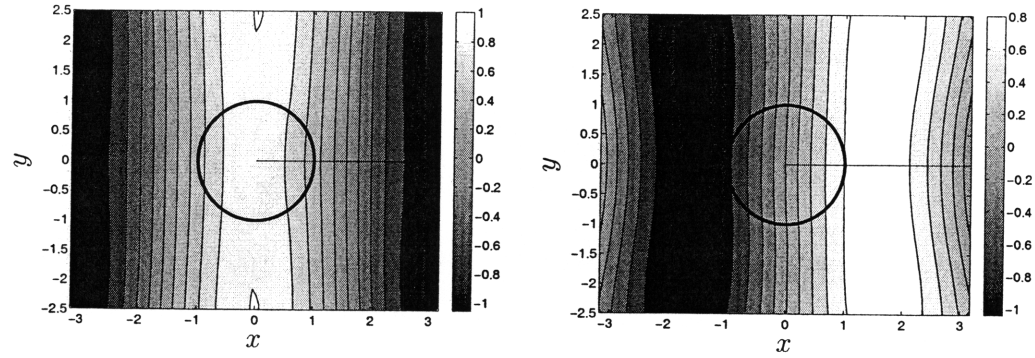

(a) $\mathrm{Re}(\eta_0)$ for $R = 1$

(b) $\mathrm{Im}(\eta_0)$ for $R = 1$

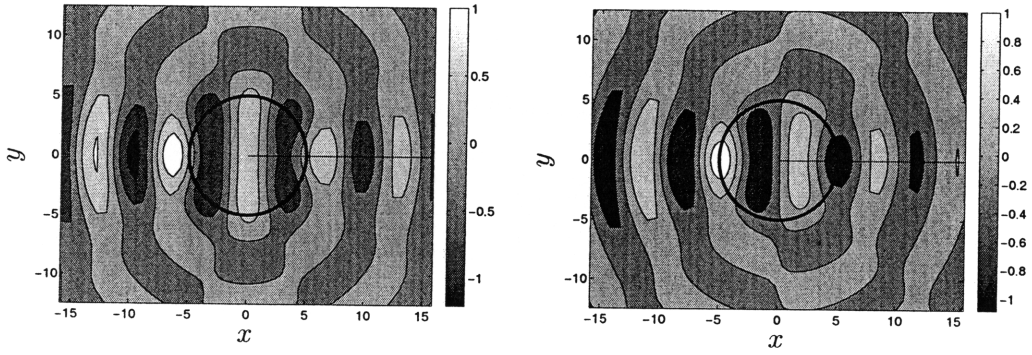

(c) $\mathrm{Re}(\eta_0)$ for $R = 5$

(d) $\mathrm{Im}(\eta_0)$ for $R = 5$

Figure 3-10: Free surface elevation in the neighbourhood of a circular array of buoys. The circumference of the array is represented by the bold circle. $\lambda_g = 0.5$, $f = 0.2$ and $k_0 = 1$. Waves are incident from the left.

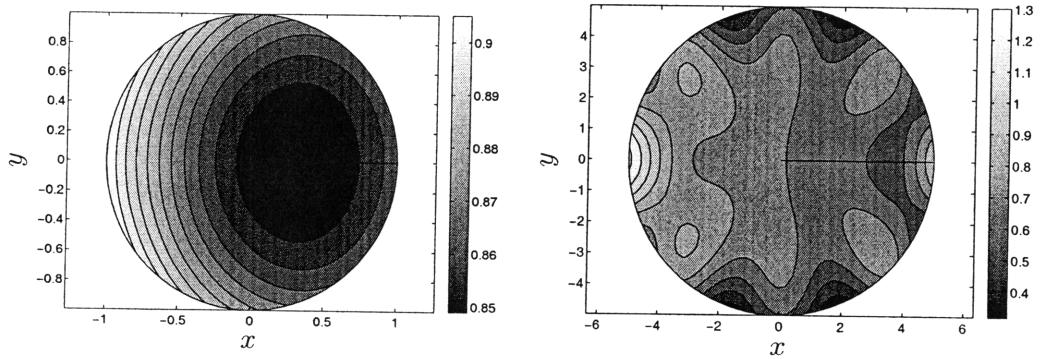

(a) $|\zeta_0|$ for $R = 1$

(b) $|\zeta_0|$ for $R = 5$

Figure 3-11: Buoy displacment inside a circular array $\lambda_g = 0.5$, $f = 0.2$ and $k_0 = 1$. Waves are incident from the left.

is

$$\mathcal{P}^* = \int_0^{2\pi} \int_{-h^*}^{0} \overline{\mathrm{i}\rho^*\omega^*\phi^* \frac{\partial \phi^{*\dagger}}{\partial r^*}} r^* \,\mathrm{d}z^* \,\mathrm{d}\theta$$
$$= \rho^* \sqrt{\frac{g^*}{h^*}} A^{*2} g^* h^* h^* \int_0^{2\pi} \int_{-1}^{0} \frac{1}{2} \mathrm{Re}\left(\mathrm{i}\phi \frac{\partial \phi^\dagger}{\partial r}\right) r \,\mathrm{d}z \,\mathrm{d}\theta \qquad (3.6.14)$$

where the overline denote time averaging over a period. Use has been made of the normalization defined in (3.2.10). The implied normalization for power output is

$$\mathcal{P}^* = \mathcal{P}\left(\rho^* \sqrt{\frac{g^*}{h^*}} A^{*2} g^* h^{*2}\right) \qquad (3.6.15)$$

In contrast, the power flux per unit length of the incoming wave crest is,

$$\frac{1}{2k_0^*} \rho^* g^* A^{*2} C_g^* = \frac{1}{2} h^* \rho^* g^* A^{*2} \sqrt{\frac{g^*}{h^*}} h^* \frac{1}{k_0} \frac{d\omega}{dk_0} = \left(\rho^* g^* A^{*2} \sqrt{\frac{g^*}{h^*}} h^{*2}\right) \frac{C_g}{2k_0}$$

The capture width $\mathcal{W}^*$ can be defined as

$$k_0^* \mathcal{W}^* = k_0 \mathcal{W} = \frac{\mathcal{P}^*}{\frac{1}{2k_0^*} \rho^* g^* A^{*2} C_g^*} = \frac{2k_0 \mathcal{P}}{C_g} \qquad (3.6.16)$$

Using the asymptotic expansions of Bessel functions for large $k_0 r$, we get from (3.6.2),

$$\phi_m(r) \approx \mathcal{A}_m \sqrt{\frac{2}{\pi k_0 r}} \mathrm{e}^{\mathrm{i}(k_0 r - \pi/4)} \frac{f_0(z)}{\mathrm{i}\omega f_0(0)} \qquad \text{for } k_0 r \gg 1 \qquad (3.6.17)$$

so that

$$\phi(r) \approx \frac{1}{\mathrm{i}\omega f_0(0)} \left(\mathrm{e}^{\mathrm{i}k_0 r \cos(\theta)} + \sum_m \mathcal{A}_m \sqrt{\frac{2}{\pi k_0 r}} \mathrm{e}^{\mathrm{i}(k_0 r - \pi/4)} \cos(m\theta)\right) f_0(z) \qquad (3.6.18)$$

where the modal amplitudes $\mathcal{A}_m$ can be computed from the solution using the asymptotic expression of the Hankel functions:

$$\mathcal{A}_m = a_{0,m} \mathrm{i}^{-m}$$

Using the method of stationary phase it can be shown that :

$$\mathcal{P} = 2\frac{1}{\omega f_0(0)^2}\left[|\mathcal{A}_0|^2 + \frac{1}{2}\sum_{m\geq 1}|\mathcal{A}_m|^2 + \mathrm{Re}\left(\sum_{m\geq 0}\mathcal{A}_m\right)\right] \tag{3.6.19}$$

Details are similar to that in (see Mei et al., 2005, p.381) and are given in Appendix B.3.1, as well as an alternative derivation of the expression from the buoy displacement. The capture width is therefore:

$$k_0^*\mathcal{W}^* = k_0\mathcal{W} = \frac{4k_0}{\omega C_g f_0(0)^2}\left[|\mathcal{A}_0|^2 + \frac{1}{2}\sum_{m\geq 1}|\mathcal{A}_m|^2 + \mathrm{Re}\left(\sum_{m\geq 0}\mathcal{A}_m\right)\right]$$

Finally, using the expression for f_0 and the dispersion relation, we find

$$C_g f_0(0)^2 = \frac{k_0}{\omega}$$

hence

$$k_0\mathcal{W} = 4\left(|\mathcal{A}_0|^2 + \frac{1}{2}\sum_{m\geq 1}|\mathcal{A}_m|^2 + \mathrm{Re}(\sum_{m\geq 0}\mathcal{A}_m)\right) \tag{3.6.20}$$

Another measure of efficiency is the ratio of the energy absorbed to the energy entering a distance $2R$,

$$\mathcal{E} = \frac{\mathcal{W}}{2R} \tag{3.6.21}$$

For the evaluation of the merits of the compact array let us recall some results known for a single buoy Newman (1979), Falnes (2002a), Mei et al. (2005) : (i) Maximum extraction is achieved at resonance. Both the heaving amplitude and the frequency at resonant peak increase as the size of a buoy decreases. (ii) The optimal $k_0\mathcal{W}$ is 1 at best for a heaving buoy of any size. It is known that a buoy with all three degrees of freedom has the maximum $k_0\mathcal{W} = 3$. If there is no external restoring force such as a spring the horizontal, then the mode of sway cannot be resonated so that the maximum is $k_0\mathcal{W} = 2$. (iii) The bandwidth of efficiency decreases when the size of the buoy increases. These have been checked by us using the semi-numerical method of Black, Mei, and Bray (1971) in Chapter 2.

In light of these let us present the results for a circular array of buoys. Figure 3-12 shows the dependence of capture width and extraction efficiency on the extraction rate λ_g. For two different array radii R, the greatest capture width and efficiency are achieved at around the same extraction rate of $\lambda_g = 0.5$. The precise optimal rate of damping depends slightly on the frequency/wave-number of the incoming wave.

Figure 3-13 shows that for a fixed packing ratio and damping rate, the capture width and efficiency naturally increases with the radius of the array. More important, the efficiency band width is very broad for all array sizes.

Figure 3-14 shows that the extraction efficiency increases monotonically with the packing ratio f, and with the incoming wave frequency. Recall that for circular buoys in a square array the maximum packing ratio is $f \leq \pi/4 \approx 0.79$.

Finally let us compare a large buoy whose radius and draft are equal, with a buoy array of the same total displaced volume $\pi f R^2 H$. Note that the value of H does not influence the energy extraction, but a value must be chosen here to define the total volume for the array. Since $H^* = O(a^*) \ll h^*$ we take $H = 0.1$ for illustration. With this choice, the radius and draft of the large buoy are both $a_b = (fR^2H)^{1/3}$. Figure 3-15 shows the comparison of capture widths over a wide range of frequencies. The solid curves gives the capture width for an array for different radii R, with fixed $f = 0.2$ and $\lambda_g = .5$. The dashed curves represent the capture width for a single-buoy absorber of corresponding radius a_b. In the range of $0 < k_0 = k_0^* h^* < 6$ the maximum $k_0 \mathcal{W}$ is at most unity for a single heaving buoy that only heaves, and can be 3 if roll and sway can also be resonated. Note however that the band width of a single buoy is always limited. Thus the circular buoy array is potentially more advantageous from the technical viewpoint of efficiency.

3.7 Conclusion

Stimulated by a recent invention in Norway, we have developed a theory for the hydrodynamics and power-extraction efficiency of a compact array of small buoys. The typical wave length is assumed to be comparable to the overall radius of the

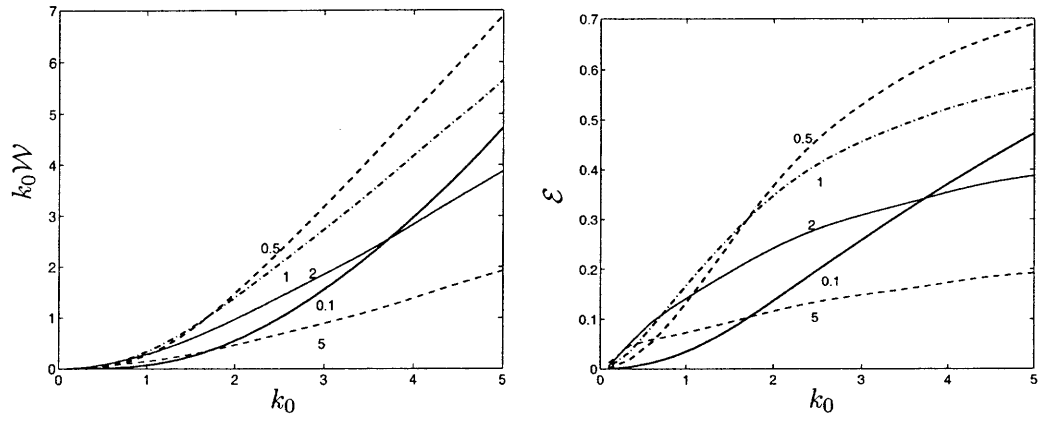

(a) Capture width for $R = 1$

(b) Efficiency for $R = 1$

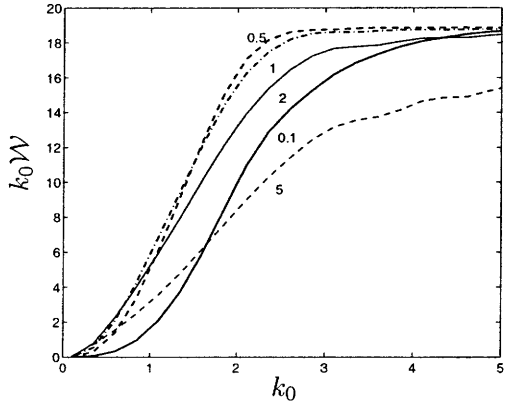

(c) Capture width for $R = 5$

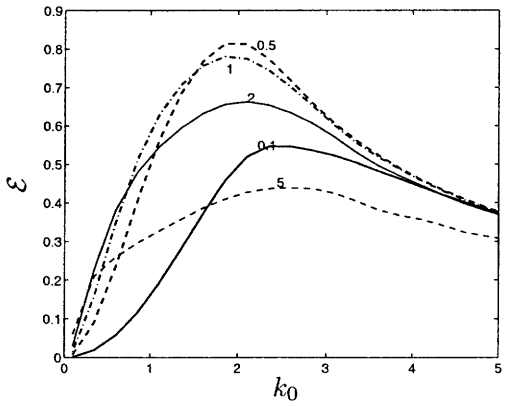

(d) Efficiency for $R = 5$

Figure 3-12: Effect of the extraction rate of the energy absorber on energy extraction The value of λ_g is indicated next to the curves. The packing ratio is $f = 0.2$.

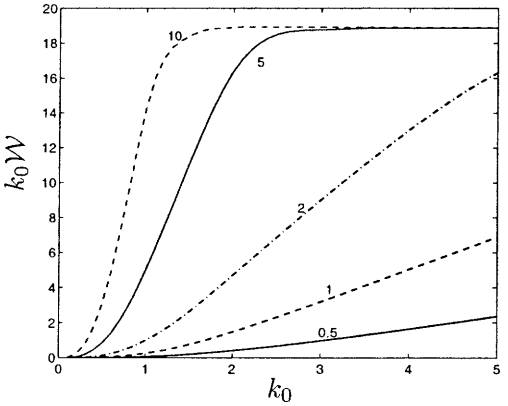

(a) Capture width

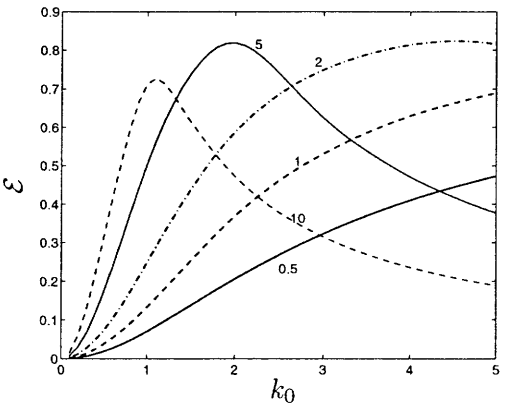

(b) Efficiency

Figure 3-13: Effect of the radius of the array on energy extraction. The value of R is indicated next to the curves. $\lambda_g = 0.5$, $f = 0.2$).

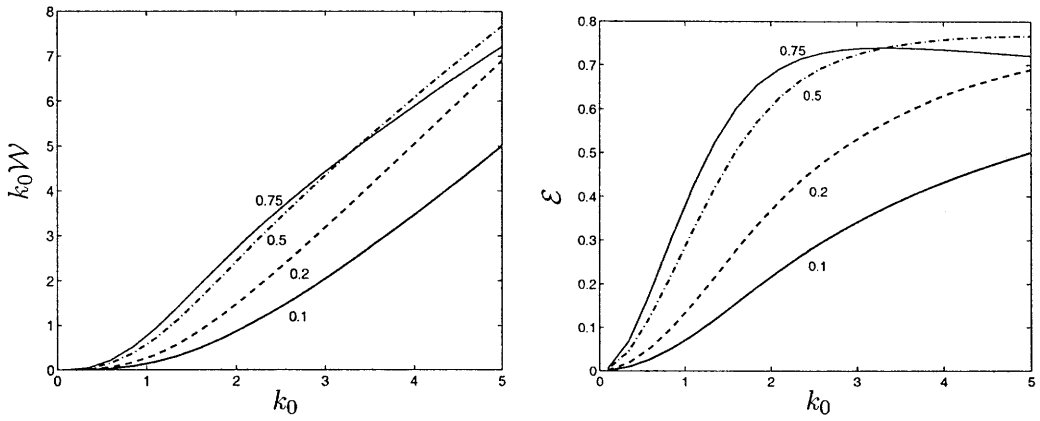

(a) Capture width (b) Efficiency

Figure 3-14: Effect of the packing ratio on energy extraction. The packing ratio f is indicated next to the curves. For $\lambda_g = 0.5$, $R = 1$).

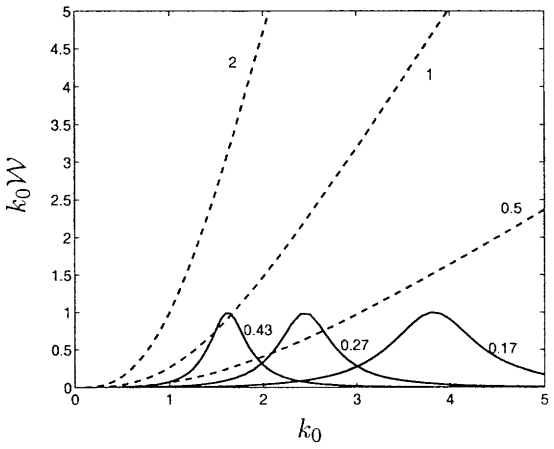

Figure 3-15: Capture widths of a circular arrays of small buoys of radii $R = 0.5, 1, 2$ are shown by dashed curves. Their drafts are $H = 1/10$. Capture widths of a large buoy of equal total volume with radii $a_b = (fR^2H)^{\frac{1}{3}} = 0.17, 0.27, 0.43$ are shown by solid curves. The draft is equal to the radius. For the array $f = 0.2$, $\lambda_g = 0.5$. For the single buoys the extraction rate is chosen to be the maximum at the peak.

array but much greater than the dimensions of individual buoys. For a periodic array the two-scale method of homogenization leads to an effective equation governing the spatial average. The energy-absorbing efficiency is studied for a long strip of buoys and for a circular array. The latter geometry is shown to be potentially advantageous in having good efficiency over a broad range of frequencies, unlike that of one large buoy.

The theory can be readily modified for wave interaction with broken ice floes floating on the sea surface, if the ice floes are idealized as identical floating bodies in a periodic array.

Chapter 4

Effect of Bragg resonance on wave-power extraction from a sparse array of buoys.

4.1 Introduction

We showed in Chapter 2 that in the usual range of frequencies of water waves a small buoy does not resonate and so can only extract very little energy, at least without control of the displacement. We may want to create another form of resonance by using a large number of buoys that will interact in such a way that their displacements will be increased. For this, we would need a constructive interaction between the

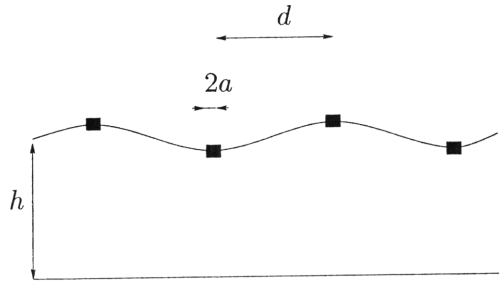

(a) Schema of the system

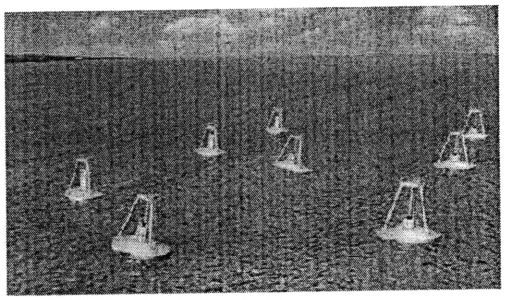

(b) Artist's view of a sparse array. Image taken from Ocean Power Technologies Inc.

Figure 4-1: Sparse array of buoys at Braggs resonance

waves generated by the movement of each buoy, which happens when the spacing is related to the wave length by

$$k^* d^* = n\pi \quad n \in \mathbb{N}$$

and is known as Braggs resonance. For these frequencies, we will also have strong scattering, as it was shown for example by Li and Mei (2007a,b) for the propagation of water waves in an array vertical cylinders and by Mei (1985) in the case of a periodic sea bed.

Numerical methods based on eigenfunction expansions have been developed to treat scattering by arrays. For example the interaction of an incoming wave with an infinite or semi-infinite line of floating objects at any frequency has been treated numerically by Peter et al. (2006), Peter and Meylan (2007). Linton and Mclver (1996) and Chamberlain (2007) considered the scattering by finite arrays of cylinders.

In this chapter, we will first investigate wave propagation in an infinite array of buoys using tools from solid state physics and standard Finite Elements procedures. This type of approach is similar to that of Chou (2000) for the scattering of a surface wave by a periodic interface. It will be a starting point to then focus on the propagation in a channel for frequencies close to Braggs resonance. Applying multiple scale analysis, we derive simple equations that will allow us to evaluate the energy extraction with very limited numerical computation.

4.2 Scales

As we did in the previous chapter, let us use asterisks to denote physical quantities. As we mentioned in the introduction, we are interested in the energy extraction from an array where a large number of small buoys are spaced of a distance d^* similar to the wave length, as shown in figure 4-1. This means that the length parameters will be related by:

$$\mu \equiv \frac{a^*}{h^*} \sim \frac{H^*}{h^*} \ll k^* d^* \sim k^* h^* \sim 1$$

As a consequence, we have three distinct sets of length scales, which are:

1. The local scale, which characterizes the flow in the neighborhood of the buoy. The proper dimensionless coordinates are

$$(\bar{x}, \bar{y}, \bar{z}) = \left(\frac{x^*}{a^*}, \frac{y^*}{a^*}, \frac{z^*}{a^*}\right)$$

2. The scale of the separation distance d^*. This will be referred to as the *short-scale* or *micro-scale*. At this scale the incoming wave length and the cell structure will be comparable. The dimensionless coordinate system associated to this scale will be

$$(x', y', z', t') = \left(\frac{x^*}{h^*}, \frac{y^*}{h^*}, \frac{z^*}{h^*}, \sqrt{\frac{g^*}{h^*}}t^*\right)$$

3. The *macro-scale*, at which the scattering effects will be significant. These effects will be characterized by the modulation of the wave envelope, so it needs to be related to space and time coordinates. Let us recall that the scattering and radiation effects of a single small heaving buoy of radius a^* on a wave of wavenumber k^* are of order $(k^*a^*)^2 \ll 1$, so in order to get significant interaction we need to consider at least $N \sim (k^*a^*)^{-2}$ buoys. Let us introduce the set of dimensionless coordinates

$$(x, y, t) = \mu^2(x', y', t')$$

to represent the effect at this scale. Given our assumption that the depth should be comparable to the incoming wave length, only the horizontal space coordinates are involved on the macro scale.

The free surface elevation, potential and buoy displacement will be respectively normalized by

$$\eta^* = A^*\eta', \qquad \phi^* = A^*\sqrt{g^*h^*}\phi, \qquad \zeta^* = A^*\zeta' \tag{4.2.1}$$

4.3 Asymptotic estimate away from Bragg scattering

Let us consider a single small buoy of radius μ. The scattered and radiated waves will be negligible (We show in Appendix E that they will be order μ for a semi-spherical buoy) compared to the incoming wave, even in the neighborhood of the buoy, so the only hydrodynamic force applied to the buoy will be due to the incoming wave. Let us assume we have an incoming wave of the form

$$\phi_i^* = \frac{A^* g^*}{\mathrm{i}\omega^*} \frac{\cosh(k^*(z^* + h^*))}{\cosh(k^* h^*)} \mathrm{e}^{\mathrm{i}k^* x^*}$$

then the exciting force is given by

$$F_{zD}^* = \mathrm{i}\rho^* \omega^* \iint_{S_B} \phi_{S,0}^* \, \mathrm{d}S^* = \mathrm{i}\rho^* \pi a^{*2} \omega^* \frac{A^* g^*}{\mathrm{i}\omega^*}$$

assuming without loss of generality that the buoy is located in $x^* = 0$. Using the following normalization

$$F_{zD}{}^* = \rho^* g^* h^{*2} A^* F_{zD}$$

we get

$$F_{zD} = \mathrm{i}\omega' \iint_{S_B} \phi_{S,0} \, \mathrm{d}S = \pi\mu^2$$

Applying Newton's law to a buoy, we get

$$-M^* \omega^{*2} \zeta^* = \pi\mu^2 \rho^* g^* h^{*2} A^* + \mathrm{i}\omega^* \lambda_g^* \zeta^* - \pi\rho^* g^* a^{*2} \zeta^* \tag{4.3.1}$$

As $M^* = \rho^* \pi a^{*2} H^*$, (4.3.1) can be rewritten as

$$0 = \pi + \mathrm{i}\omega' \pi \lambda_g \zeta - \pi\zeta$$

in dimensionless form, with

$$\lambda_g \equiv \frac{\lambda_g^*}{\pi \rho^* a^{*2} \sqrt{g^* h^*}}$$

It follows that

$$\zeta = \frac{1}{1 - \mathrm{i}\omega' \lambda_g}$$

From this, we can compute the energy extracted as

$$\begin{aligned} E^* &= \frac{1}{2} \omega^{*2} \lambda_g^* |\zeta^*|^2 \\ &= \frac{1}{2} \rho^* \sqrt{g^* h^*}^3 A^{*2} \mu^2 \pi \lambda_g |\zeta^2| \end{aligned}$$

Let us recall that the energy incoming on a width W^* is given by

$$\frac{1}{2} \rho^* \sqrt{g^* h^*}^3 A^{*2} W' C_g'$$

so a single buoy extracts a ratio

$$d' \mu^2 \frac{\pi}{W' d' C_g'} \frac{\lambda_g \omega'^2}{1 + \omega'^2 \lambda_g^2}$$

of the incoming energy. Let us introduce

$$\mathcal{R} \equiv \frac{\pi}{W' d' C_g'} \frac{\lambda_g \omega'^2}{1 + \omega'^2 \lambda_g^2} \tag{4.3.2}$$

Let us now assume that we have many of such buoys spaced of a distance $\delta x = \mu^2 d'$ in the long scale set of coordinates. Neglecting the interaction of the buoys, the energy e of the incoming wave at a position x would be related to the amplitude at $x + \delta x$ by

$$e(x + \delta x) = (1 - \delta x \mathcal{R}) e(x)$$

so

$$\frac{\mathrm{d}e}{\mathrm{d}x} = \mathcal{R} e(x)$$

The energy remaining at the end of the array would therefore be

$$e(L) = \mathrm{e}^{-\mathcal{R}L}$$

and so the extracted energy in this approximation would be

$$\mathcal{E}_0 \equiv 1 - \mathrm{e}^{-\mathcal{R}L} \tag{4.3.3}$$

Note that the fraction of the incoming energy that is extracted depends only on:

- The number of buoys through L/d'. The number of cells is in fact $L/(\mu^2 d')$.
- The frequency of the incoming wave through ω'/C'_g.
- The energy extraction rate
- The width of the array

The dependency of $\mathcal{E}_0$ with the number of buoys, the damping rate and the frequency is represented in figure 4-2. We see that it increases with the number of buoys, and that the optimum damping rate is independent of the length of the array. Indeed, in the limits of this approximation, the extracted energy will be maximum for

$$\frac{\mathrm{d}\mathcal{E}_0}{\mathrm{d}\lambda_g} = 0$$

that is to say

$$-\left(-\frac{\frac{\pi}{d'^2 C'_g}\omega' L}{1+\lambda_g^2\omega'^2} + 2\frac{\frac{\pi}{d'^2 C'_g}\lambda_g^2\omega'^3 L}{\left(1+\lambda_g^2\omega'^2\right)^2}\right)\mathrm{e}^{-\mathcal{R}L} = 0$$

which gives

$$\lambda_g = \frac{1}{\omega'}$$

***Remark* 4.3.1** (Neighborhood of Bragg resonance.). *Recall that we want to consider frequencies that are close to Bragg resonance (but not too much so that scattering*

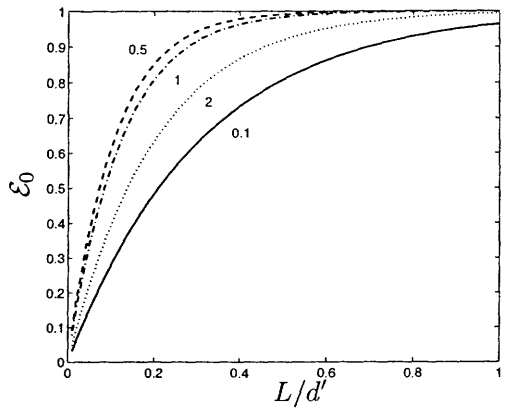

(a) Influence of the number of buoys. The value of λ_g is indicated next to the curves and $k' = \pi$.

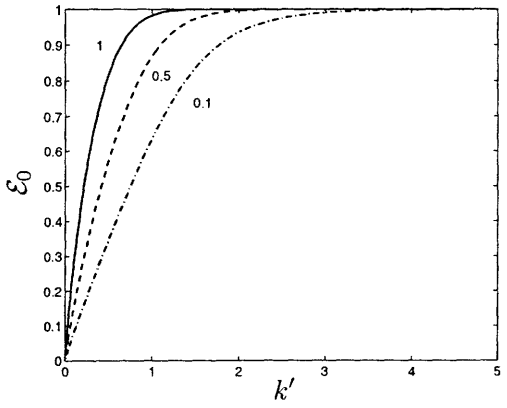

(b) Influence of the frequency on the the $\mathcal{E}_0$. λ_g is set to its optimal value, and the value of L/d' is indicated next to the curves.

Figure 4-2: Energy extraction $\mathcal{E}_0$ for $W' = 1$.

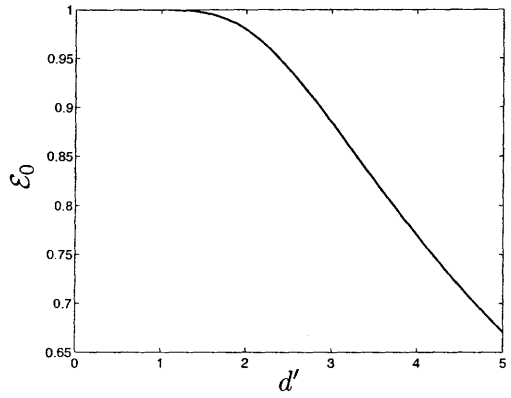

Figure 4-3: $\mathcal{E}_0$ around Bragg scattering for $L/d' = 1$ and for the optimum damping rate λ_g. $W' = 1$

effects remain negligible), so

$$\omega' = \sqrt{k' \tanh(k')} \approx \sqrt{\frac{\pi}{d'} \tanh\left(\frac{\pi}{d'}\right)}$$

In this case, the energy extracted will depend on d' through the resonant frequency. This dependency is represented in figure 4-3.

From now on, we will set the dimensionless width of the channel to be equal to the spacing: $W' = d'$.

4.4 Periodicity: Bloch solutions

Let us first give some general properties of the wave propagation in an infinite periodic domain, following an approach that is common in solid state physics. The important point that we emphasize here is that the periodicity of the domain does not imply the periodicity of the solution.

4.4.1 Bloch theorem

Due to periodicity in the two horizontal directions, Bloch theorem states that any bounded solution in an infinite periodic domain can be decomposed into a linear combination of Bloch states (sometimes also called Floquet modes) ψ for which there exists a real vector $\boldsymbol{k}' = (k'_x, k'_y, 0)$ such that

$$\widetilde{\psi}(\boldsymbol{x}') = \psi(\boldsymbol{x}') \exp(-\mathrm{i}\boldsymbol{k}' \cdot \boldsymbol{x}')$$

is a periodic function. See Appendix D for some insight on the derivation of this theorem. In physical terms, it means that the solution will behave like a plane wave of wave vector equal to the Bloch wave vector, but with a periodic envelope. Therefore determining the vector $\boldsymbol{k}'$ will give us a good insight into the wave propagation.

4.4.2 Symmetry

For now, the wave vector coordinates k'_x and k'_y can be any real number. We can however note that for any $\boldsymbol{k}'$ and for any integer n and m the vector

$$\boldsymbol{k}'_{n,m} \equiv \boldsymbol{k}' + (n\frac{2\pi}{d'}, m\frac{2\pi}{d'})$$

will also be such that

$$\widetilde{\psi}_{n,m}(\boldsymbol{x}') = \psi(\boldsymbol{x}') \exp(-\mathrm{i}\boldsymbol{k}'_{n,m} \cdot \boldsymbol{x}')$$

is a periodic function. From the point of view of Bloch theorem, $\boldsymbol{k}'$ and $\boldsymbol{k}'_{n,m}$ are equivalent. We can therefore consider only the vectors such that

$$-\frac{\pi}{d'} \leq k'_x \leq \frac{\pi}{d'} \qquad\qquad -\frac{\pi}{d'} \leq k'_y \leq \frac{\pi}{d'}$$

in order to avoid redundancy. This region is called the first Brilloin zone. We can also note that our problem is invariant under the changes

$$x' \leftrightarrow -x' \qquad y' \leftrightarrow -y' \qquad x' \leftrightarrow y' \qquad t' \leftrightarrow -t'$$

so if we find a Bloch state $\psi(x', y', z')$ associated with the vector (k'_x, k'_y), then we will also have (See Joannopoulos et al. (2008))

1. $\psi(y', x', z')$ associated with (k'_y, k'_x)
2. $\psi(-x', y', z')$ associated with $(-k'_x, k'_y)$
3. $\psi(-x', -y', z')$ associated with $(-k'_x, -k'_y)$
4. $\psi(x', -y', z')$ associated with $(k'_x, -k'_y)$

As a consequence, we only need to consider wave vectors in the area shown in figure 4-4(b), called irreducible zone. Indeed, knowing the solution for $\boldsymbol{k}$ in area I of figure 4-4(b) we can use 1. to deduce the solution in area II, and then 2., 3. and 4. to obtain the solutions in areas III, IV and V, so the solution is known in the entire Brilloin zone. The irreducible zone is the smaller region in which the problems associated to the Bloch vectors are not related by symmetry (See Joannopoulos et al. (2008)).

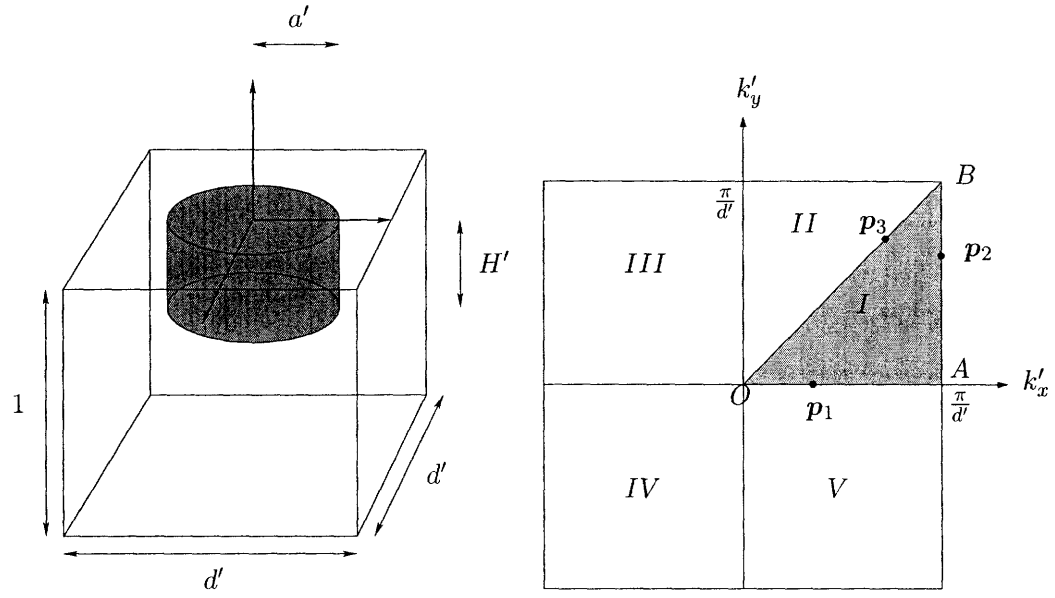

(a) Cell

(b) The irreducible Brilloin zone for our problem.

Figure 4-4: Geometry

4.5 Wave propagation in an infinite array of fixed bodies

4.5.1 Equations

Let us first study the propagation of a wave by fixed buoys. We employ the following symbols for physical domains: Ω_f is the fluid domain, S_f is the free surface, S_W is the lateral surface of the buoys, and S_B is the bottom surface of the buoys. In terms of the short scale alone, the set of equation characterizing the linearized scattering of an incoming wave is

$$\begin{aligned}
\Delta'\phi_S &= 0, \quad \boldsymbol{x}' \in \Omega_f \\
\left(\frac{\partial}{\partial z'} - \omega'^2\right)\phi_S &= 0, \quad \boldsymbol{x}' \in S_F \\
\frac{\partial \phi_S}{\partial z'} &= 0, \quad \boldsymbol{x}' \in S_B \\
\frac{\partial \phi_S}{\partial z'} &= 0, \quad z' = -1 \\
\frac{\partial \phi_S}{\partial r'} &= 0, \quad \boldsymbol{x}' \in S_W
\end{aligned} \tag{4.5.1}$$

where Δ' is the three dimensional with respect to the short scale coordinates. The derivation of this system is classic. The first equation expresses the fact that we consider a potential flow, the second gives the free surface condition and the last three impose that there should be no flux of mass into the buoy or the sea bottom.

As we mentioned in §4.4, determining the Bloch wave vector is very important to understand the wave propagation inside a periodic domain. In solid state physics, band diagrams are used to represent the dependence of these vectors with the frequency. Let us follow this approach to get a first idea of how a sinusoidal wave will propagate in an array of buoys. This is also the approach followed by Chou (2000) to study the scattering of water waves by a periodic interface. Let us look for a Bloch state ϕ_S that solves (4.5.1). We know that

$$\phi_S(\boldsymbol{x}') = \mathrm{e}^{\mathrm{i}\boldsymbol{k}'\cdot\boldsymbol{x}'}\widetilde{\phi}_S(\boldsymbol{x}') \tag{4.5.2}$$

where $\widetilde{\phi}_S$ is a $d'-$periodic function in x and y. Therefore, in terms of $\widetilde{\phi}_S$ we have:

$$\begin{aligned}
\Delta'\widetilde{\phi}_S + 2\mathrm{i}\boldsymbol{k}'\cdot\boldsymbol{\nabla}'_2\widetilde{\phi}_S - \|\boldsymbol{k}'\|^2\widetilde{\phi}_S = 0, &\qquad \boldsymbol{x}' \in \Omega_f \\
\left(\frac{\partial}{\partial z'} - \omega'^2\right)\widetilde{\phi}_S = 0, &\qquad \boldsymbol{x}' \in S_F \\
\frac{\partial\widetilde{\phi}_S}{\partial z'} = 0, &\qquad \boldsymbol{x}' \in S_B \\
\frac{\partial\widetilde{\phi}_S}{\partial z'} = 0, &\qquad z' = -1 \\
\frac{\partial\widetilde{\phi}_S}{\partial r'} = -\mathrm{i}\boldsymbol{k}'\cdot\boldsymbol{e}_r\widetilde{\phi}_S, &\qquad \boldsymbol{x}' \in S_W
\end{aligned} \tag{4.5.3}$$

where $\boldsymbol{\nabla}_2$ denotes the gradient with represents to the horizontal coordinates

The more logic approach to solve this problem would be to look for the values of $\boldsymbol{k}'$ for which there exists a solution to (4.5.3) for a given ω', as it will be imposed by the incoming wave, but this is not a standard problem. Instead, for any real vector $\boldsymbol{k}'$, (4.5.3) is an eigen-problem for which the eigenvalue is the square of the frequency, and so usual methods can be used to get the frequencies associated to any $\boldsymbol{k}'$.

Before going to the scattering by buoys, let us consider the situation where the array is made of piles. This is the case studied by Li and Mei (2007a,b) using different methods, so their theory will provide us a way to check our results.

4.5.2 Vertical cylinders extending to the bottom of the sea

Solution method

In this case we can apply separation of variables to (4.5.3). Writing $\widetilde{\phi}_S(x', y', z') = \varphi(x', y')\chi(z')$, we get [1]

$$\frac{\Delta'_2\varphi + 2\mathrm{i}\boldsymbol{k}'\cdot\boldsymbol{\nabla}'_2\varphi - \|\boldsymbol{k}'\|^2\varphi}{\varphi} = -\frac{1}{\chi}\frac{\mathrm{d}^2\chi}{\mathrm{d}z'^2} = -\kappa^2, \quad \kappa \in \mathbb{C} \tag{4.5.4}$$

where κ is an eigenvalue. As we did for the gradient, Δ_2 denotes the two dimensional Laplacian. Equation (4.5.4) gives us a new eigenvalue problem that involves only

[1] $\mathbb{C}$ is the set of complex numbers.

horizontal coordinates:

$$\begin{aligned} \Delta'_2\varphi + 2\mathrm{i}\boldsymbol{k}'\cdot\boldsymbol{\nabla}'_2\varphi - \|\boldsymbol{k}'\|^2\varphi &= -\kappa^2\varphi, \qquad \boldsymbol{x}' \in \Omega_f \\ \frac{\partial\varphi}{\partial r'} &= -\mathrm{i}\boldsymbol{k}'\cdot\boldsymbol{e}_r\varphi, \quad \boldsymbol{x}' \in S_W \end{aligned} \tag{4.5.5}$$

In order to solve it numerically with `FreeFEM++` (Cf. Hecht et al.), we need the following weak formulation: $\forall\psi \in H^1_{per}$ [2]

$$\iint_{\Omega_f} \left(\boldsymbol{\nabla}'_2\phi_S\cdot\boldsymbol{\nabla}'_2\psi^\dagger + \|\boldsymbol{k}'\|^2\varphi\psi^\dagger\right) - \mathrm{i}\boldsymbol{k}'\cdot\left(\boldsymbol{\nabla}'_2\varphi\psi^\dagger - \boldsymbol{\nabla}'_2\psi^\dagger\varphi\right)\mathrm{d}S' = \kappa^2\iint_{\Omega_f}\varphi\psi^\dagger\,\mathrm{d}S' \tag{4.5.6}$$

Let us define

$$\begin{aligned} b(\varphi,\psi) &= \iint_{\Omega_f} \left(\boldsymbol{\nabla}'_2\varphi\cdot\boldsymbol{\nabla}'_2\psi^\dagger + \|\boldsymbol{k}'\|^2\varphi\psi^\dagger\right) - \mathrm{i}\boldsymbol{k}'\cdot\left(\boldsymbol{\nabla}'_2\varphi\psi^\dagger - \boldsymbol{\nabla}'_2\psi^\dagger\varphi\right)\mathrm{d}S' \\ l(\varphi,\psi) &= \iint_{\Omega_f}\varphi\psi^\dagger\,\mathrm{d}S' \end{aligned}$$

then $\forall\psi \in H^1_{per}$ we can make use of the fact that $b(\varphi,\varphi) \in \mathbb{R}$ as b is Hermitian, and apply Cauchy-Schwartz inequality twice (to the scalar products in $\mathbb{R}^2$ and L^2) to get:

$$\begin{aligned} b(\varphi,\varphi) &= \|\boldsymbol{\nabla}'_2\varphi\|^2 + \|\boldsymbol{k}'\|^2\|\varphi\|^2 - 2\boldsymbol{k}'\cdot\iint_{\Omega_f}\mathrm{Im}\left(\varphi\boldsymbol{\nabla}'_2\varphi\right)\mathrm{d}S' \\ &\geq \|\boldsymbol{\nabla}'_2\varphi\|^2 + \|\boldsymbol{k}'\|^2\|\varphi\|^2 - 2\|\boldsymbol{k}'\|\iint_{\Omega_f}|\varphi\boldsymbol{\nabla}'_2\varphi|\,\mathrm{d}S' \\ &\geq \|\boldsymbol{\nabla}'_2\varphi\|^2 + \|\boldsymbol{k}'\|^2\|\varphi\|^2 - 2\|\boldsymbol{k}'\|\|\boldsymbol{\nabla}'_2\varphi\|\|\varphi\| \\ &\geq \left(\|\boldsymbol{\nabla}'_2\varphi\| - \|\boldsymbol{k}'\|\|\varphi\|\right)^2 \end{aligned}$$

As we also have $l(\varphi,\varphi) \geq 0$, then the eigenvalues κ^2 will be real and positive, so we can choose $\kappa \in \mathbb{R}^+$. The vertical dependency will thus be

$$\chi(z') \propto \cosh(\kappa(z'+1))$$

[2] H^1_{per} is the space of 'periodic' functions in L^2 that have a weak derivative in L^2. For a more precise definition, we refer to Cioranescu and Donato (1999)

We can now make use of the free surface boundary condition to relate κ to the frequency by

$$\omega'^2 = \kappa \tanh(\kappa) \tag{4.5.7}$$

We further note that if $b(\varphi, \varphi) = 0$ then

$$\boldsymbol{\nabla}'_2 \varphi \propto \varphi$$

and

$$\boldsymbol{\nabla}'_2 \varphi \propto \boldsymbol{k}'$$

which implies that $\exists \alpha \in \mathbb{C}$ such that

$$\boldsymbol{\nabla}'_2 \varphi = \alpha \varphi \boldsymbol{k}'$$

and so

$$\varphi = \beta \exp(\alpha \boldsymbol{k}' \cdot \boldsymbol{x}), \quad \beta \in \mathbb{C}$$

In order to satisfy the boundary condition on the cylinder S_W, we must have $\alpha = \mathrm{i}$. As φ should be periodic and $\boldsymbol{k}'$ should be in the irreducible Brillouin zone, we are only left with $\boldsymbol{k}' = 0$, and so $\varphi = 0$. The bilinear form b is therefore Hermitian positive definite. This shows that $\kappa > 0$ for $\boldsymbol{k} \neq 0$.

This shows us that for any $\boldsymbol{k}'$ in the irreducible Brillouin zone, we can compute the eigenvalues κ from (4.5.6) and then get the corresponding frequency from (4.5.7). Due to the eigenvalue structure of the problem, a sequence of frequencies $\omega_n(\boldsymbol{k})$ will correspond to any Bloch wave vector. Numerical results for these frequencies are represented in figure 4-5. Note that this numerical approach is not limited to small radius $k^* a^* \ll 1$.

A band gap is a range of frequency for which no propagation is possible. This corresponds to frequencies that are not associated to any vector $\boldsymbol{k}'$. We see that this phenomenon does not appear here, but we should however note that for a given direction of propagation (given by the direction of $\boldsymbol{k}'$) only certain frequencies are

possible.

***Remark* 4.5.1** (Representation of the dispersion relation). *First one should note that figure 4-5 does not represent the frequencies associated to all vectors in the irreducible Brilloin zone, but only to the vectors on its boundaries. The reason for this is that contour or surface representation are not suitable to represent all the eigenvalues associated to each vector in the same plot. The only vectors* $\boldsymbol{k}'$ *that are considered in such a representation are those that are along the path* $OABO$*. The plot in composed of three sections, respectively represented on the horizontal axis by the segments* OA*,* AB *and* BO*. The first section corresponds to vectors* $(k'_x, 0, 0)$ *for* $0 \leq k'_x \leq \pi/d'$*, the second to vectors of the form* $(\pi/d', k'_y, 0)$ *for* $0 \leq k_y \leq \pi/d'$ *and finally the last one to* $(k', k', 0)$ *for* k' *decreasing from* π/d' *to* 0*.*

The representation of the dispersion shown in figure 4-5 can be surprising as it does not look like the representation of a function $\omega'(k')$*. A sequence of values of* ω' *correspond to each value of* $\boldsymbol{k}'$*, which seems contradicting with the usual dispersion relation* $\omega' = k' \tanh(k')$*. This corresponds to the fact that from the point of view of the Bloch theorem only the value of the function at the lateral boundaries of the cell are relevant, so for example there is no difference between a function that is* $d'-$*periodic and a function that is* $d'/2-$*periodic, so they correspond to the same abscissa. However these two functions would correspond to different frequency, this is why for a given* $\boldsymbol{k}'$ *in the irreducible Brillouin zone there are several frequencies associated. This is like if we represented the usual curve* $\omega'^2 = k' \tanh(k')$ *on a bounded interval folding itself.*

Particular case: piles in a channel

In the case of a 2D array of buoys $\boldsymbol{k}'$ varies in the area shown in figure 4-4(b), so we can in general expect that all values of $\boldsymbol{k}'$ along a curve will correspond to a given frequency. In order to make this situation simpler, a possibility is to consider that $\boldsymbol{k}' \propto \boldsymbol{e}_x$ (i.e. consider one dimensional propagation) so that only the first section of the band diagram shown in figure 4-5 (i.e. the segment OA) has to be considered.

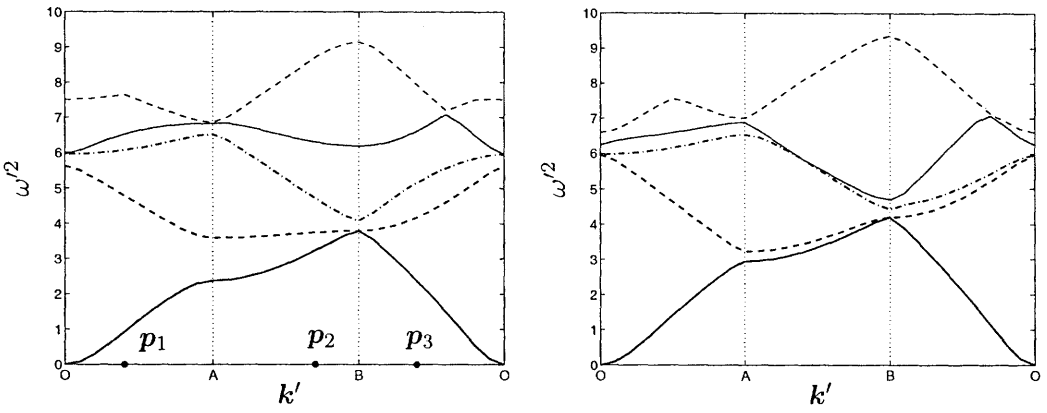

(a) $a' = 0.25$, $d' = 1$ (b) $a' = 0.1$, $d' = 1$

Figure 4-5: Smaller eigenvalues of (4.5.6) as $\boldsymbol{k}'$ moves along the path $OABO$ described in figure 4-4(b). The position $\boldsymbol{p}_1$, $\boldsymbol{p}_2$ and $\boldsymbol{p}_3$ on the horizontal axis correspond to the vectors $\boldsymbol{k}'$ represented in figure 4-4(b). For more explanation, see Remark 4.5.1. Numerical solution was carried out using `FreeFEM++` for the generation of the Finite Element matrices and `Matlab` for the computation of the eigenvalues.

It greatly simplifies the problem as now only one value of $\boldsymbol{k}'$ *in the Brillouin zone* corresponds to a frequency.

Due to symmetry, solutions of the problem for $k'_y = 0$ are even in y', so the periodicity condition is equivalent to stating that the normal flux in $y' = \pm d'$ is zero, which corresponds to propagation in a channel.

Band gaps If we restrict ourselves to a 1D propagation then propagation is not possible for certain ranges of frequency (See a graphical illustration in figure 4-7(e)). This appears to be a general feature of 1D propagation (Cf. Joannopoulos et al. (2008)). As one could expect, band gaps are more important when bigger buoys are considered, and for small buoys the dispersion relation is very similar to that we have with no buoy. Let us quantify this observation.

Comparison with the band gap width in Li and Mei (2007b). Analytic study in Li and Mei (2007b) shows that there is a band gap for

$$\omega'_0 - 2\pi^2\mu^2\Omega_0^c \leq \omega' \leq \omega'_0 + \pi^2\mu^2\Omega_0^c$$

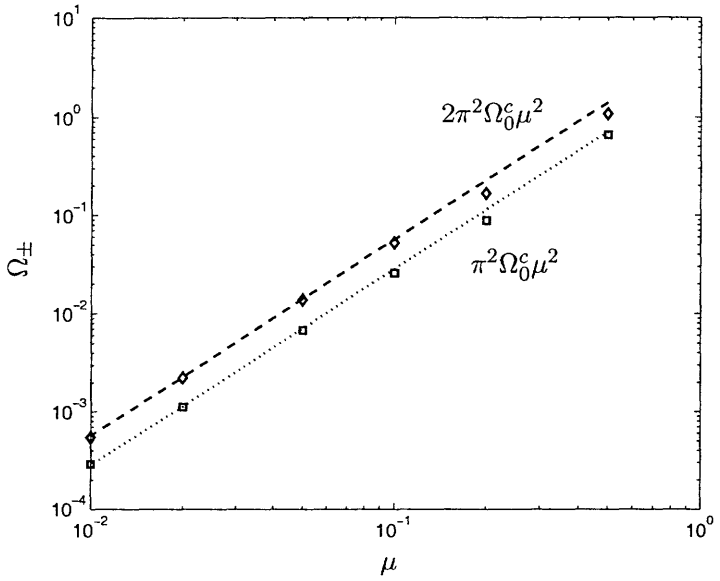

Figure 4-6: Upper and lower limits of the band gap for the wave propagation in an array of piles in a channel for $d' = 1$. Ω_+ is represented by the squares, Ω_- by the diamonds.

with

$$\Omega_0^c = \frac{C_g'}{d'} \qquad\qquad \omega_0' = \sqrt{\pi \tanh(\pi)} \tag{4.5.8}$$

in the limit $\mu \ll 1$. The approach we described allows us to evaluate the limits of the band gap by looking at the first two eigenvalues for $k' = \pi$. Writing these two values as $\omega_0' + \Omega_+$ and $\omega_0' - \Omega_-$, we can represent Ω_+ and Ω_- as a function of μ. Numerical results are shown in figure 4-6. We note a very good agreement between the analytical and numerical studies.

4.5.3 3D buoys.

Let us derive the weak form of (4.5.3) in order to get theoretical and numerical insight on the solution. For this, let us multiply (4.5.3) by an arbitrary test function $\psi^\dagger \in H^1_{per}$ and integrate by parts

$$\iiint_\Omega \Delta' \widetilde{\phi}_S \psi^\dagger + 2i\boldsymbol{k}' \cdot \boldsymbol{\nabla}_2' \widetilde{\phi}_S \psi^\dagger - \|\boldsymbol{k}'\|^2 \widetilde{\phi}_S \psi^\dagger \, \mathrm{d}V' = 0$$

so [3]

$$\iiint_\Omega -\boldsymbol{\nabla}'\widetilde{\phi}_S\cdot\boldsymbol{\nabla}'\psi^\dagger+\mathrm{i}\boldsymbol{k}'\cdot\left(\boldsymbol{\nabla}'_2\widetilde{\phi}_S\psi^\dagger-\psi^\dagger\boldsymbol{\nabla}'_2\widetilde{\phi}_S\right)-\|\boldsymbol{k}'\|^2\widetilde{\phi}_S\psi^\dagger\,\mathrm{d}V'$$
$$=-\iint_{\partial\Omega}\frac{\partial\widetilde{\phi}_S}{\partial n'}\psi^\dagger+\mathrm{i}\boldsymbol{k}'\cdot\boldsymbol{e}_n\widetilde{\phi}_S\psi^\dagger\,\mathrm{d}S'$$

This expression can be simplified to:

$$\iiint_\Omega \boldsymbol{\nabla}'\widetilde{\phi}_S\cdot\boldsymbol{\nabla}'\psi^\dagger-\mathrm{i}\boldsymbol{k}'\cdot\left(\boldsymbol{\nabla}'_2\widetilde{\phi}_S\psi^\dagger-\psi^\dagger\boldsymbol{\nabla}'_2\widetilde{\phi}_S\right)+\|\boldsymbol{k}'\|^2\widetilde{\phi}_S\psi^\dagger\,\mathrm{d}V'$$
$$=\omega'^2\iint_{S_f}\widetilde{\phi}_S\psi^\dagger\,\mathrm{d}S' \quad (4.5.9)$$

We can define

$$b(\widetilde{\phi}_S,\psi)=\iiint_\Omega\left(\boldsymbol{\nabla}'\widetilde{\phi}_S\cdot\boldsymbol{\nabla}'\psi^\dagger+|\boldsymbol{k}'|^2\widetilde{\phi}_S\psi^\dagger\right)-\mathrm{i}\boldsymbol{k}'\cdot\left(\boldsymbol{\nabla}'_2\widetilde{\phi}_S\psi^\dagger-\boldsymbol{\nabla}'_2\psi^\dagger\widetilde{\phi}_S\right)\mathrm{d}V'$$
$$l(\widetilde{\phi}_S,\psi)=\iint_{S_f}\widetilde{\phi}_S\psi^\dagger\,\mathrm{d}S'$$

As in the 2D case, b and l are Hermitian and positive, which tells us that the eigenvalues are real and positive. However, only b is definite (for $\boldsymbol{k}'\neq 0$) as for example $l(z',z')=0$, so the problem that should be solved in practice is:

$$l(\widetilde{\phi}_S,\psi)=\frac{1}{\omega'^2}b(\widetilde{\phi}_S,\psi),\quad\forall\psi\in H^1_{per} \quad (4.5.10)$$

This problem can be solved numerically using the Finite Elements Method (FEM), as described in Appendix C. An example of numerical result is shown in figure 4-7. We can see that the appearance of the band diagram is similar to what we had in 2D. In particular, we note that band gaps are present for the scattering by a line of buoys inside a channel.

[3] $\partial\Omega$ is the boundary of Ω

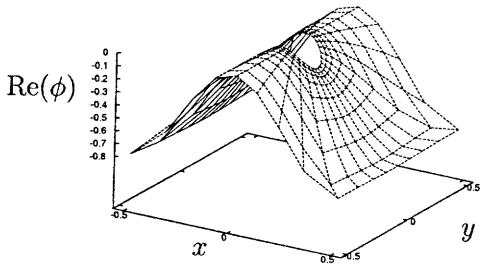

(a) Real part of the first eigenvector for $k'_x = \pi$

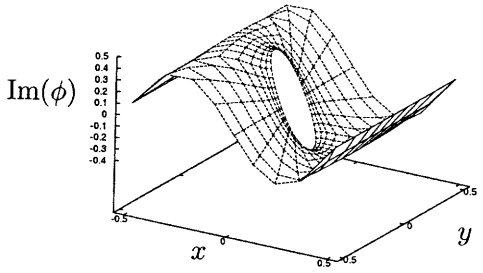

(b) Imaginary part of the first eigenvector for $k'_x = \pi$

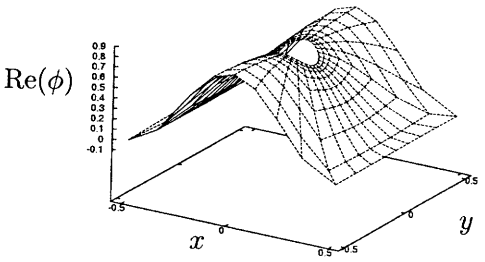

(c) Real part of the second eigenvector for $k'_x = \pi$

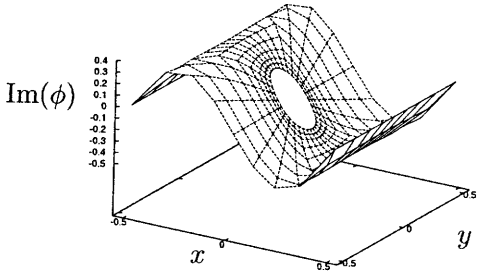

(d) Imaginary part of the second eigenvector for $k'_x = \pi$

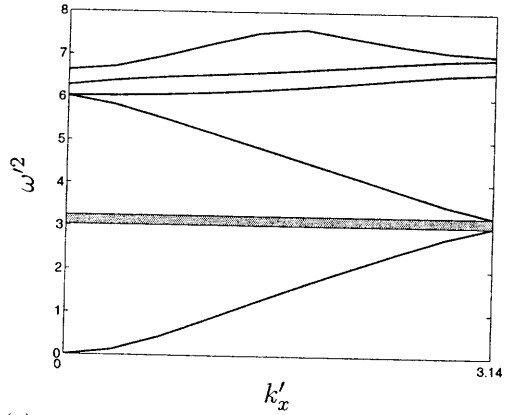

(e) Band diagram for 1D propagation. The band gap is represented in gray.

Figure 4-7: Finite element simulation of the propagation in an array of buoys ($d' = 1$, $a' = 0.1$ and $H' = 0.1$).

4.6 Multiple scales analysis of the scattering problem

The analysis of band gaps we carried out confirms that strong scattering can be expected for some particular frequencies, and gives us information about the limits of the band gap. However it does not give us information about the rate of decay of the solution, or about the influence of the finite length of the array. For this purpose, let us apply the method of multiple scales to the problem of Bragg scattering by a line of buoys in a channel.

Expressing the derivatives in terms of short and long scale coordinates in (4.5.1) and expanding the potential as $\phi_S = \phi_{S,0} + \mu^2\phi_{S,1} + ...$, we get the following set of equations:

$$\begin{aligned}
\left(\Delta' + 2\mu^2\frac{\partial^2}{\partial x\partial x'} + \mu^4\frac{\partial^2}{\partial x^2}\right)\left(\phi_{S,0} + \mu^2\phi_{S,1} + ...\right) = 0, \quad & \boldsymbol{x}' \in \Omega_f \\
\left(\frac{\partial}{\partial z'} - \omega'^2 - 2\mu^2 \mathrm{i}\omega'\frac{\partial}{\partial t} - \mu^4\frac{\partial^2}{\partial t'^2}\right)\left(\phi_{S,0} + \mu^2\phi_{S,1} + ...\right) = 0, \quad & \boldsymbol{x}' \in S_F \\
\frac{\partial}{\partial z'}\left(\phi_{S,0} + \mu^2\phi_{S,1} + ...\right) = 0, \quad & \boldsymbol{x}' \in S_B \\
\frac{\partial}{\partial z'}\left(\phi_{S,0} + \mu^2\phi_{S,1} + ...\right) = 0, \quad & z' = -1 \\
\left(\frac{\partial}{\partial r'} + \mu^2\frac{\partial}{\partial r}\right)\left(\phi_{S,0} + \mu^2\phi_{S,1} + ...\right) = 0, \quad & \boldsymbol{x}' \in S_W
\end{aligned} \tag{4.6.1}$$

In comparison to the case of a compact array, we can note two main points:

- There is no ambiguity in the notion of long and short scales, as the unit cell now has comparable dimensions in both x', y' and z'. The volume of the buoy is now smaller than the volume of the cell by a factor μ^2, which is also the ratio between the two scales.

- The free surface is not a rigid boundary on the short scale.

4.6.1 Zeroth order

At the leading order, (4.6.1) gives the following set of equations:

$$\begin{aligned}
\Delta'\phi_{S,0} &= 0, \quad \boldsymbol{x}' \in \Omega_f \\
\left(\frac{\partial}{\partial z'} - \omega'^2\right)\phi_{S,0} &= 0, \quad \boldsymbol{x}' \in S_F \\
\frac{\partial \phi_{S,0}}{\partial z'} &= 0, \quad \boldsymbol{x}' \in S_B \\
\frac{\partial \phi_{S,0}}{\partial z'} &= 0, \quad z' = -1 \\
\frac{\partial \phi_{S,0}}{\partial r'} &= 0, \quad \boldsymbol{x}' \in S_W
\end{aligned} \tag{4.6.2}$$

As we assumed that $\mu = a' \sim H' \ll d' \sim 1$, then the areas of the surfaces S_B and S_W are negligible compared to that of S_f. As we did for the compact array, let us ignore this boundary condition for the moment and keep it for the next order, so that the problem becomes:

$$\begin{aligned}
\Delta'\phi_{S,0} &= 0, \quad \boldsymbol{x}' \in \Omega_f \\
\left(\frac{\partial}{\partial z'} - \omega'^2\right)\phi_{S,0} &= 0, \quad \boldsymbol{x}' \in S_F \\
\frac{\partial \phi_{S,0}}{\partial z'} &= 0, \quad z = -1
\end{aligned} \tag{4.6.3}$$

Let us introduce

$$Z(z') = \frac{1}{\mathrm{i}\omega'} \frac{\cosh(k'(z'+1))}{\cosh(k')} \tag{4.6.4}$$

and recall that on the short scale, solution should be propagating, then solutions to (4.6.3) are known to be of the form

$$\phi_{S,0} = \alpha^+(x,t)Z(z')\mathrm{e}^{\mathrm{i}k'x'} + \alpha^+(x,t)Z(z')\mathrm{e}^{-\mathrm{i}k'x'} \tag{4.6.5}$$

with

$$\omega'^2 = k' \tanh(k')$$

The long scale functions $\alpha^{\pm}$ represent the amplitude of the modulation of the right and left going waves, and can for the moment be arbitrary. In order to get their

expressions, we need to proceed to the next order.

4.6.2 First order

Let us recall that we are interested in Bragg resonance for which

$$k'd' \sim \pi$$

which means that

$$\phi_{S,0}(d',y') = -\phi_{S,0}(-d',y'), \quad \left.\frac{\partial\phi_{S,0}}{\partial x'}\right|_{x'=-d'} = -\left.\frac{\partial\phi_{S,0}}{\partial x'}\right|_{x'=d'}, \quad \left.\frac{\partial\phi_{S,0}}{\partial y'}\right|_{y'=\pm d'} = 0$$

This also gives us boundary conditions on the lateral boundaries of the cell and allows us to proceed with this analysis. The first order problem of (4.6.1) is given by

$$\Delta'\phi_{S,1} = -2\frac{\partial^2\left[\alpha^+Z(z')\mathrm{e}^{\mathrm{i}k'x'} + \alpha^-Z(z')\mathrm{e}^{-\mathrm{i}k'x'}\right]}{\partial x\partial x'}, \qquad \boldsymbol{x}' \in \Omega_f \qquad (4.6.6a)$$

$$\left(\frac{\partial}{\partial z'} - \omega'^2\right)\phi_{S,1} = 2\mathrm{i}\omega'\frac{\partial\left[\alpha^+Z(z')\mathrm{e}^{\mathrm{i}k'x'} + \alpha^-Z(z')\mathrm{e}^{-\mathrm{i}k'x'}\right]}{\partial t}, \qquad \boldsymbol{x}' \in S_F \qquad (4.6.6b)$$

$$\frac{\partial\phi_{S,1}}{\partial z'} = -\frac{1}{\mu^2}\frac{\partial\left[\alpha^+Z(z')\mathrm{e}^{\mathrm{i}k'x'} + \alpha^-Z(z')\mathrm{e}^{-\mathrm{i}k'x'}\right]}{\partial z'}, \qquad \boldsymbol{x}' \in S_B \qquad (4.6.6c)$$

$$\frac{\partial\phi_{S,1}}{\partial z'} = 0, \qquad z' = -1 \qquad (4.6.6d)$$

$$\frac{\partial\phi_{S,1}}{\partial r'} = -\frac{1}{\mu^2}\frac{\partial\left[\alpha^+Z(z')\mathrm{e}^{\mathrm{i}k'x'} + \alpha^-Z(z')\mathrm{e}^{-\mathrm{i}k'x'}\right]}{\partial r'}, \qquad \boldsymbol{x}' \in S_W \qquad (4.6.6e)$$

together with the lateral boundary conditions:

$$\phi_{S,1}(d',y') = -\phi_{S,1}(-d',y'), \quad \left.\frac{\partial\phi_{S,1}}{\partial x'}\right|_{x'=-d'} = -\left.\frac{\partial\phi_{S,1}}{\partial x'}\right|_{x'=d'}, \quad \left.\frac{\partial\phi_{S,1}}{\partial y'}\right|_{y'=\pm d'} = 0$$

that come from the Bloch theorem. We see that now the boundary conditions on the surface of the buoy are of order μ^{-2}. As they are applied on surfaces of order μ^2, we can expect them to produce effects of order 1 all over the cell.

The usual way to get a solvability condition is to find a solution of the homogeneous problem and to apply Green's formula. This way, boundary conditions can be used

to simplify the surface integrals, and to get an equation that depends only on the solution of the leading order problem. In our case, it does not seem possible to do so without resorting to numerical solution. We can however follow Li and Mei (2007a,b) and look for an approximate inner solution in the neighborhood of the buoy (i.e. at a distance $O(a^*)$ from the buoy), and use this approximation in the solvability condition. This is done in Appendix E for a semi spherical buoy, but we note that even for a cylindrical buoy, we have

$$\frac{\partial \phi_{S,1}}{\partial n'} \sim \frac{\phi_{S,1}}{\mu} \gg \phi_{S,1} \tag{4.6.7}$$

in the neighborhood of the buoy, for which $r' \sim \mu$. Using (4.6.6c) and (4.6.6e), we know that

$$\frac{\partial \phi_{S,1}}{\partial n'} \sim \frac{1}{\mu^2} \tag{4.6.8a}$$

which gives us

$$\phi_{S,1} \sim \frac{1}{\mu} \tag{4.6.8b}$$

in the neighborhood of the buoy.

A solvability condition for $\phi_{S,1}$ can be obtained by applying Green's formula to $\phi_{S,1}$ and $Z(z')\exp(\pm \mathrm{i}k'x')$ over the volume of any cell Ω_f:

$$\begin{aligned}
\iiint_{\Omega_f} \left[\phi_{S,1}\Delta'(Z(z)\mathrm{e}^{\mp \mathrm{i}k'x'}) - Z(z')\mathrm{e}^{\mp \mathrm{i}k'x'}\Delta'\phi_{S,1}\right] \mathrm{d}V' = \\
- \iiint_{\Omega_f} \left[\boldsymbol{\nabla}'\phi_{S,1} \cdot \boldsymbol{\nabla}'(Z(z')\mathrm{e}^{\mp \mathrm{i}k'x'}) - \boldsymbol{\nabla}'(Z(z')\mathrm{e}^{\mp \mathrm{i}k'x'}) \cdot \boldsymbol{\nabla}'\phi_{S,1}\right] \mathrm{d}V' \\
+ \iint_{\partial\Omega_f} \left[\phi_{S,1}\frac{\partial Z(z')\mathrm{e}^{\mp \mathrm{i}k'x'}}{\partial n'} - Z(z')\mathrm{e}^{\mp \mathrm{i}k'x'}\frac{\partial \phi_{S,1}}{\partial n'}\right] \mathrm{d}S'
\end{aligned}$$

Using (4.6.6) we can rewrite this expression to

$$2\iiint_{\Omega_f} Z(z')\mathrm{e}^{\mp \mathrm{i}k'x'}\frac{\partial^2}{\partial x\partial x'}\left(\alpha^+ Z(z')\mathrm{e}^{\mathrm{i}k'x'}+\alpha^- Z(z')\mathrm{e}^{-\mathrm{i}k'x'}\right)\mathrm{d}V' =$$
$$-2\mathrm{i}\omega'\iint_{S_f} Z(z')\mathrm{e}^{\mp \mathrm{i}k'x'}\frac{\partial\left[\alpha^+ Z(z')\mathrm{e}^{\mathrm{i}k'x'}+\alpha^- Z(z')\mathrm{e}^{-\mathrm{i}k'x'}\right]}{\partial t}\mathrm{d}S'$$
$$+\frac{1}{\mu^2}\iint_{S_B\cup S_W} Z(z')\mathrm{e}^{\mp \mathrm{i}k'x'}\frac{\partial\left[\alpha^+ Z(z')\mathrm{e}^{\mathrm{i}k'x'}+\alpha^- Z(z')\mathrm{e}^{-\mathrm{i}k'x'}\right]}{\partial n'}\mathrm{d}S'$$
$$+\iint_{S_B\cup S_W}\phi_{S,1}\frac{\partial Z(z')\mathrm{e}^{\mp \mathrm{i}k'x'}}{\partial n'}\mathrm{d}S' \quad (4.6.9)$$

Using (4.6.8), we see that the last term can be dropped as it is or order μ whereas all other are of order 1. To the leading order, the left hand side of (4.6.9) can be simplified to

$$LHS(4.6.9) = \pm 2\mathrm{i}k'd'^2\frac{\partial\alpha^\pm}{\partial x}\int_{-1}^{0} Z(z')^2\,\mathrm{d}z' + O(\mu^3)$$

The integral over the free surface on the right hand side gives

$$I_{S_f} = -\frac{2d'^2}{\mathrm{i}\omega'}\frac{\partial\alpha^\pm}{\partial t} + O(\mu^2)$$

Concerning the integral on the surface of the buoy, we get [4]

$$I_1 \equiv \frac{1}{\mu^2}\iint_{S_B\cup S_W} Z(z')\mathrm{e}^{\mp \mathrm{i}k'x'}\frac{\partial\left[\alpha^+ Z(z')\mathrm{e}^{\mathrm{i}k'x'}+\alpha^- Z(z')\mathrm{e}^{-\mathrm{i}k'x'}\right]}{\partial n'}\mathrm{d}S'$$
$$= -\frac{1}{\mu^2}\iint_{S_W} Z(z')\mathrm{e}^{\pm \mathrm{i}k'x'}\left(\alpha^+\mathrm{i}k' Z(z')\mathrm{e}^{\mathrm{i}k'x'}+\alpha^-(-\mathrm{i}k')Z(z')\mathrm{e}^{-\mathrm{i}k'x'}\right)\boldsymbol{e}_r.\boldsymbol{e}_x\,\mathrm{d}S'$$
$$+\frac{1}{\mu^2}\iint_{S_B} Z(z')\mathrm{e}^{\pm \mathrm{i}k'x'}\left(\alpha^+\frac{\mathrm{d}Z(z')}{\mathrm{d}z'}\mathrm{e}^{\mathrm{i}k'x'}+\alpha^-\frac{\mathrm{d}Z(z')}{\mathrm{d}z'}\mathrm{e}^{-\mathrm{i}k'x'}\right)\mathrm{d}S'$$

Let us now make use of the fact that the buoy draft is $H' \sim \mu$ so

$$Z \approx \frac{1}{\mathrm{i}\omega'} \qquad \text{and} \qquad \frac{\mathrm{d}Z}{\mathrm{d}z'} \approx -\mathrm{i}\omega' \qquad \text{on} \qquad S_W \cup S_B \qquad (4.6.10)$$

[4] $\bar{r} = r^*/a^*$ and $\bar{z} = z^*/a^*$

which gives us

$$I_1 \approx -(\alpha^+ - \alpha^-) \int_0^{2\pi} \int_{-\bar{H}}^0 \mathrm{i}k' \cos(\theta)\, d\bar{z}\, \mathrm{d}\theta - (\alpha^+ + \alpha^-) \int_0^{2\pi} \int_0^1 \bar{r}\, \mathrm{d}\bar{r}\, \mathrm{d}\theta$$
$$\approx -\pi(\alpha^+ + \alpha^-)$$

so (4.6.9) gives

$$\frac{2d'^2}{\mathrm{i}\omega'} \frac{\partial \alpha^\pm}{\partial t} \pm 2\mathrm{i}k'd'^2 \frac{\partial \alpha^\pm}{\partial x} \int_{-1}^0 Z(z)^2\, \mathrm{d}z = -\pi \left(\alpha^+ + \alpha^-\right) + O(\mu)$$

or in simplified form

$$\boxed{\frac{\partial \alpha^\pm}{\partial t} \pm C_g' \frac{\partial \alpha^\pm}{\partial x} = -\mathrm{i}\Omega_0 \left(\alpha^+ + \alpha^-\right)} \tag{4.6.11}$$

with

$$\Omega_0 = \frac{\pi\omega'}{2d'^2} \qquad\qquad C_g' = \frac{\mathrm{d}\omega'}{\mathrm{d}k'} \tag{4.6.12}$$

Equation (4.6.11) can be rewritten in physical coordinates as

$$\frac{\partial \alpha^{*\pm}}{\partial t^*} \pm C_g^* \frac{\partial \alpha^{*\pm}}{\partial x^*} = -\mathrm{i}\frac{\omega^* a^{*2}}{2d^{*2}} \left(\alpha^{*+} + \alpha^{*-}\right) \tag{4.6.13}$$

This equation gives us the evolution of the wave amplitude inside an array of small buoys. We see that the waves in both directions are coupled. This is due to reflection, and is consistent with Li and Mei (2007a,b), Naciri and Mei (1988). We also see that the coupling term on the right hand side of the above equation is proportional to μ^2. This shows us that the scattering effects are of order μ^2, which is consistent with the study of a single buoy. We can also note that in the limit $\mu \to 0$, we find the usual equation for the wave amplitude.

***Remark* 4.6.1** (Comparison with Li and Mei (2007b)). *We find that the scattering effects are of the same order of magnitude as in Li and Mei (2007b) although the area of the surface of the bodies is smaller by a factor μ, which can be surprising. The*

difference is that in our case scattering effect come from the bottom of the buoy, that is not present in the case of vertical piles extending to the bottom of the sea. In the case of piles, in the equivalent of integral I_1 the leading order term of the integrand gave a zero contribution, and so the relevant integrand was order μ, which compensates with the area of the lateral surface of the buoy (which is of order μ) and the factor $1/\mu^2$ to give an order 1 term in the solvability condition.

4.6.3 Long scale dispersion relation and band gap

Let us consider the envelope modification by an infinite array, and let us look for long scale amplitudes such that

$$\alpha^{\pm} \propto \mathrm{e}^{\mathrm{i}(\pm K_S x - \Omega t)}$$

that is to say that we consider waves that are slightly detuned from Bragg resonance. Equation (4.6.11) gives:

$$\begin{aligned} -\mathrm{i}\left(\Omega - C_g' K_S\right)\alpha^+ &= -\mathrm{i}\Omega_0\left(\alpha^+ + \alpha^-\right) \\ -\mathrm{i}\left(\Omega + C_g' K_S\right)\alpha^+ &= -\mathrm{i}\Omega_0\left(\alpha^+ + \alpha^-\right) \end{aligned}$$

This system has non zero solutions under the condition:

$$\begin{vmatrix} \Omega - \Omega_0 - C_g' K_S & -\Omega_0 \\ -\Omega_0 & \Omega - \Omega_0 + C_g' K_S \end{vmatrix} = 0$$

This gives us the following dispersion relation:

$$C_g'^2 K_S^2 = \Omega(\Omega - 2\Omega_0) \tag{4.6.14}$$

which is represented in figure 4-8(a). For $\Omega \in \mathbb{R}$ we can distinguish 3 regions:

- $\Omega \leq 0$, which means that the frequency of the incoming wave is slightly smaller than the frequency of Bragg scattering. In this case K_S is real, so we have propagating waves.

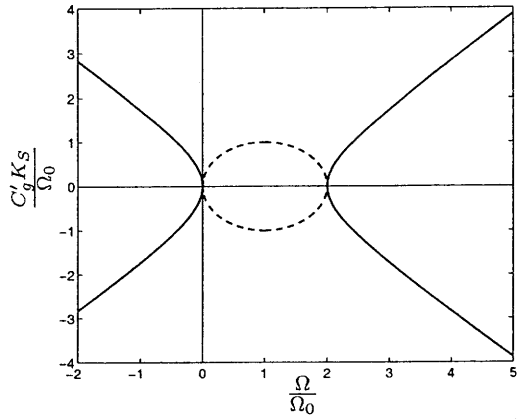

(a) Dispersion relation for the envelope. Real values are plotted in solid lines, and imaginary values in dashed line.

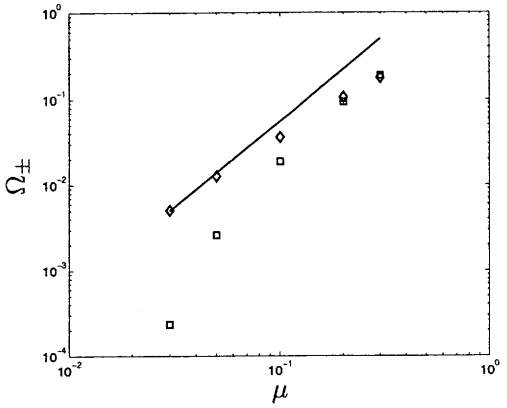

(b) Limits of the band gap obtained by the Finite Element Method. $\Omega_\pm$ are respectively represented by the diamonds and the squares, and the solid line represents the upper bound found by multiple scale analysis, $2\mu^2\Omega_0$. $d' = 1$

Figure 4-8: Dispersion in an infinite periodic array

- $0 \leq \Omega \leq 2\Omega_0$: K_S is now imaginary, which means that no traveling wave can be present. The imaginary part of K_S, that characterizes the rate of decay of the wave amplitude, is maximum for $\Omega = \Omega_0$.
- $2\Omega_0 \leq \Omega$: propagation is possible again.

***Remark* 4.6.2.** *Without the presence of the buoys, $K_S \to K = \Omega/C_g'$. The long scale dispersion relation would be*

$$C_g' K = \Omega$$

from the dispersion relation, which is the limit of (4.6.14) *as the presence of the buoys becomes negligible. This is also the limit of the dispersion relation as $|\Omega| \gg |\Omega_0|$. This is consistent with the fact that away from Bragg resonance the scattering effects are not significant and the interaction between buoys is negligible.*

In terms of the short scale coordinates, which are independent of the size of the buoys, the band gap width varies like μ^2. Numerical results for the band gap limits $\Omega_\pm$ obtained as described in §4.5 are represented in figure 4-8(b) together with the result of multiple scales. We note a good agreement between the two approaches.

As we mentioned in §4.5.2, Li and Mei (2007b) showed that for the propagation of a surface wave in an infinite array of vertical piles, the band gap extends in the range

$$\omega_0' - 2\pi^2\mu^2\Omega_0^c \leq \omega' \leq \omega_0' + \pi^2\mu^2\Omega_0^c$$

where Ω_0^c is defined in (4.5.8). The order of magnitude of the width of the band gap is the same, but in the case of buoys the band gap is defined by

$$\omega_0' \leq \omega' \leq \omega_0' + 2\mu^2\Omega_0$$

This difference in the location of the band gap is due to the fact that whereas reflection was caused by the lateral surface of the cylinder in the case of piles, it is due to the vertical surface in the case of buoys.

4.6.4 Scattering by an array of finite width

Potential outside the array and matching conditions

Let us consider the situation of a finite array of length $L \sim 1$. Equations (4.6.11) gives us two coupled first order partial differential equations. In order to solve them, we need to find the appropriate boundary conditions. These will come from the matching with the outer region and will couple the flow inside the array to the excitation by an incoming wave.

Let us assume that the array is excited by an incoming wave slightly detuned from Bragg resonance and of unit amplitude, that is to say

$$\phi_{in} = Z(z')\mathrm{e}^{\mathrm{i}k'x'}\mathrm{e}^{\mathrm{i}(Kx-\Omega t)}$$

with

$$K \equiv C_g'\Omega$$

We will only focus on the time harmonic response so we can factor out the slow time

dependency $\exp(-\mathrm{i}\Omega t)$ by writing

$$\alpha^{\pm}(x,t) = \widehat{\alpha}^{\pm}(x)\mathrm{e}^{-\mathrm{i}\Omega t} \tag{4.6.15}$$

With this assumption, we can write the scattering potential outside of the array as

$$\begin{aligned} \phi_{S,0} &= \left(Z(z')\mathrm{e}^{\mathrm{i}k'x'}\mathrm{e}^{\mathrm{i}Kx} + RZ(z')\mathrm{e}^{-\mathrm{i}k'x'}\mathrm{e}^{-\mathrm{i}Kx}\right)\mathrm{e}^{-\mathrm{i}\Omega t}, \quad x' < 0 \\ \phi_{S,0} &= TZ(z')\mathrm{e}^{\mathrm{i}k'(x'-L)}\mathrm{e}^{\mathrm{i}Kx}\mathrm{e}^{-\mathrm{i}\Omega t}, \qquad\qquad\qquad\quad x' > L \end{aligned} \tag{4.6.16}$$

The complex coefficients R and T introduced above are respectively called reflection and transmission coefficients. Let us now express that the horizontal velocity and the pressure should be continuous at the limits of the array. Note that to the leading order, the velocity is given by the short scale derivative in the x direction, so we must have

$$\phi_{S,0}\left(0^{-}\right) = \phi_{S,0}\left(0^{+}\right) \qquad \phi_{S,0}\left(L^{-}\right) = \phi_{S,0}\left(L^{+}\right) \tag{4.6.17a}$$

$$\left.\frac{\partial\phi_{S,0}}{\partial x'}\right|_{0^{-}} = \left.\frac{\partial\phi_{S,0}}{\partial x'}\right|_{0^{+}} \qquad \left.\frac{\partial\phi_{S,0}}{\partial x'}\right|_{L^{-}} = \left.\frac{\partial\phi_{S,0}}{\partial x'}\right|_{L^{+}} \tag{4.6.17b}$$

As the dependency of the potentials with the long time and the depth are the same everywhere, (4.6.17) will give us boundary conditions for $\widehat{\alpha}^{\pm}(x)$. We see that we introduced 2 new scalar unknowns, the reflection and transmission coefficients, but (4.6.17) gives us 4 equations, so the matching the problem can in general be solved uniquely. Let us now express the matching explicitly. Recall first that the potentials inside the array are given by

$$\phi_{S,0} = \left(\widehat{\alpha}^{+}\mathrm{e}^{\mathrm{i}k'x'} + \widehat{\alpha}^{-}\mathrm{e}^{-\mathrm{i}k'x'}\right)\mathrm{e}^{-\mathrm{i}\Omega t} \tag{4.6.18}$$

Boundary conditions for the scattering problem

Using (4.6.16) and (4.6.18), we find that

$$\begin{aligned}
\phi_{S,0}\left(0^-\right) &= (1+R)\,\mathrm{e}^{-\mathrm{i}\Omega t} & \phi_{S,0}\left(0^+\right) &= \left(\widehat{\alpha}^+(0)+\widehat{\alpha}^-(0)\right)\mathrm{e}^{-\mathrm{i}\Omega t} \\
\phi_{S,0}\left(L^-\right) &= \left(\widehat{\alpha}^+(L)+\widehat{\alpha}^-(L)\right)\mathrm{e}^{-\mathrm{i}\Omega t} & \phi_{S,0}\left(L^+\right) &= T\mathrm{e}^{-\mathrm{i}\Omega t} \\
\left.\frac{\partial\phi_{S,0}}{\partial x'}\right|_{0^-} &= (1-R)\,\mathrm{e}^{-\mathrm{i}\Omega t} & \left.\frac{\partial\phi_{S,0}}{\partial x'}\right|_{0^+} &= \left(\widehat{\alpha}^+(0)-\widehat{\alpha}^-(0)\right)\mathrm{e}^{-\mathrm{i}\Omega t} \\
\left.\frac{\partial\phi_{S,0}}{\partial x'}\right|_{L^-} &= \left(\widehat{\alpha}^+(L)-\widehat{\alpha}^-(L)\right)\mathrm{e}^{-\mathrm{i}\Omega t} & \left.\frac{\partial\phi_{S,0}}{\partial x'}\right|_{L^+} &= T\mathrm{e}^{-\mathrm{i}\Omega t}
\end{aligned}$$

so (4.6.17) gives

$$1+R=\widehat{\alpha}^+(0)+\widehat{\alpha}^-(0) \qquad T=\widehat{\alpha}^+(L)+\widehat{\alpha}^-(L) \tag{4.6.19a}$$

$$1-R=\widehat{\alpha}^+(0)-\widehat{\alpha}^-(0) \qquad T=\widehat{\alpha}^+(L)-\widehat{\alpha}^-(L) \tag{4.6.19b}$$

It follows that

$$\widehat{\alpha}^-(L)=0, \quad \widehat{\alpha}^+(0)=1 \tag{4.6.20}$$

Solution

Differentiating (4.6.11), we can see that the amplitudes $\widehat{\alpha}^\pm$ satisfy the following uncoupled second order ODEs

$$\frac{\mathrm{d}^2\widehat{\alpha}^+}{\mathrm{d}x^2}+K_S^2\alpha^+=0 \tag{4.6.21a}$$

$$\frac{\mathrm{d}^2\widehat{\alpha}^-}{\mathrm{d}x^2}+K_S^2\alpha^-=0 \tag{4.6.21b}$$

with

$$\Omega_S\equiv\sqrt{\Omega(\Omega-2\Omega_0)} \qquad\qquad K_S\equiv\frac{\Omega_S}{C_g'}$$

which shows us that

$$\widehat{\alpha}^\pm=C_1^\pm\cos(K_Sx)+C_2^\pm\sin(K_Sx)$$

The coefficients $C_1^{\pm}$ and $C_2^{\pm}$ can be found using the coupling between between $\widehat{\alpha}^+$ and $\widehat{\alpha}^-$ and the boundary conditions. We find that the solutions to (4.6.11) and (4.6.20) are given by

$$\widehat{\alpha}^+(x) = \frac{\mathrm{i}(\Omega - \Omega_0)\sin(K_S(x-L))) + \Omega_S \cos(K_S(x-L))}{-\mathrm{i}(\Omega - \Omega_0)\sin(K_S L) + \Omega_S \cos(K_S L)} \tag{4.6.22a}$$

$$\widehat{\alpha}^-(x) = \frac{\mathrm{i}\Omega_0 \sin(K_S(x-L))}{-\mathrm{i}(\Omega - \Omega_0)\sin(K_S L) + \Omega_S \cos(K_S L)} \tag{4.6.22b}$$

This allows us to get the transmission and reflection coefficients:

$$T = \frac{\Omega_S}{-\mathrm{i}(\Omega - \Omega_0)\sin(K_S L) + \Omega_S \cos(K_S L)} \tag{4.6.23a}$$

$$R = \frac{-\mathrm{i}\Omega_0 \sin(K_S L)}{-\mathrm{i}(\Omega - \Omega_0)\sin(K_S L) + \Omega_S \cos(K_S L)} \tag{4.6.23b}$$

These results are represented in figure 4-9. We see that reflection and scattering coefficients depend strongly on the detuning. Away from Bragg resonance, the scattering effects of the array are weak, as $R \to 0$ and $T \to 1$. In §4.5 and §4.6.3, we saw that propagation is not possible in an infinite array within the band gap, $0 \leq \Omega \leq \Omega_0$. In the case of a finite array, these frequencies are characterized by a very strong scattering. We see that in this range of frequencies the reflection coefficient becomes close to 1: the wave is reflected because it can not propagate through the array. The difference between frequencies inside and outside the band gap in terms of free surface displacement is shown in figure 4-9(c-d): we clearly see that $|\eta|$ has an oscillatory behavior for $\Omega = -2\Omega_0$ whereas it decays exponentially in x for $\Omega = \Omega_0$.

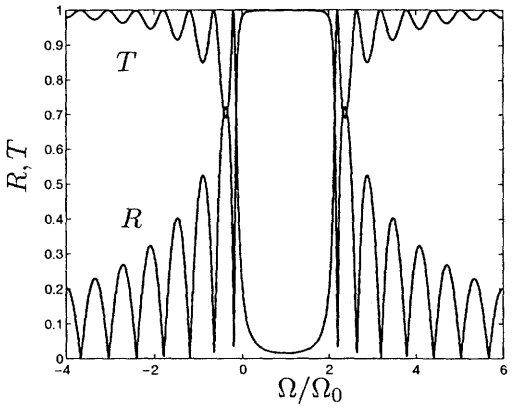

(a) Reflection and transmission coefficients for $L = 1/2$

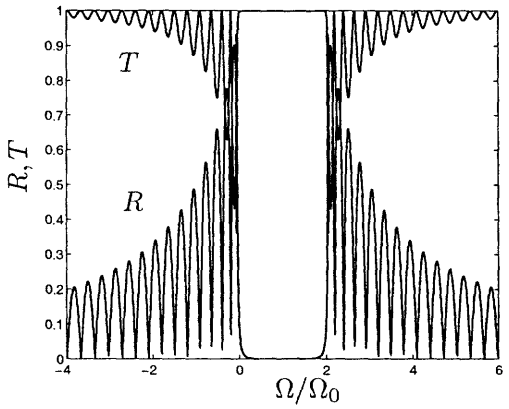

(b) Reflection and transmission coefficients for $L = 1$

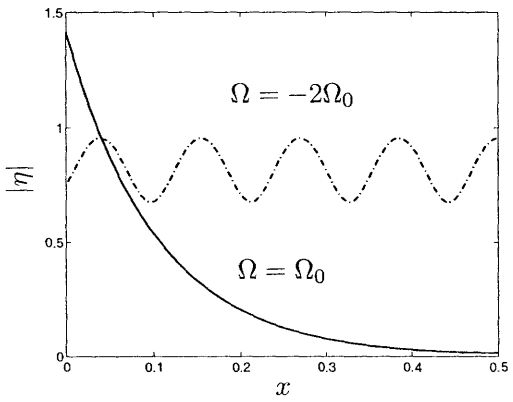

(c) Free surface elevation for $L = 1/2$

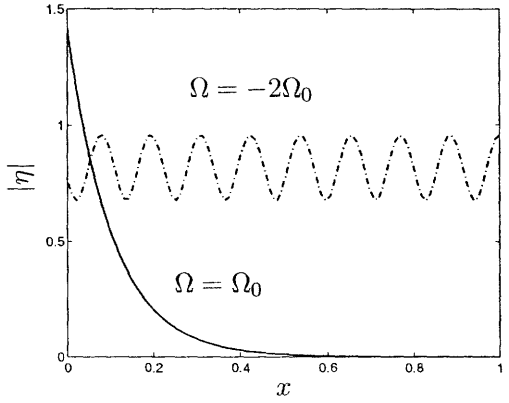

(d) Free surface elevation for $L = 1$

Figure 4-9: Scattering by a finite array of length L around Bragg resonance. $d' = 1$

4.7 Multiple scales analysis of the radiation problem

In this section, the objective it to obtain the flow generated by the movement of buoys. As we consider Bragg resonance, the wave length is such that if one buoy goes up then its neighbors will go down, and the amplitude of displacement will be a slowly varying function. The displacement of the n^{th} buoy can therefore be expressed as

$$\zeta_n = (-1)^n \zeta(x,t) \tag{4.7.1}$$

where ζ depends on the long scale coordinates. As the center of the n^{th} buoy is located at $x'_n = nd'$, we can re-express the term $(-1)^n$ as

$$(-1)^n = \mathrm{e}^{\mathrm{i}k'x_n}$$

as $k'\pi$. This exponential does not have the meaning of a traveling wave, but is only here to take into account the fact that we consider frequencies close to Bragg resonance. This allows us to express the radiation problem as

$$\begin{aligned}
\left(\Delta' + 2\mu^2 \frac{\partial^2}{\partial x \partial x'} + \mu^4 \Delta\right)\left(\phi_{R,0} + \mu^2 \phi_{R,1} + ...\right) &= 0, && \boldsymbol{x}' \in \Omega_f \\
\left(\frac{\partial}{\partial z'} - \omega'^2 - 2\mu^2 \mathrm{i}\omega' \frac{\partial}{\partial t} - \mu^4 \frac{\partial^2}{\partial t^2}\right)\left(\phi_{R,0} + \mu^2 \phi_{R,1} + ...\right) &= 0, && \boldsymbol{x}' \in S_F \\
\frac{\partial}{\partial z'}\left(\phi_{R,0} + \mu^2 \phi_{R,1} + ...\right) &= -\mathrm{i}\omega' \zeta \mathrm{e}^{\mathrm{i}k'x'_n}, && \boldsymbol{x}' \in S_B^{(n)} \\
\frac{\partial}{\partial z'}\left(\phi_{R,0} + \mu^2 \phi_{R,1} + ...\right) &= 0, && z' = -1 \\
\left(\frac{\partial}{\partial r'} + \mu^2 \frac{\partial}{\partial r}\right)\left(\phi_{R,0} + \mu^2 \phi_{R,1} + ...\right) &= 0, && \boldsymbol{x}' \in S_W^{(n)}
\end{aligned} \tag{4.7.2}$$

where $S_B^{(n)}$ and $S_W^{(n)}$ are respectively the bottom and lateral boundaries of the n^{th} buoy. From (4.7.2), we see that the zeroth order problem is the same as for the

scattering problem, so let us write the zeroth order solution as

$$\phi_{R,0} = \beta^+(x,t)Z(z')\mathrm{e}^{\mathrm{i}k'x'} + \beta^-(x,t)Z(z')\mathrm{e}^{-\mathrm{i}k'x'} \tag{4.7.3}$$

As before, the long scale functions $\beta^{\pm}$ represent the unknown amplitudes of the waves. The first order problem is

$$\Delta'\phi_{R,1} = -2\frac{\partial^2\left[\beta^+Z(z')\mathrm{e}^{\mathrm{i}k'x'} + \beta^-Z(z')\mathrm{e}^{-\mathrm{i}k'x'}\right]}{\partial x\partial x'}, \qquad \boldsymbol{x}' \in \Omega_f \quad (4.7.4a)$$

$$\left(\frac{\partial}{\partial z'} - \omega'^2\right)\phi_{R,1} = 2\mathrm{i}\omega' Z(z')\frac{\partial\left[\beta^+\mathrm{e}^{\mathrm{i}k'x'} + \beta^-\mathrm{e}^{-\mathrm{i}k'x'}\right]}{\partial t}, \qquad \boldsymbol{x}' \in S_F \quad (4.7.4b)$$

$$\frac{\partial\phi_{R,1}}{\partial z'} = \frac{-\mathrm{i}\omega'\zeta\mathrm{e}^{\mathrm{i}k'x'_n}}{\mu^2} - \frac{1}{\mu^2}\left[\beta^+\mathrm{e}^{\mathrm{i}k'x'} + \beta^-\mathrm{e}^{-\mathrm{i}k'x'}\right]\frac{\mathrm{d}Z}{\mathrm{d}z'}, \qquad \boldsymbol{x}' \in S_B^{(n)} \quad (4.7.4c)$$

$$\frac{\partial\phi_{R,1}}{\partial z'} = 0, \qquad z' = -1 \quad (4.7.4d)$$

$$\frac{\partial\phi_{R,1}}{\partial r'} = -\frac{1}{\mu^2}Z(z')\frac{\partial\left[\beta^+\mathrm{e}^{\mathrm{i}k'x'} + \beta^-\mathrm{e}^{-\mathrm{i}k'x'}\right]}{\partial r'}, \qquad \boldsymbol{x}' \in S_W^{(n)} \quad (4.7.4e)$$

Note that as the buoys radii and drafts are of order μ, we have $x' = x'_n + O(\mu)$ for $\boldsymbol{x}' \in S_W^{(n)} \cup S_B^{(n)}$. The problem (4.7.4) is similar to the scattering problem, except for the addition of the term

$$\frac{\mathrm{i}\omega'\zeta\mathrm{e}^{\mathrm{i}k'x'_n}}{\mu^2}$$

in (4.7.4c). It expresses the fact that the vertical velocity of the flow must be equal to the velocity of the buoy.

As we did for the scattering problem, the solvability condition for $\phi_{R,1}$ can be obtained by applying Green's formula to $\phi_{R,1}$ and $Z(z')\exp(\pm\mathrm{i}k'x')$ over Ω_f:

$$\begin{aligned}\iiint_{\Omega_f}\left[\phi_{R,1}\Delta'(Z(z)\mathrm{e}^{\mp\mathrm{i}k'x'}) - Z(z')\mathrm{e}^{\mp\mathrm{i}k'x'}\Delta'\phi_{R,1}\right]\mathrm{d}V' = \\ -\iiint_{\Omega_f}\left[\boldsymbol{\nabla}'\phi_{R,1}\cdot\boldsymbol{\nabla}'(Z(z')\mathrm{e}^{\mp\mathrm{i}k'x'}) - \boldsymbol{\nabla}'(Z(z')\mathrm{e}^{\mp\mathrm{i}k'x'})\cdot\boldsymbol{\nabla}'\phi_{R,1}\right]\mathrm{d}V' \\ +\iint_{\partial\Omega_f}\left[\phi_{R,1}\frac{\partial Z(z')\mathrm{e}^{\mp\mathrm{i}k'x'}}{\partial n'} - Z(z')\mathrm{e}^{\mp\mathrm{i}k'x'}\frac{\partial\phi_{R,1}}{\partial n'}\right]\mathrm{d}S' \end{aligned} \tag{4.7.5}$$

Equation (4.7.4) allows us to rewrite (4.7.5) as

$$
\begin{aligned}
2\iiint_{\Omega_f} Z(z')\mathrm{e}^{\mp \mathrm{i}k'x'}\frac{\partial^2}{\partial x\partial x'}\left(\beta^+ Z(z')\mathrm{e}^{\mathrm{i}k'x'}+\beta^- Z(z')\mathrm{e}^{-\mathrm{i}k'x'}\right)\mathrm{d}V' = \\
-2\mathrm{i}\omega'\iint_{S_f} Z(z')\mathrm{e}^{\mp \mathrm{i}k'x'}\frac{\partial\left[\beta^+ Z(z')\mathrm{e}^{\mathrm{i}k'x'}+\beta^- Z(z')\mathrm{e}^{-\mathrm{i}k'x'}\right]}{\partial t}\mathrm{d}S' \\
+\frac{1}{\mu^2}\iint_{S_B\cup S_W} Z(z')\mathrm{e}^{\mp \mathrm{i}k'x'}\frac{\partial\left[\beta^+ Z(z')\mathrm{e}^{\mathrm{i}k'x'}+\beta^- Z(z')\mathrm{e}^{-\mathrm{i}k'x'}\right]}{\partial n'}\mathrm{d}S' \\
-\frac{1}{\mu^2}\iint_{S_B} Z(z')\mathrm{e}^{\mp \mathrm{i}k'x'}\mathrm{i}\omega'\zeta\mathrm{e}^{\mathrm{i}k'x'}\,\mathrm{d}S' + \iint_{S_B\cup S_W}\phi_{R,1}\frac{\partial Z(z')\mathrm{e}^{\mp \mathrm{i}k'x'}}{\partial n'}\mathrm{d}S' \qquad (4.7.6)
\end{aligned}
$$

In this, we made use of the fact that the radius of the buoy is $\mu \ll 1$, so $x'_n \approx x'$. As we had for the scattering potential

$$\frac{\partial\phi_{R,1}}{\partial n'} \sim \frac{\phi_{R,1}}{\mu} \gg \phi_{R,1} \qquad (4.7.7)$$

in the neighborhood of the buoy. Using the boundary condition on the surface of the body, we find

$$\frac{\partial\phi_{R,1}}{\partial n'} \sim \frac{1}{\mu^2} \qquad (4.7.8a)$$

which gives us

$$\phi_{R,1} \sim \frac{1}{\mu} \qquad (4.7.8b)$$

on the surface of the buoy. This allows us to see that the last term in (4.7.6) can be dropped as it is smaller than all other terms by a factor μ. The left hand side of (4.7.6) can be rewritten as

$$LHS(4.7.6) = \pm 2\mathrm{i}k'd'^2\frac{\partial\beta^\pm}{\partial x}\int_{-1}^{0} Z(z')^2\,\mathrm{d}z' + O(\mu^3)$$

The integral over the free surface gives

$$I_{S_f} = -\frac{2d'^2}{\mathrm{i}\omega'}\frac{\partial\beta^\pm}{\partial t} + O(\mu^2)$$

and finally the integral on the surface of the buoy gives

$$\begin{aligned}
I_1 \equiv & \frac{1}{\mu^2}\iint_{S_B\cup S_W} Z(z')\mathrm{e}^{\mp \mathrm{i}k'x'}\frac{\partial\left[\beta^+ Z(z')\mathrm{e}^{\mathrm{i}k'x'}+\beta^- Z(z')\mathrm{e}^{-\mathrm{i}k'x'}\right]}{\partial n'}\,\mathrm{d}S' \\
& -\frac{1}{\mu^2}\iint_{S_B} Z(z')\mathrm{e}^{\mp \mathrm{i}k'x'}\mathrm{i}\omega'\zeta\mathrm{e}^{\mathrm{i}k'x'}\,\mathrm{d}S' \\
= & -\frac{1}{\mu^2}\iint_{S_W} Z(z')\mathrm{e}^{\pm \mathrm{i}k'x'}\left(\mathrm{i}k'Z(z')\mathrm{e}^{\mathrm{i}k'x'}\beta^+ + \beta^-(-\mathrm{i}k')Z(z')\mathrm{e}^{-\mathrm{i}k'x'}\right)\boldsymbol{e}_r.\boldsymbol{e}_x\,\mathrm{d}S' \\
& +\frac{1}{\mu^2}\iint_{S_B} Z(z')\mathrm{e}^{\pm \mathrm{i}k'x'}\left(\beta^+\frac{\mathrm{d}Z(z')}{\mathrm{d}z'}\mathrm{e}^{\mathrm{i}k'x'}+\beta^-\frac{\mathrm{d}Z(z')}{\mathrm{d}z'}\mathrm{e}^{-\mathrm{i}k'x'}\right)\mathrm{d}S' \\
& -\frac{1}{\mu^2}\iint_{S_B} Z(z')\mathrm{e}^{\mp \mathrm{i}k'x'}\mathrm{i}\omega'\zeta\mathrm{e}^{\mathrm{i}k'x'}\,\mathrm{d}S'
\end{aligned}$$

Using (4.6.10), we finally get

$$\begin{aligned}
I_1 &\approx -(\beta^+-\beta^-)\int_0^{2\pi}\int_{-\bar{H}}^0 \mathrm{i}k'\cos(\theta)\,d\bar{z}\,\mathrm{d}\theta - (\beta^++\beta^--\zeta)\int_0^{2\pi}\int_0^1 \bar{r}\,\mathrm{d}\bar{r}\,\mathrm{d}\theta \\
&\approx -\pi(\beta^++\beta^--\zeta)
\end{aligned}$$

This finally gives us the long scale equations

$$\frac{2d'^2}{\mathrm{i}\omega'}\frac{\partial\beta^\pm}{\partial t}\pm 2\mathrm{i}k'd'^2\frac{\partial\beta^\pm}{\partial x}\int_{-1}^0 Z(z)^2\,\mathrm{d}z = -\pi\left(\beta^++\beta^--\zeta\right)+O(\mu)$$

that is to say:

$$\boxed{\frac{\partial\beta^\pm}{\partial t}\pm C_g'\frac{\partial\beta^\pm}{\partial x} = -\mathrm{i}\Omega_0\left(\beta^++\beta^--\zeta\right)} \tag{4.7.9}$$

where Ω_0 was defined in (4.6.12). In terms of the physical coordinates, (4.7.9) gives

$$\frac{\partial\beta^{*\pm}}{\partial t^*}\pm C_g^*\frac{\partial\beta^{*\pm}}{\partial x^*} = -\mathrm{i}\frac{\omega^*a^{*2}}{2d^{*2}}\left(\beta^{*+}+\beta^{*-}-\zeta^{*-}\right) \tag{4.7.10}$$

These two equations express the coupling between the amplitude of the right- and left-going waves and the unknown buoy motion. As it was the case for scattering, the coupling is still of order μ^2. Equation (4.7.9) also expresses how radiation will be forced by the movement of the buoys, given by ζ. Let us now express that the buoy displacement is induced by the waves, in order to relate ζ to $\alpha^\pm$ and $\beta^\pm$ in (4.7.9).

4.7.1 Buoy dynamics

The forcing term ζ in the long scale equation for the radiation problem is for the moment unknown. Let us relate it to the scattering and radiation potentials, that are respectively given by

$$\phi_{S,0} = \alpha^+ \mathrm{e}^{\mathrm{i}k'x'} + \alpha^- \mathrm{e}^{-\mathrm{i}k'x'} \qquad \phi_{R,0} = \beta^+ \mathrm{e}^{\mathrm{i}k'x'} + \beta^- \mathrm{e}^{-\mathrm{i}k'x'}$$

according to the results of the previous sections. The hydrodynamic forces applied to a buoy by these potentials to the n^{th} buoy are given by

$$F_{zD}^{(n)} = \mathrm{i}\omega' \iint_{S_B^{(n)}} \phi_{S,0}\, \mathrm{d}S = \mathrm{i}\pi\mu^2\omega' \frac{(-1)^n}{\mathrm{i}\omega'} \left(\alpha^+ + \alpha^-\right)$$
$$F_{zz}^{(n)} = \mathrm{i}\omega' \iint_{S_B^{(n)}} \phi_{R,0}\, \mathrm{d}S = \mathrm{i}\pi\mu^2\omega' \frac{(-1)^n}{\mathrm{i}\omega'} \left(\beta^+ + \beta^-\right)$$

where the forces are normalized in the following way:

$$F_{zD}^{(n)^*} = \rho^* g^* h^{*2} A^* F_{zD}^{(n)}$$

As before, let us assume that the energy extraction device applies a force $-\lambda_g \dot{\zeta}$ to the buoys. Applying Newton's law to a buoy, we get

$$-M^* \omega^{*2} \zeta_n^* = F_{zD}^{(n)^*} + F_{zz}^{(n)^*} + \mathrm{i}\omega^* \lambda_g^* \zeta_n^* - \pi\rho^* g^* a^{*2} \zeta_n^* \tag{4.7.11}$$

As $M^* = \rho^* \pi a^{*2} H^*$, (4.7.11) can be rewritten as

$$-\rho^* \pi a^{*2} H^* \frac{g^*}{h^*} A^* \omega'^2 = \rho^* g^* h^{*2} A^* \left(F_{zD}^{(n)} + F_{zz}^{(n)}\right) - \mathrm{i}\sqrt{\frac{g^*}{h^*}} \pi\rho^* a^{*2} \sqrt{g^* h^*} A^* \omega' \lambda_g \zeta_n - \pi\rho^* g^* a^{*2} A^* \zeta_n \tag{4.7.12}$$

where the damping rate is normalized in the same way as for a compact array, i.e.

$$\lambda_g \equiv \frac{\lambda_g^*}{\pi\rho^* a^{*2} \sqrt{g^* h^*}}$$

This gives us in dimensionless form

$$-\omega'^2\mu^3\pi\bar{H}\zeta(-1)^n = \pi\mu^2\left(\alpha^+ + \alpha^-\right)(-1)^n + \pi\mu^2\left(\beta^+ + \beta^-\right)(-1)^n + \mathrm{i}\pi\omega'\mu^2\zeta(-1)^n\lambda_g - \pi\mu^2\zeta(-1)^n \quad (4.7.13)$$

We see that the mass of the buoy can be ignored in (4.7.13), which gives

$$\zeta = \frac{1}{1-\mathrm{i}\omega'\lambda_g}\left[\left(\alpha^+ + \alpha^-\right) + \left(\beta^+ + \beta^-\right)\right] \quad (4.7.14)$$

For brevity, we shall introduce

$$\mathcal{G} \equiv \frac{1}{1-\mathrm{i}\omega'\lambda_g} \quad (4.7.15)$$

Using (4.7.14) we can rewrite (4.7.9) as:

$$\begin{aligned}\frac{\partial\beta^+}{\partial t} + C_g'\frac{\partial\beta^+}{\partial x} &= -\mathrm{i}\Omega_0\left[(1-\mathcal{G})(\beta^+ + \beta^-) - \mathcal{G}(\alpha^+ + \alpha^-)\right]\\ \frac{\partial\beta^-}{\partial t} - C_g'\frac{\partial\beta^-}{\partial x} &= -\mathrm{i}\Omega_0\left[(1-\mathcal{G})(\beta^+ + \beta^-) - \mathcal{G}(\alpha^+ + \alpha^-)\right]\end{aligned} \quad (4.7.16)$$

that express the coupling between radiation and scattering. The scattering potential has been derived in the previous section, and acts as forcing term.

4.7.2 Radiation in an array of finite width

Potential outside the array and matching conditions

Let us consider again the situation of a finite array of length $L \sim 1$. As we did for scattering, let us consider the time harmonic response so we can factor out the slow time dependency $\exp(-\mathrm{i}\Omega t)$

$$\beta^\pm(x,t) = \widehat{\beta}^\pm(x)\mathrm{e}^{-\mathrm{i}\Omega t} \quad (4.7.17)$$

Using the radiation condition, the potential outside of the array as

$$\begin{aligned} \phi_{R,0} &= C_L Z(z') \mathrm{e}^{-\mathrm{i}k'x'} \mathrm{e}^{-\mathrm{i}Kx} \mathrm{e}^{-\mathrm{i}\Omega t}, \qquad x' < 0 \\ \phi_{R,0} &= C_R Z(z') \mathrm{e}^{\mathrm{i}k'(x'-L)} \mathrm{e}^{-\mathrm{i}Kx} \mathrm{e}^{-\mathrm{i}\Omega t}, \quad x' > L \end{aligned} \tag{4.7.18}$$

for some unknown complex coefficients C_R and C_L. As before, continuity of the potential and its $x-$ derivative gives

$$\phi_{R,0}\left(0^-\right) = \phi_{R,0}\left(0^+\right) \qquad \phi_{R,0}\left(L^-\right) = \phi_{R,0}\left(L^+\right) \tag{4.7.19a}$$

$$\left.\frac{\partial \phi_{R,0}}{\partial x'}\right|_{0^-} = \left.\frac{\partial \phi_{R,0}}{\partial x'}\right|_{0^+} \qquad \left.\frac{\partial \phi_{R,0}}{\partial x'}\right|_{L^-} = \left.\frac{\partial \phi_{R,0}}{\partial x'}\right|_{L^+} \tag{4.7.19b}$$

Let us recall that inside the array we have

$$\phi_{R,0} = \left(\widehat{\beta}^+ \mathrm{e}^{\mathrm{i}k'x'} + \widehat{\beta}^- \mathrm{e}^{-\mathrm{i}k'x'}\right) \mathrm{e}^{-\mathrm{i}\Omega t} \tag{4.7.20}$$

Boundary conditions for the scattering problem

Using (4.7.18) and (4.7.20), we find that

$$\begin{aligned} \phi_{R,0}\left(0^-\right) &= C_L \mathrm{e}^{-\mathrm{i}\Omega t} & \phi_{R,0}\left(0^+\right) &= \left(\widehat{\beta}^+(0) + \widehat{\beta}^-(0)\right) \mathrm{e}^{-\mathrm{i}\Omega t} \\ \phi_{R,0}\left(L^-\right) &= \left(\widehat{\beta}^+(L) + \widehat{\beta}^-(L)\right) \mathrm{e}^{-\mathrm{i}\Omega t} & \phi_{R,0}\left(L^+\right) &= C_R \mathrm{e}^{-\mathrm{i}\Omega t} \\ \left.\frac{\partial \phi_{R,0}}{\partial x'}\right|_{0^-} &= -C_L \mathrm{e}^{-\mathrm{i}\Omega t} & \left.\frac{\partial \phi_{R,0}}{\partial x'}\right|_{0^+} &= \left(\widehat{\beta}^+(0) - \widehat{\beta}^-(0)\right) \mathrm{e}^{-\mathrm{i}\Omega t} \\ \left.\frac{\partial \phi_{R,0}}{\partial x'}\right|_{L^-} &= \left(\widehat{\beta}^+(L) - \widehat{\beta}^-(L)\right) \mathrm{e}^{-\mathrm{i}\Omega t} & \left.\frac{\partial \phi_{S,0}}{\partial x'}\right|_{L^+} &= C_R \mathrm{e}^{-\mathrm{i}\Omega t} \end{aligned}$$

so (4.7.19) gives

$$\begin{aligned} C_L &= \widehat{\beta}^+(0) + \widehat{\beta}^-(0) & C_R &= \widehat{\beta}^+(L) + \widehat{\beta}^-(L) \\ -C_L &= \widehat{\beta}^+(0) - \widehat{\beta}^-(0) & C_R &= \widehat{\beta}^+(L) - \widehat{\beta}^-(L) \end{aligned}$$

It follows that

$$\widehat{\beta}^-(L) = 0, \quad \widehat{\beta}^+(0) = 0 \tag{4.7.21}$$

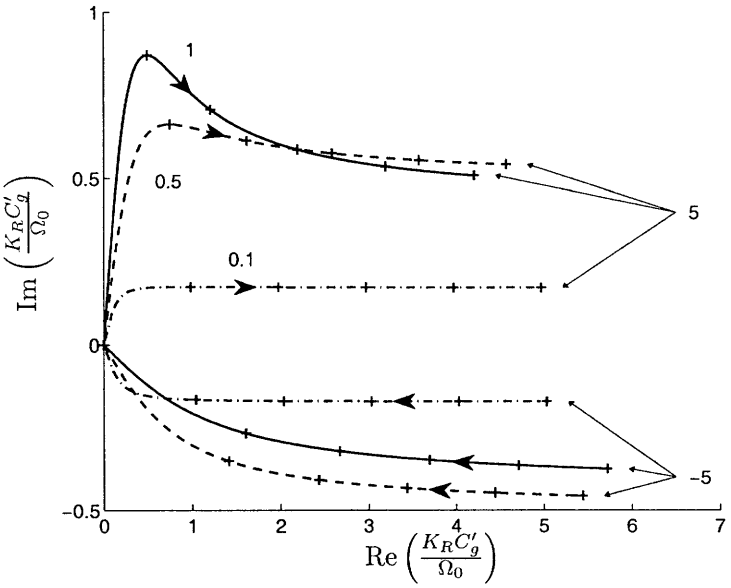

Figure 4-10: Wave-number for the radiation, represented for $\Omega/\Omega_0 \in [-5, 5]$ following the arrows. Extreme values are given on the graph. The crosses correspond to $\Omega/\Omega_0 = -5, -4, \ldots, 5$. The value of λ_g is given next to the curves. For comparison, the scattering wave number is represented in figure 4-8.

An analytic formula for the solutions of this problem, together with a numerical method of solution, are given in Appendix F. The derivation of the solution is long, but it is interesting to see that the natural wave number for the radiation problem is given by

$$K_R \equiv \frac{\sqrt{\Omega\left(\Omega - 2(1-\mathcal{G})\Omega_0\right)}}{C_g'}$$

where $\mathcal{G}$ is a complex number that expresses energy extraction, as defined in (4.7.15). K_R is represented in figure 4-10. We see that it differs from K_S, which is the wave number of the forcing in (4.7.16), so no resonance between buoys is to be expected at any frequency. We also see that, as long as $\lambda_g \neq 0$, K_R will be complex, so the radiated wave will be decaying with x. The absence of resonance between buoys, together with the strong reflection leads us to expect low energy extraction at Bragg resonance.

Case of free buoys

Let us look at the effect of totally free buoys. In this case we have $\mathcal{G} = 1$ so the evolution equations for $\beta^{\pm}$ are not coupled anymore

$$-\mathrm{i}\Omega\widehat{\beta}^{+} + C_g'\frac{\partial\widehat{\beta}^{+}}{\partial x} = -\mathrm{i}\Omega_0(\widehat{\alpha}^{+} + \widehat{\alpha}^{-})$$
$$-\mathrm{i}\Omega\widehat{\beta}^{-} - C_g'\frac{\partial\widehat{\beta}^{-}}{\partial x} = -\mathrm{i}\Omega_0(\widehat{\alpha}^{+} + \widehat{\alpha}^{-})$$

It is easy to see that the solutions are of the form

$$\widehat{\beta}^{+} = C_1\mathrm{e}^{\mathrm{i}Kx} - \frac{K_0\mathcal{A}^{+}}{K - K_S}\mathrm{e}^{\mathrm{i}K_Sx} - \frac{K_0\mathcal{A}^{-}}{K + K_S}\mathrm{e}^{-\mathrm{i}K_Sx} \tag{4.7.22}$$
$$\widehat{\beta}^{-} = C_2\mathrm{e}^{-\mathrm{i}Kx} - \frac{K_0\mathcal{A}^{+}}{K + K_S}\mathrm{e}^{\mathrm{i}K_Sx} - \frac{K_0\mathcal{A}^{-}}{K - K_S}\mathrm{e}^{-\mathrm{i}K_Sx} \tag{4.7.23}$$

with some constant C_1 and C_2. Note that

$$\frac{K_0\mathcal{A}^{+}}{K - K_S} + \frac{K_0\mathcal{A}^{+}}{K + K_S} = 2\frac{K_0K}{K^2 - K_S^2} = 1$$

using the fact that the scattering wave number is given by $K_S = \sqrt{K^2 - 2KK_0}$. This gives us that

$$\zeta = \left(\widehat{\alpha}^{+} + \widehat{\alpha}^{-} + \widehat{\beta}^{+} + \widehat{\beta}^{-}\right)\mathrm{e}^{-\mathrm{i}\Omega t} = C_1\mathrm{e}^{\mathrm{i}(Kx - \Omega t)} + C_2\mathrm{e}^{-\mathrm{i}(Kx + \Omega t)}$$

Using the expressions of $\mathcal{A}\pm$ and the boundary conditions (4.7.21), or matching directly the total potential $\phi_{S,0} + \phi_{R,0}$ with the outside of the array, we see that

$$C_1 = 1, \qquad C_2 = 0 \tag{4.7.24}$$

Let us recall that $\alpha^{\pm}$ and $\beta^{\pm}$ correspond to wave amplitudes, and that the free surface elevation is given by

$$\eta = \alpha^{+} + \alpha^{-} + \beta^{+} + \beta^{-}$$

If we assume that buoys are free then from (4.7.14) we find that $\zeta = \eta$. This agrees with the expectation that small buoy move with the free surface, and we have from (4.7.22) and (4.7.24)

$$\eta = \zeta = \mathrm{e}^{\mathrm{i}(Kx - \Omega t)}$$

or

$$\phi_{S,0} + \phi_{R,0} = Z(z)\mathrm{e}^{\mathrm{i}k'x'}\mathrm{e}^{\mathrm{i}(Kx-\Omega t)} = \phi_{in}$$

which shows that to the leading order a sparse array of small free buoys does not affect the incoming wave. This comes from the fact that mass was negligible in the equation of conservation of the vertical momentum of the buoys, so the buoys have no effect on the displacement of the free surface.

4.7.3 Energy extraction

Now that the flow is known, we can compute the buoy displacement, and the main quantity we are interested in is the energy extraction. It is well known that the extraction *from the j^{th} buoy alone* is given by:

$$E_j^* \equiv \frac{1}{2}\omega^{*2}\lambda_g^*|\zeta_j^*|^2$$

so the total energy extracted by N buoys will be given by

$$E^* = \sum_{j=1}^{N} E_j^* = \frac{1}{d^*}\sum_{j=1}^{N} E_j^* d^*$$

Using the fact that $N \gg 1$, we can see the above expression as a Riemann sum, so we can approximate it by an integral:

$$\begin{aligned} E^* &\approx \frac{1}{2d^*}\omega^{*2}\lambda_g^* \int_0^{L^*} |\zeta^*|^2 \,\mathrm{d}x^* \\ &\approx \frac{\pi}{d'}\frac{1}{2}\rho^*\sqrt{g^*h^*}^3 A^{*2}\omega'^2\lambda_g \int_0^{L} |\zeta|^2 \,\mathrm{d}x \end{aligned} \tag{4.7.25}$$

This quantity can be compared to the energy incoming on a length d^* which is known to be (See Mei et al. (2005), p. 19)

$$\frac{1}{2}\rho^* \sqrt{g^* h^*}^3 A^{*2} C_g' d' \tag{4.7.26}$$

So a measure of the absorbed power is the ratio of (4.7.25) and (4.7.26):

$$\mathcal{E} \equiv \frac{\pi}{d'^2 C_g'} \omega'^2 \lambda_g \int_0^L |\zeta|^2 \, \mathrm{d}x$$

Another approach would have been to look at the energy incoming and outgoing, and the difference would correspond to the energy extraction. Expressing the modified radiation and transmission coefficients due to radiation, we find

$$\mathcal{E}' \equiv 1 - \left(\left| \widehat{\alpha}^-(0) + \widehat{\beta}^-(0) \right|^2 + \left| \widehat{\alpha}^+(L) + \widehat{\beta}^+(L) \right|^2 \right)$$

It is shown in Appendix G that $\mathcal{E}' = \mathcal{E}$.

4.7.4 Numerical results

Let us now present some numerical results. Figure 4-11, shows how the the extracted energy varies with the detuning, the length of the array and the energy extraction rate. The first thing we see is that energy extraction can be reduced in a very important way due to Bragg resonance. In order to measure this drop, let us introduce

$$\mathcal{D} = \mathcal{E}_0 - \min_{\Omega} \mathcal{E} \tag{4.7.27}$$

We see in figure 4-11 that the minimum is reached around $\Omega = 0$. Figure 4-12 shows that $\mathcal{D}$ increases with the length of the array and and with the energy extraction rate increase, and can be superior to 90% of $\mathcal{E}$. Note that $\mathcal{D}$ increases when when scattering is more important (see §4.6.4).

The results show that, as one could have expected, the maximum extracted energy increases with the length of the array, and is maximum for some optimum λ_g, as it

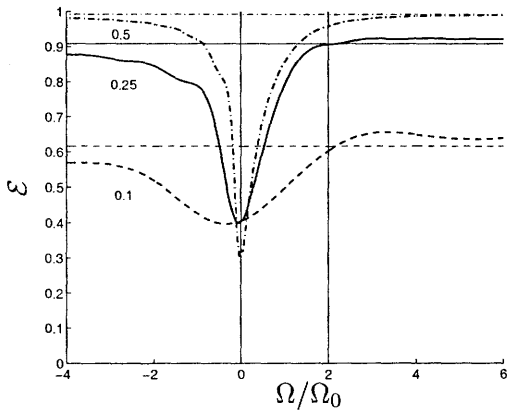

(a) $\lambda_g = 1/2$, and the value of L is given next to the curves

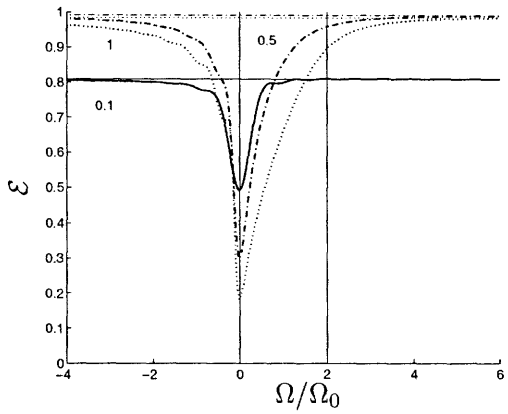

(b) $L = 1/2$, and the value of λ_g is given next to the curves

Figure 4-11: Influence of (a) L and (b) λ_g on the energy extraction, as indicated next to the curves. The vertical lines represents the limits of band gap. The horizontal lines give the results obtained by (4.3.3). $d' = 1$

was the case for a compact array and for a single buoy. Note however that at Bragg scattering, the extraction rate should be reduced in order to increase the extracted energy (see figure 4-12(a)). What is maybe more surprising is that shorter arrays can yield more energy than longer ones for small detuning.

We finally see that away from Bragg resonance (i.e. for important detuning), the energy extracted seems to tend to a constant value, and that there is a good agreement between this value and the result of the asymptotic estimate (4.3.3).

Let us now try to explain why energy extraction is reduced in such an important manner.

As we mentioned earlier, scattering effect are negligible for free buoys but can be very important for fixed buoys when the detuning is such that $0 \leq \Omega \leq \Omega_0$. Figures 4-13 and 4-14 show how the amplitudes of the reflected and transmitted waves vary with the array length L, the damping rate λ_g and the detuning Ω. As it was the case for fixed buoys, reflection is increased in the neighborhood of Bragg resonance, and specially for values of Ω inside the band gap. This augmentation of reflection increases with the energy extraction rate and with the length of the array. In particular, reflection is maximum for fixed buoys. The behavior of the transmitted wave is more surprising, as we see that depending on the value of Ω it can be increased or decreased

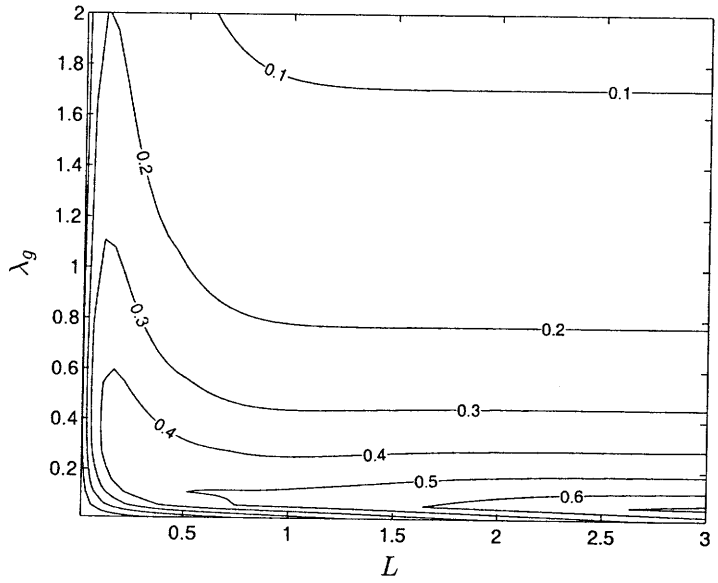

(a) $\min_\Omega \mathcal{E}$

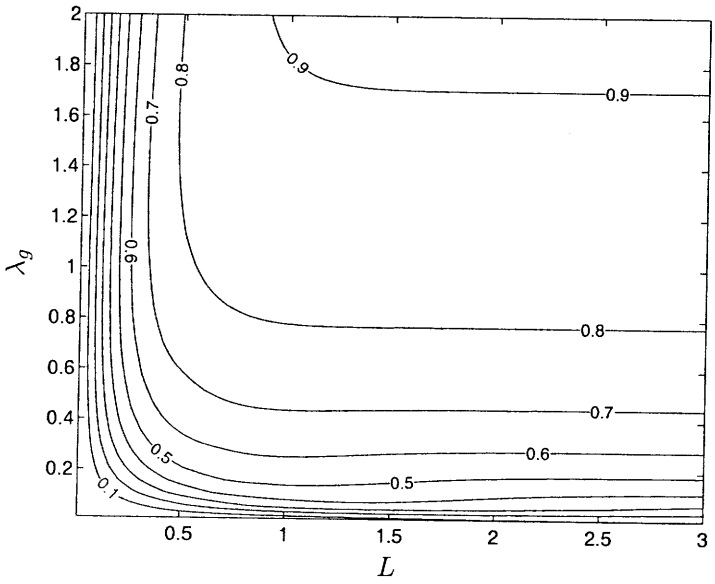

(b) $\mathcal{D}$

Figure 4-12: Influence of L and λ_g on the the minimum energy extracted and on drop due to Bragg resonance. $d' = 1$

by radiation. Note finally that the detuning corresponding to the maximum reflection is not $\Omega = \Omega_0$, that corresponded to the maximum reflection in the case of fixed buoys, but that it is shifted towards $\Omega = 0$. All this shows that in the neighborhood of Bragg resonance and when the effect of the energy extraction device on the buoys is significant, most of the energy of the incoming wave is reflected.

Figures 4-15 and 4-16 show the amplitudes of the displacements of the free surface and of the buoy. As we mentioned earlier, the amplitude of the free surface displacement remains constant when the buoys are totally free. We see that increasing λ_g does not necessary means having smaller free surface elevation, but it results in smaller buoy displacement. Note that the buoy displacement is significant over a much smaller distance for frequencies in the band gap due to strong reflection. As the wave does not propagate through the array it can not induce a displacement of the buoys, and so only little energy can be extracted.

4.8 Conclusion

We saw in this chapter that the method of multiple scales, that was previously successfully applied to several scattering problems can also be applied to study radiation by moving buoys. This allowed us to derive simple equations governing the long scale evolution of the wave envelopes and the buoy displacement, providing us an easy way to compute the energy extracted from the array. We checked the consistency of the result of the homogenization using numerical simulation and asymptotic estimates.

We showed that buoys of small draft produce scattering effect of the same order of magnitude as vertical piles, as the horizontal surface of the buoys, or its projection onto the horizontal plane in the case of semi-spherical buoys, has a much bigger influence on the wave than the lateral surface. In particular, we showed that one dimensional wave propagation is not possible in an array of buoys for some range of frequencies around Bragg resonance. This phenomena is known in solid state physics as a band gap.

Multiple scale analysis also allowed us to show that, in the limits of our approx-

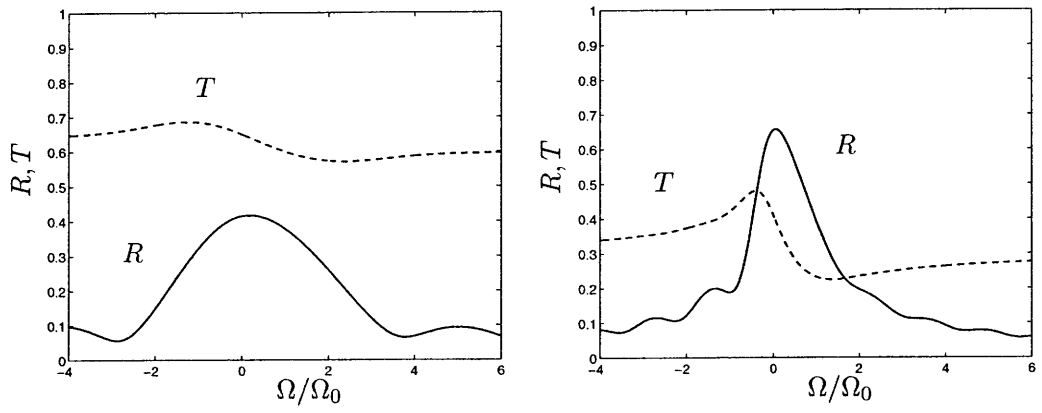

(a) $L = 0.1$

(b) $L = 0.25$

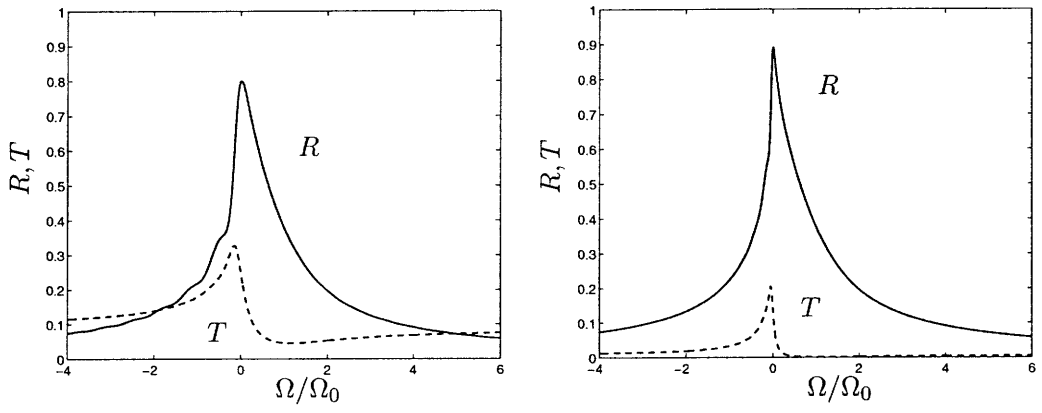

(c) $L = 0.5$

(d) $L = 1$

Figure 4-13: Influence of L on the reflection and transmission coefficients. The energy extraction rate is set to $\lambda_g = 1/2$. $d' = 1$

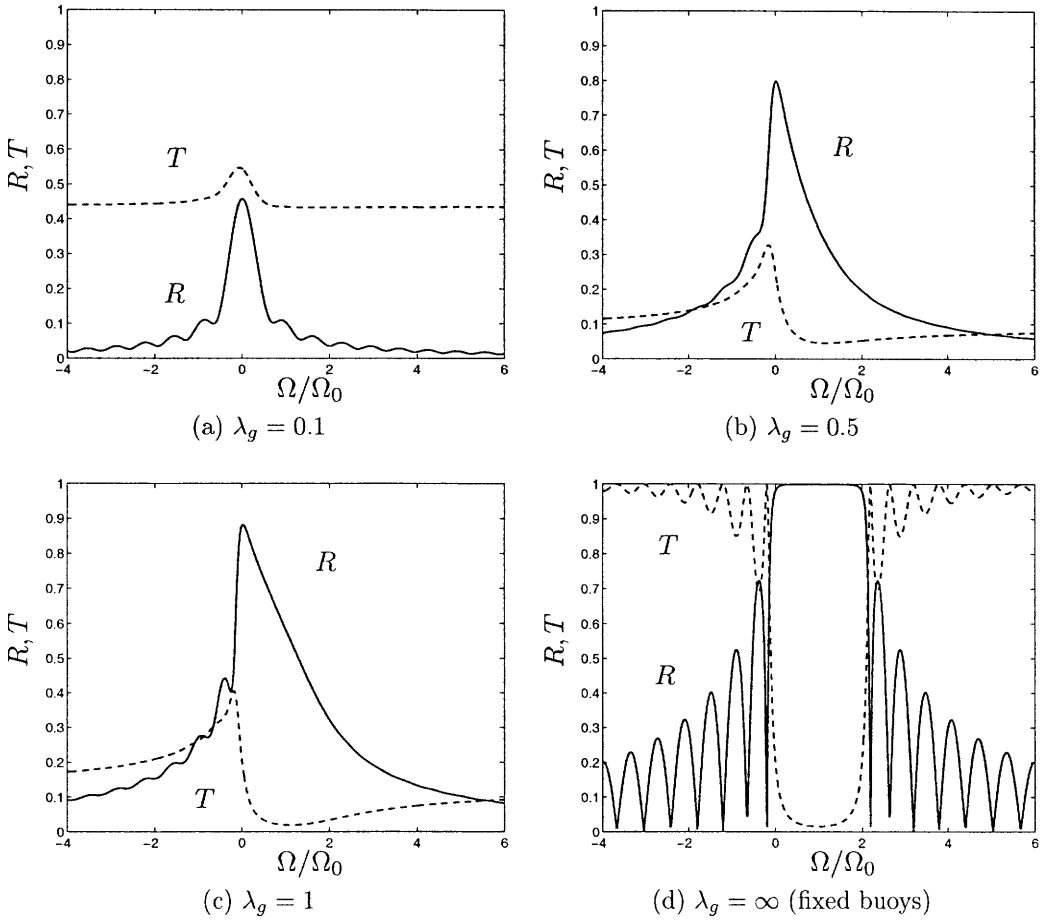

(a) $\lambda_g = 0.1$ (b) $\lambda_g = 0.5$

(c) $\lambda_g = 1$ (d) $\lambda_g = \infty$ (fixed buoys)

Figure 4-14: Influence of λ_g on the reflection and transmission coefficients. The length of the array is $L = 1/2$ and $d' = 1$

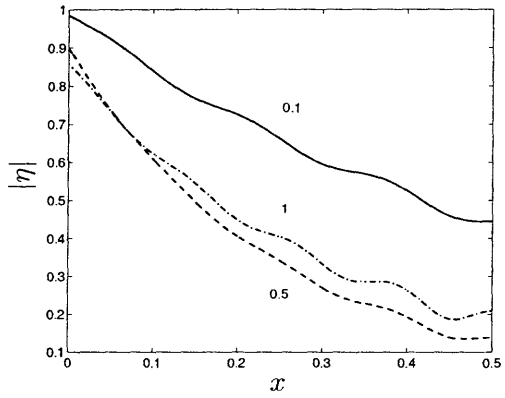

(a) η for $\Omega = -2\Omega_0$. The value of λ_g is indicated next to the curves.

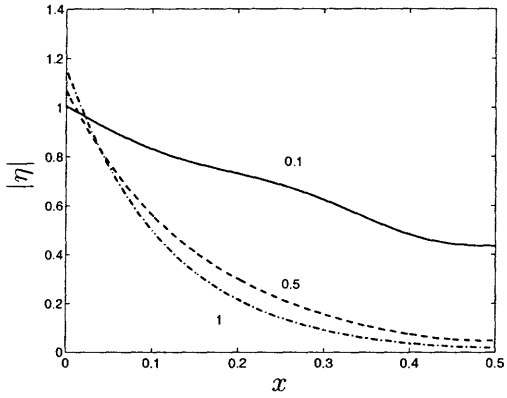

(b) η for $\Omega = \Omega_0$. The value of λ_g is indicated next to the curves.

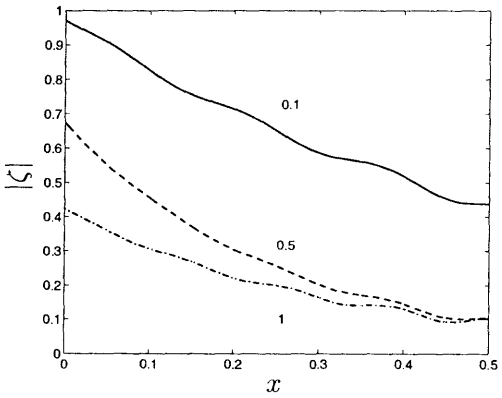

(c) ζ for $\Omega = -2\Omega_0$. The value of λ_g is indicated next to the curves.

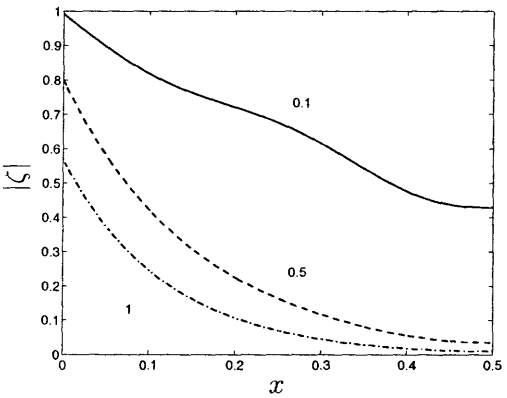

(d) ζ for $\Omega = \Omega_0$. The value of λ_g is indicated next to the curves.

Figure 4-15: Influence of the extraction rate on the free surface elevation η and buoy displacement ζ in the array. $L = 1/2$ and $d' = 1$

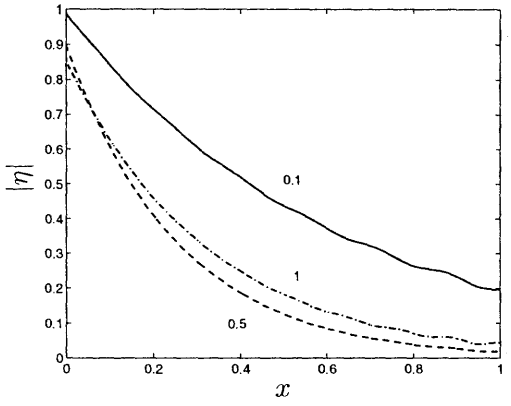

(a) η for $\Omega = -2\Omega_0$. The value of λ_g is indicated next to the curves.

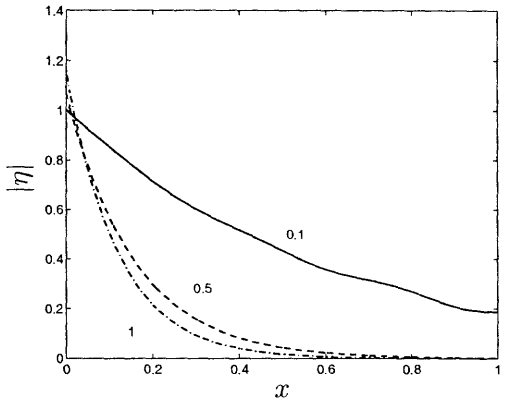

(b) η for $\Omega = \Omega_0$. The value of λ_g is indicated next to the curves.

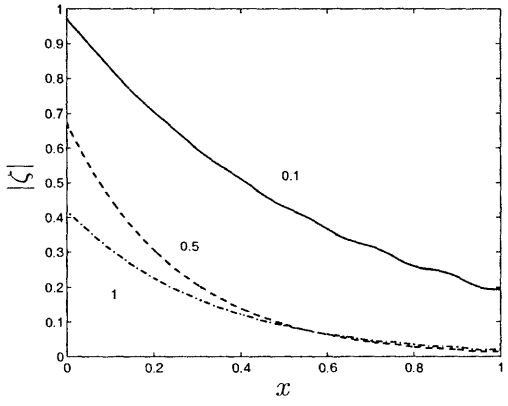

(c) ζ for $\Omega = -2\Omega_0$. The value of λ_g is indicated next to the curves.

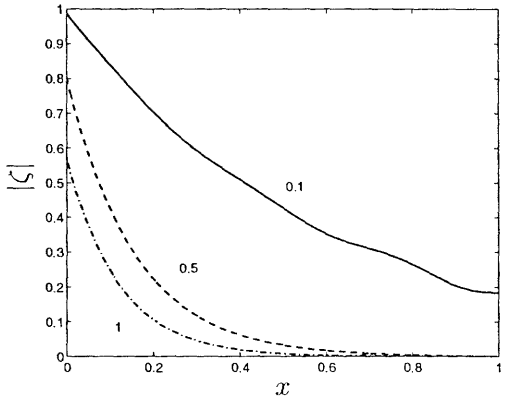

(d) ζ for $\Omega = \Omega_0$. The value of λ_g is indicated next to the curves.

Figure 4-16: Influence of the extraction rate on the free surface elevation η and buoy displacement ζ in the array. $L = 1$ and $d' = 1$

imation, an array of totally free buoys have no effect on a propagating wave, as the inertia of the buoys can be neglected.

We finally saw that the power extraction in a channel is much reduced in the neighborhood of Bragg resonance due to very strong reflection, and that this reduction increases with the length of the array L and with the energy extraction rate λ_g. In particular when λ_g is set to its optimal value for a single small buoy, Bragg scattering can result in a drop of more than 70% of the energy extracted. As a consequence, for industrial wave energy extraction the spacing should be kept smaller than half of the smaller relevant incoming wave lengths in terms of incoming energy. Equation (4.3.3), that gives an asymptotic expression for energy extraction far away from Bragg resonance, can help the designer to find a balance between the number of buoys used and the energy extracted.

Note that our analysis is limited to one dimensional propagation, and the situation could be very different if the waves were able to propagate in the two horizontal direction. We can in particular expect that reflection will be much less important as band gaps are not present anymore.

Chapter 5

Conclusion

Although it has been shown that the maximum possible capture width is one for heaving buoys of any size, the analysis conducted in Chapter 2 showed that this happens when the buoy resonates with the incoming wave, and that the resonant frequency increases as the size of the buoy decreases. In practice, only big buoys would operate in optimal conditions for common wave length, and for these the bandwidth would be very limited. Phase control methods have been proposed in order to obtain the resonance of small point absorbers under typical conditions, but the focus of this thesis was to study energy extraction by arrays of 'small' buoys (compared to the wave length), and in particular to see whether or not it is possible to place them in such a way that they would resonate.

Different configurations have been studied: first we considered a compact array, in which the spacing is of the same order of magnitude as the radii of the buoys. We proposed an analytical method to treat this problem, and showed that although an infinitely long array would not produce results as good as that one could obtain with a Salter's cam, gathering the buoys into a circle seems promising. In particular it is possible to get capture width much bigger than one even in the usual range of frequencies, and with a broad bandwidth. We then looked at another limiting case, in which the spacing is much larger than the size of the buoy, and focused mainly of Braggs resonance, for which the spacing is equal to half the wave length. For simplicity, we restricted ourselves to the propagation inside a channel. Theoretical

and numerical results showed that strong reflection of the incoming wave should be expected, leading to a reduced energy extraction as the wave do not propagate inside the array.

This results can give some insight for designing 'wave farms' in order to produce electrical energy, but one should however keep in mind that our analysis is restricted to linear waves, and that the viscosity of water has not been taken into account.

From a more theoretical perspective, we applied the method of multiple scale to new type of problems. This method had already been used to study a wide variety of problems. We showed in this thesis that this is a powerful tool even if the unit cell has different length scales, as it is the case for a compact array. In the last chapter, this method also proved useful to treat a radiation problem.

Appendix A

Numerical solution of the energy extraction buoy with one buoy.

A.1 Analytical value of the coefficients in (2.1.23)

A.1.1 Change of base

The scalar products are given by

$$\langle f_0, F_0\rangle = \frac{\sinh(k(1-H))c_0}{k\sqrt{1-H}}$$
$$\langle f_n, F_0\rangle = \frac{\sin(k_n(1-H))c_n}{k_n\sqrt{1-H}}$$
$$\langle f_0, F_n\rangle = (-1)^n \frac{\sqrt{2}k(1-H)^{3/2}c_0\sinh(k(1-H))}{(k^2(1-H)^2+n^2\pi^2)}$$
$$\langle f_n, F_m\rangle = (-1)^m \frac{\sqrt{2}k_n(1-H)^{3/2}c_n\sin(k_n(1-H))}{(k_n^2(1-H)^2-m^2\pi^2)}$$

A.1.2 Particular solution for the scattering problem

We find:

$$\langle U_p, f_0\rangle = -\mathrm{i}^m\varepsilon_m\frac{-\mathrm{i}}{\omega\cosh(k)}\frac{c_0}{2}J'_m(ka)\left(\sinh(k(1-H))\cosh(k(1-H))+k(1-H)\right)$$

$$\langle U, f_n\rangle = -\mathrm{i}^m\varepsilon_m\frac{-\mathrm{i}}{\omega\cosh(k)}\frac{c_n k J'_m(ka)}{k^2+k_n^2}\left(k_n\sin(k_n(1-H))\cosh(k(1-H))\right.$$
$$\left.+k\cos(k_n(1-H))\sinh(k(1-H))\right)$$

$$\langle \Phi^p_m, F_0\rangle = -\mathrm{i}^m\varepsilon_m\frac{-\mathrm{i}}{\omega\cosh(k)}\frac{J_m(ka)}{k\sqrt{1-H}}\sinh(k(1-H))$$

$$\langle \Phi^p_m, F_n\rangle = -\mathrm{i}^m\varepsilon_m\frac{-\mathrm{i}}{\omega\cosh(k)}\frac{(-1)^n}{k^2(1-H)^2+\pi^2n^2}\frac{kJ_m(ka)\sqrt{2}(1-H)^2\sinh(k(1-H))}{\sqrt{1-H}}$$

A.1.3 Particular solution for the radiation problem

We can perform an analytical integration, and we get:

$$\langle U^p_r, f_0\rangle = -\frac{c_0 a}{2k(1-H)}\sinh(k(1-H))$$

$$\langle U^p_r, f_n\rangle = -\frac{c_n a}{2k_n(1-H)}\sin(k_n(1-H))$$

$$\langle \Phi^p_r(r,z), F_0\rangle = \frac{1}{2\sqrt{1-H}}\left\{\frac{(1-H)^2}{3}-\frac{a^2}{2}\right\}$$

$$\langle \Phi^p_r(r,z), F_n\rangle = \frac{(-1)^n}{n^2}\frac{\sqrt{2}(1-H)^{3/2}}{\pi^2}$$

A.1.4 Boundary condition on S_W

For the radiation problem, we have $U^W_r = 0$. For the scattering, one can notice that

$$\langle U^p_m, f_n\rangle_{-h,-H} + \langle U^W_m, f_n\rangle_{-H,0} = \frac{-\mathrm{i}^m\varepsilon_m}{\mathrm{i}\omega\cosh(k)}\frac{c_0}{2}J'_m(ka)\delta_{0n}$$

A.1.5 Asymptotic expansions

In order to examine the convergence of the series, it is interesting to study the asymptotic value of the coefficients. We find that all series are absolutely convergent, at least as fast as $\sum 1/n^2$. It is also interesting to examine the asymptotic expansions

for large arguments of Bessel functions. To begin with, as k_n is defined by

$$k_n . \tan k_n = -\omega^2 \tag{A.1.1}$$

with $k_n \geq 0$, we have $-\frac{\omega^2}{k_n} \to 0^-$ when $n \to \infty$, so

$$k_n \sim n\pi \quad \text{as } n \to \infty \tag{A.1.2}$$

As

$$\alpha_{n,m} = \frac{K_m^2(ka)}{\frac{m}{a}K_m(ka) - kK_{m+1}(ka)} \tag{A.1.3}$$

we have

$$\alpha_{n,m} \sim -\frac{1}{k_n} \tag{A.1.4}$$

Similarly, we have

$$\beta_{n,m} = \frac{I_m^2(ka)}{\frac{m}{a}I_m(ka) + kI_{m+1}(ka)} \tag{A.1.5}$$

so

$$\beta_{n,m} \sim \frac{1}{K_n} \tag{A.1.6}$$

Finally, we have

$$c_n \sim \sqrt{\frac{2}{h_n}} \tag{A.1.7}$$

A.2 Accuracy of the numerical approximation.

A.2.1 Matching.

Figure A-1 shows an example of the solutions computed in $r = a$. We see that oscillations are present in the velocity, but that the pressure is smoother. We can also see that oscillations affect the matching between the solutions as well as between the outer solution and the boundary condition.

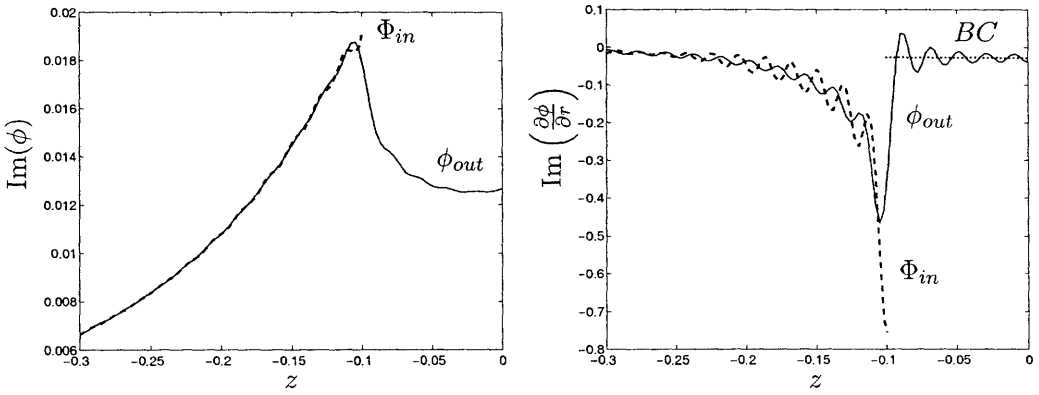

(a) Potential, imaginary part

(b) Flux, imaginary part

Figure A-1: Matching of the inner (Φ_{in}) and outer (ϕ_{out}) solutions ($N = 100$, $a = H = .1$). For the flux, the boundary condition is indicated by BC

A.2.2 Convergence of the capture width.

As we do not know the exact value of the capture width, we can evaluate the error for a solution with N vertical modes by:

$$e_n = \frac{|kW_N - kW_\infty|}{|kW_\infty|} \approx \frac{|kW_N - kW_{N_0}|}{|kW_{N_0}|}$$

where $N_0 \gg N$. In figure A-2, results are given for $N_0 = 500$. We see that $N = 50$ already gives us a relative precision smaller than 10^{-3}. The same thing can be done with the angular modes, and we see that

$$\frac{|kW_{N_\theta=2} - kW_{N_\theta=50}|}{|kW_{N_\theta=50}|} \sim 10^{-13}$$

so we used $N_\theta = 2$. This shows us that despite the oscillations shown in §A.2.1, our result are still accurate.

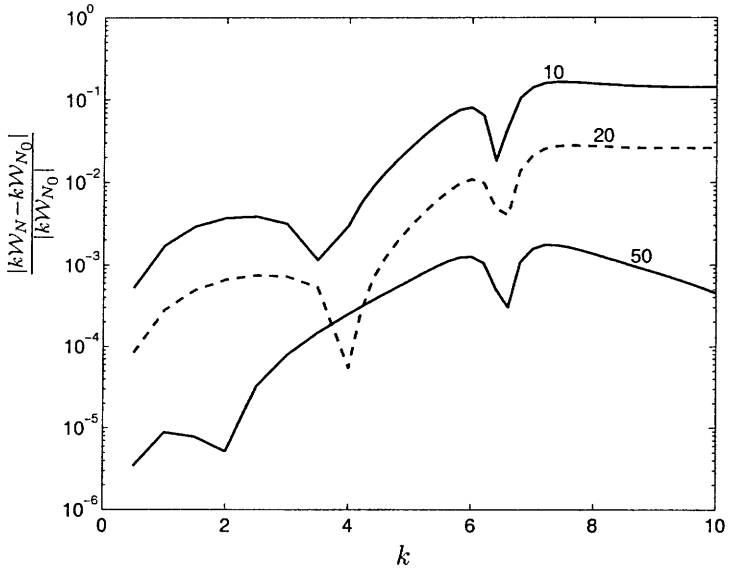

Figure A-2: Convergence of capture width. The solution takes into account N vertical modes and N_θ angular modes. The value of N is given next to the curves, and $N_\theta = 2$ ($a = H = .1$)

Appendix B

Numerical solution of the matching problem for a compact array

For both the 1D and the 2D geometries we found that energy extraction can be obtained through the solution of a linear system. In order to build the matrices, the more challenging part is to find the complex wave numbers in each region. Then, some care should be taken when truncating the series.

B.1 Determination of wave numbers

The roots of (3.4.12) have to be computed numerically, but unlike in the case open sea or one single buoy, we do not have bounds for each eigenvalue. In order to get a first idea of the solutions, let us go back to the boundary value problem from which it is coming, (3.4.9). Such an eigenvalue problem can be solved in an approximate way using Finite Elements. Let $H^1(-1,0)$ be the Sobolev space of L^2 functions on $(-1,0)$ that have a weak derivative in L^2. A variational formulation of (3.4.9) is found multiplying (3.4.9) by an arbitrary function $\phi \in H^1(-1,0)$ and integrating by parts:

$$\int_{-1}^{0} f''(z)\phi(z)\,\mathrm{d}z = f'\phi|_{-1}^{0} - \int_{-1}^{0} f'(z)\phi'(z)\,\mathrm{d}z$$

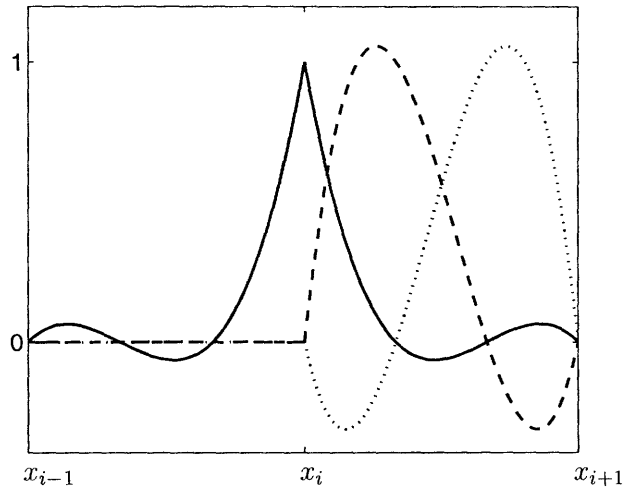

Figure B-1: Cubic Lagrange base functions. Solid: ϕ_i, dashed: $\phi_{i+1/3}$, dotted: $\phi_{i+2/3}$

making use of the boundary conditions, we finally get

$$\alpha f(0)\phi(0) - \int_{-1}^{0} f'(x)\phi'(x)\,\mathrm{d}x = \kappa^2 \int_{-1}^{0} f(x)\phi(x)\,\mathrm{d}x \qquad \forall \phi \in H^1(-1,0) \qquad \text{(B.1.1)}$$

Let us define

$$
\begin{aligned}
x_{n+i/3} &= -1 + (n + i/3)\delta x && -1 \leq x_{n+i/3} \leq 0 \\
\Phi_1(x) &= \frac{-9}{2}(x - 1/3)(x - 2/3)(x - 1) && 0 \leq x \leq 1 \\
&= \frac{-9}{2}(-x - 1/3)(-x - 2/3)(-x - 1) && -1 \leq x \leq 0 \\
&= 0 && \text{else} \\
\Phi_2(x) &= \frac{27}{2}x(x - 2/3)(x - 1) && 0 \leq x \leq 1 \\
&= 0 && \text{else} \\
\Phi_3(x) &= \frac{-27}{2}(x - 1/3)(x - 1) && 0 \leq x \leq 1 \\
&= 0 && \text{else} \\
\phi_i &= \Phi_1(\frac{x - x_i}{\delta x}) \\
\phi_{i+1/3} &= \Phi_2(\frac{x - x_i}{\delta x}) \\
\phi_{i+2/3} &= \Phi_3(\frac{x - x_i}{\delta x})
\end{aligned}
$$

A numerical approximation of the solution of (3.4.9) can then be obtained replacing $H^1(-1, 0)$ by $\text{Span}(\phi_{n+i/3})$. Theses base functions, called Lagrange cubic elements, are represented in figure B-1. On this set (B.1.1) can be expressed as an matrix generalized eigenvalue problem [1]

$$(\alpha A - K)f = \lambda M f \tag{B.1.2}$$

where

$$A = \text{diag}(1, 0, \cdots, 0)$$

enforces the boundary condition in $z = 0$. The matrix K, called rigidity matrix, contains the scalar products of the derivatives of the base functions, and M contains

[1] Functions $\phi_0, \phi_{1/3}, \cdots$ are renumbered to $\phi_1, \cdots, \phi_n$

the scalar products of the functions themselves:

$$K_{i,j} = \langle \phi_i' | \phi_j' \rangle$$
$$M_{i,j} = \langle \phi_i | \phi_j \rangle$$

Note that K and M are symmetric. Their analytic expression are:

$$K_{i,j} = \begin{pmatrix} \frac{37}{10} & \frac{-189}{40} & \frac{27}{20} & \frac{-13}{40} & 0 & \cdots \\ * & \frac{54}{5} & \frac{-297}{40} & \frac{27}{20} & 0 & \cdots \\ * & * & \frac{54}{5} & \frac{-189}{40} & 0 & \cdots \\ * & * & * & \frac{74}{10} & \frac{-189}{40} & \cdots \\ & & & & & \ddots \end{pmatrix}$$

$$M_{i,j} = \begin{pmatrix} \frac{8}{105} & \frac{33}{560} & \frac{-3}{140} & \frac{19}{1680} & 0 & \cdots \\ * & \frac{27}{70} & \frac{-27}{560} & \frac{-3}{140} & 0 & \cdots \\ * & * & \frac{27}{70} & \frac{33}{560} & 0 & \cdots \\ * & * & * & \frac{16}{105} & \frac{33}{560} & \cdots \\ & & & & \ddots & \end{pmatrix}$$

The vector f contains the value of the eigenfunction at any point of our grid, and the values of κ are approximated by the square root of λ. As we know that all κ_n should verify $\kappa_n \tanh(\kappa_n) = \alpha$, we can then refine this estimation, for example using Matlab built-in function `fsolve`.

B.2 Truncation error

B.2.1 Convergence of the series expansion for the linear array.

In order to solve (3.5.13), we need to truncate the series after a finite number of vertical modes. As we do not know the exact solution of our problem, we need to use as a reference the solution $k\mathcal{W}_{N_0}$ computed with a 'high' number of terms N_0, and

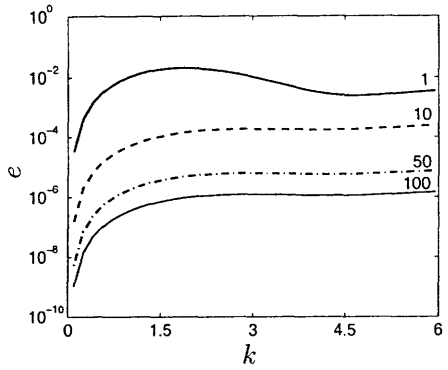

(a) Relative error e between the value of energy extraction obtained for $N = 1, 10, 50, 100$. The value of N is indicated next to the curve. We take the results for $N = 200$ as a reference. $f = .5$, $L = 1$ and $\lambda = 1$

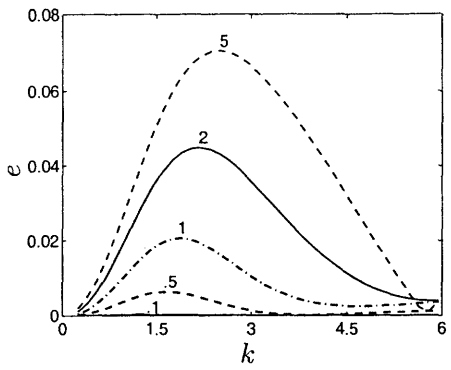

(b) Influence of damping coefficient on error: relative error e between results for $N = 1$ and $N = 30$. The value of λ is indicated next to the curve, $f = .5$ and $L = 1$.

Figure B-2: Precision of the numerical solution.

define the error e as

$$e_{n,N_0} \equiv \frac{|k\mathcal{W}_n - k\mathcal{W}_{N_0}|}{|k - \mathcal{W}_{N_0}|}$$

figure B-2(a) shows this error converges to 0, which indicates that our solution method is valid. On figure B-2(b), we see that the error depends on the damping coefficient. We can generally see that a good precision is obtained with relatively few terms.

B.2.2 Convergence of the series expansion in the 2D case

Several verification of the validity of the problem can be made: first, we can check numerically that if the buoys are fixed of totally free, we find that $k_0\mathcal{W} = 0$, which is the equivalent of the optical theorem. This means that energy is conserved. Figure B-3(c) shows the good verification of this relation. We can also check that the truncation errors are negligible. For this, figures B-3(a) and B-3(b) show the convergence of this solution method to the solution in terms of number of vertical and angular modes taken into account.

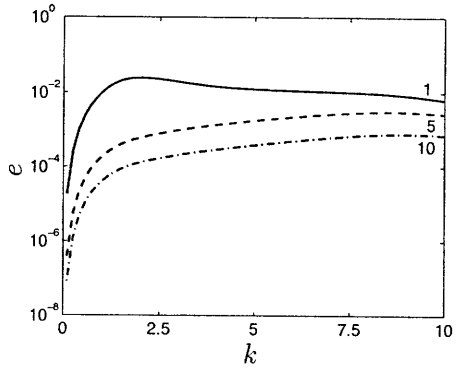

(a) Relative error e between the value of energy extraction obtained for $N = 1, 5, 10$. The value of N is indicated next to the curve. We take the results for $N = 50$ as a reference.($f = .5$, $R = 1$, $\lambda_g = 1$ and $M = 5$)

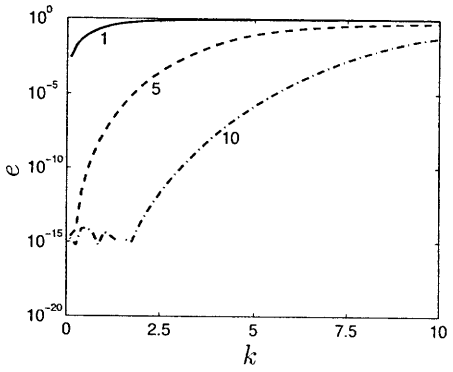

(b) Relative error e between the value of energy extraction obtained for $M = 1, 5, 10$. The value of M is indicated next to the curve. We take the results for $M = 50$ as a reference.($f = .5$, $R = 1$, $\lambda_g = 1$ and $N = 10$)

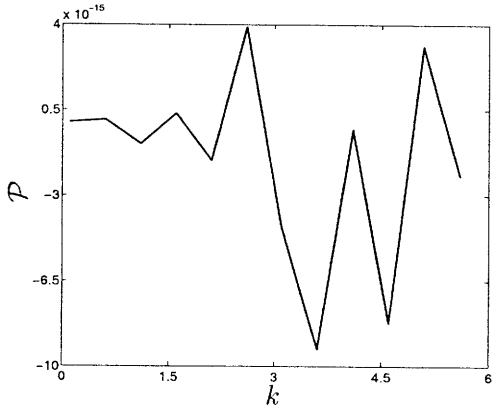

(c) Verification of the optical theorem ($f = .5$, $R = 1$, $\lambda_g = \infty$, $N = 10$, $M = 5$)

Figure B-3: Verifications of the numerical solution.

B.3 Energy absorption by a circular array: details of the derivation

B.3.1 From the far field potential

Let us define

$$\mathcal{A}(\theta) = \sum_m \mathcal{A}_m \cos(m\theta)$$

Replacing the expression of the potential given in (3.6.18) in the definition of $\mathcal{P}$, we get

$$\begin{aligned}
\mathcal{P} &= -\frac{1}{\omega^2 f_0(0)^2}\int_{-h}^{0} f_0(z)^2\, dz. \int_0^{2\pi} \frac{1}{2}\mathrm{Re}\left(\mathrm{i}\omega\phi\frac{\partial\phi^\dagger}{\partial r}\right) r\,\mathrm{d}\theta \\
&= -\frac{1}{2}\frac{1}{\omega^2 f_0(0)^2}\int_{-h}^{0} f_0(z)^2\, dz.\mathrm{Re}\left(\mathrm{i}\omega\int_0^{2\pi}\left(\mathrm{e}^{\mathrm{i}k_0 r\cos(\theta)} + \mathcal{A}(\theta)\sqrt{\frac{2}{\pi k_0 r}}\mathrm{e}^{\mathrm{i}(k_0 r-\pi/4)}\right)\right. \\
&\quad \left.\left(\mathrm{i}k_0\cos(\theta)\mathrm{e}^{\mathrm{i}k_0 r\cos(\theta)} + \mathcal{A}(\theta)\sqrt{\frac{2}{\pi k_0 r}}\mathrm{i}k_0\mathrm{e}^{\mathrm{i}(k_0 r-\pi/4)}\right)^\dagger r\,\mathrm{d}\theta\right) \\
&= -\frac{1}{2}\frac{1}{\omega f_0(0)^2}\int_{-h}^{0} f_0(z)^2\, dz.\mathrm{Re}\left(k_0\int_0^{2\pi}\left(\mathrm{e}^{\mathrm{i}k_0 r\cos(\theta)} + \mathcal{A}(\theta)\sqrt{\frac{2}{\pi k_0 r}}\mathrm{e}^{\mathrm{i}(k_0 r-\pi/4)}\right)\right. \\
&\quad \left.\left(k_0\cos(\theta)\mathrm{e}^{-\mathrm{i}k_0 r\cos(\theta)} + \mathcal{A}^*(\theta)\sqrt{\frac{2}{\pi k_0 r}}k_0\mathrm{e}^{-\mathrm{i}(k_0 r-\pi/4)}\right)^\dagger r\,\mathrm{d}\theta\right) \\
&= \frac{1}{2}\frac{1}{\omega f_0(0)^2}\int_{-h}^{0} f_0(z)^2\, dz.\mathrm{Re}\left(k_0\int_0^{2\pi}\left(\cos(\theta) + \frac{2}{\pi k_0 r}|\mathcal{A}(\theta)|^2 + \right.\right. \\
&\quad \left.\left.\sqrt{\frac{2}{\pi k_0 r}}\left(\mathcal{A}(\theta)\cos(\theta)\mathrm{e}^{\mathrm{i}(k_0 r(1-\cos(\theta))-\pi/4)} + \mathcal{A}^\dagger(\theta)\mathrm{e}^{\mathrm{i}(-k_0 r(1-\cos(\theta))-\pi/4))}\right)\right) r\,\mathrm{d}\theta\right) \\
&= \frac{1}{2}\frac{1}{\omega f_0(0)^2}\int_{-h}^{0} f_0(z)^2\, dz.\mathrm{Re}\left(\int_0^{2\pi}\left(\sqrt{\frac{2k_0}{\pi r}}\mathcal{A}(\theta)(1+\cos(\theta))\mathrm{e}^{\mathrm{i}(k_0 r(1-\cos(\theta))-\pi/4)}\right.\right. \\
&\quad \left.\left. + \frac{2}{\pi r}|\mathcal{A}(\theta)|^2\right) r\,\mathrm{d}\theta\right)
\end{aligned}$$

In the last line, we made use of the fact that the real part of a complex number is equal to that of its complex conjugate. In order to perform further simplifications for large $k_0 r$, we apply the stationary phase approximation. The phase $k_0 r(1-\cos(\theta)) - \pi/4$ has two stationary points in the full range of θ: 0 and π. Only $\theta = 0$ will contribute

because of the factor in front. We finally get:

$$\mathcal{P} = 2\frac{1}{\omega f_0(0)^2}\left(\frac{1}{2\pi}\int |\mathcal{A}(\theta)|^2\,\mathrm{d}\theta + \mathrm{Re}(\mathcal{A}(0))\right)$$

Using the orthogonilty of cosines, we can express the integral above in terms of its Fourier coefficients,

$$\mathcal{P} = 2\frac{1}{\omega f_0(0)^2}\left(|\mathcal{A}_0|^2 + \frac{1}{2}\sum_{m\geq 1}|\mathcal{A}_m|^2 + \mathrm{Re}\left(\sum_{m\geq 0}\mathcal{A}_m\right)\right)$$

B.3.2 From the displacement of the buoys

If we consider a single buoy at a time, the extracted power will be

$$\frac{1}{2}\lambda_g^*\omega^{*2}|\zeta|^2$$

so the total extracted power is:

$$\begin{aligned}
\mathcal{P}'^* &= \frac{1}{2}\lambda_g^*\omega^{*2}\sum_j |\zeta_j|^2 \\
&= \frac{1}{2}\rho^* g^*\sqrt{\frac{g^*}{h^*}}A^* h^{*2}\lambda\omega^2\sum_j \frac{\pi a^2}{h^2}|\zeta_j|^2 \\
&= \frac{1}{2}\rho^* g^*\sqrt{\frac{g^*}{h^*}}A^* h^{*2}\lambda\omega^2\sum_j f\frac{d^2}{h^2}|\zeta_j|^2 \\
&\approx \frac{1}{2}\rho^* g^*\sqrt{\frac{g^*}{h^*}}A^* h^{*2}\lambda\omega^2 f\iint |\zeta|^2\,\mathrm{d}S
\end{aligned}$$

where the surface integral is considered over the surface of the array, S_a. In dimensionless form, this gives:

$$\mathcal{P}' = \frac{1}{2}\lambda_g\omega^2 f\iint_{S_a}|\zeta|^2\,\mathrm{d}S$$

Using Green's formula, we have

$$0 = \iiint_{\Omega_f}\phi\Delta\phi^\dagger - \phi^\dagger\Delta\phi\,\mathrm{d}V = \iint_{S_\infty\cup S_a\cup S_f}\phi\frac{\partial\phi^\dagger}{\partial n} - \phi^\dagger\frac{\partial\phi}{\partial n}\,\mathrm{d}S$$

so

$$\mathrm{Im}\left(\iint_{S_\infty} \phi \frac{\partial \phi^\dagger}{\partial n}\,\mathrm{d}S\right) = -\mathrm{Im}\left(\iint_{S_a} \phi \frac{\partial \phi^\dagger}{\partial z}\,\mathrm{d}S + \iint_{S_f} \phi \frac{\partial \phi^\dagger}{\partial z}\,\mathrm{d}S\right)$$

Using the boundary condition at the surface, we have:

$$-\mathrm{Re}\left(\iint_{S_\infty} \mathrm{i}\phi \frac{\partial \phi^\dagger}{\partial n}\,\mathrm{d}S\right) = -\mathrm{Im}\left(\iint_{S_a} \sigma^2 |\phi|^2\,\mathrm{d}S + \iint_{S_f} \omega^2 |\phi|\,\mathrm{d}S\right)$$

Let us recall that ω is real, and

$$\mathrm{Im}\left(\sigma^2\right) = \frac{f\omega^3\lambda}{|1-\mathrm{i}\omega\lambda|^2}$$

so

$$-\mathrm{Re}\left(\iint_{S_\infty} \mathrm{i}\phi \frac{\partial \phi^\dagger}{\partial n}\,\mathrm{d}S\right) = -\frac{f\omega^3\lambda}{|1-\mathrm{i}\omega\lambda|^2} \iint_{S_a} |\phi|^2\,\mathrm{d}S$$

We can finally use

$$\zeta = \frac{1}{1-\mathrm{i}\omega\lambda}\eta = \frac{\mathrm{i}\omega}{1-\mathrm{i}\omega\lambda}\,\phi|_{z=0}$$

to get

$$-\mathrm{Re}\left(\iint_{S_\infty} \mathrm{i}\phi \frac{\partial \phi^\dagger}{\partial n}\,\mathrm{d}S\right) = -f\omega\lambda \iint_{S_a} |\zeta|^2\,\mathrm{d}S \tag{B.3.1}$$

that is to say

$$\mathcal{P}' = \mathcal{P}$$

We can check numerically that these two ways to get the extracted power give the same result.

Appendix C

Finite Elements program

Let us give a brief overview of the Finite Element Method to give the choices done in our numerical solution. For a more details about the method, we refer to Ciarlet and Lions (1990).

C.1 Method

In order to solve the eigenvalue problem (4.5.9) numerically, a possible method is to use the Finite Elements Method (FEM). The idea behind this method is to start from the variational formulation, and to approximate the Sobolev space H^1_{per} by a finite dimensional space $\mathcal{H}_h = \text{Span}(\phi_1, \ldots, \phi_n)$. In order to do so, the first step is do define a mesh. Given our geometry the easiest way to mesh the volume was to use two types of elements: 'bricks' and 'wedges'. The 'brick' reference element is

$$\mathcal{B} = [-1, 1]^3$$

and the reference wedge is

$$\mathcal{W} = \{(x, y, z) | 0 \leq x \leq 1, 0 \leq y \leq 1, -1 \leq z \leq 1, y \leq 1 - x\}$$

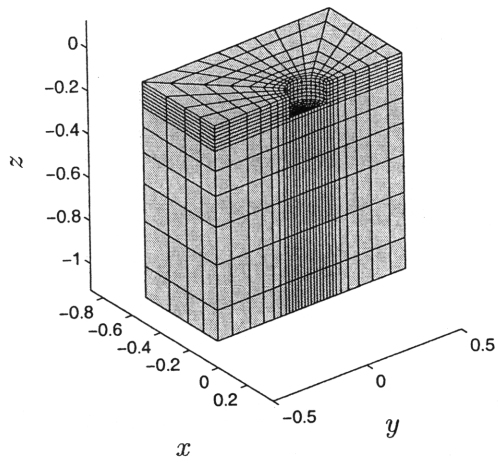

Figure C-1: Example of mesh. The volume is cut and only the region $x \leq 0$ is represented.

On each element are respectively 20 and 15 nodes placed at the vertices and at the mid edges. These two types elements are shows in figure C-2. We then need to

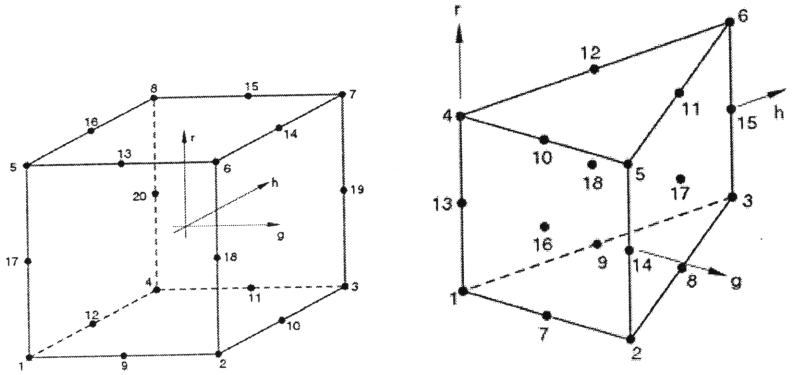

(a) 20-nodes brick (b) 15-nodes wedge

Figure C-2: Reference elements used in the mesh. The images are copied from ABAQUS

define base functions f_i corresponding to each node $\boldsymbol{p}_i$ of an element. On the 'brick', they are chosen to be the unique 2nd order polynomial that verifies $f_i(\boldsymbol{p}_j) = \delta_{i,j}$. If

$\boldsymbol{p}_i = (\xi_i, \eta_i, \zeta_i)$. These functions are given by:

$$f_i(\xi, \eta, \zeta) = \frac{1}{8}(1 + \xi\xi_i)(1 + \eta\eta_i)(1 + \zeta\zeta_i)(\xi\xi_i + \eta\eta_i - 2)$$

$$\xi_i, \eta_i, \zeta_i = \pm 1$$

$$f_i(\xi, \eta, \zeta) = \frac{1}{4}(1 - \xi^2)(1 + \eta\eta_i)(1 + \zeta\zeta_i)$$

$$\xi_i = 0$$

$$f_i(\xi, \eta, \zeta) = \frac{1}{4}(1 + \xi\xi_i)(1 - \eta^2)(1 + \zeta\zeta_i)$$

$$\eta_i = 0$$

$$f_i(\xi, \eta, \zeta) = \frac{1}{4}(1 + \xi\xi_i)(1 + \eta\eta_i)(1 - \zeta^2)$$

$$\zeta_i = 0$$

On a 15-nodes wedge, the definition should be compatible with that of a brick, so we have (see ABAQUS):

$$f_i(\xi,\eta,\zeta) = \frac{1}{2}\left((1-\xi-\eta)(1-2(\xi+\eta))(1+\zeta\zeta_i) - (1-\xi-\eta)(1-\zeta^2)\right)$$
$$i = 1,4$$
$$f_i(\xi,\eta,\zeta) = \frac{1}{2}\left(\xi(2\xi-1)(1+\zeta\zeta_i) - \xi(1-\zeta^2)\right)$$
$$i = 2,5$$
$$f_i(\xi,\eta,\zeta) = \frac{1}{2}\left(\eta(2\eta-1)(1+\zeta\zeta_i) - \eta(1-\zeta^2)\right)$$
$$i = 3,6$$
$$f_i(\xi,\eta,\zeta) = 2(1-\xi-\eta)\xi(1-\zeta\zeta_i)$$
$$i = 7,10$$
$$f_i(\xi,\eta,\zeta) = 2\xi\eta(1-\zeta\zeta_i)$$
$$i = 8,11$$
$$f_i(\xi,\eta,\zeta) = 2(1-\xi-\eta)\eta(1-\zeta\zeta_i)$$
$$i = 9,12$$
$$f_{13}(\xi,\eta,\zeta) = (1-\xi-\eta)(1-\zeta^2)$$
$$f_{14}(\xi,\eta,\zeta) = \xi(1-\zeta^2)$$
$$f_{15}(\xi,\eta,\zeta) = \eta(1-\zeta^2)$$

These functions are used to map the reference element onto an arbitrarily oriented one. If the nodal coordinates are $X = (\boldsymbol{x}_1, \ldots, \boldsymbol{x}_q)$, the global (="real") coordinates of a point $P = (x, y, z)^T$ are related to its local coordinates $\Pi = (\xi, \eta, \zeta)^T$ by

$$P = X(f_1(\Pi), \ldots, f_q(\Pi))^T$$

Listing C.1: Computation of the Jacobian matrix.

```
subroutine jacobian_3D(points_el, x ,y , z, res)

   !points_el contains the coordinates of the nodal points
   !res contains the jacobian matrix in (x,y,z)
   implicit none
   real*8, intent(in) :: points_el(20,3), x, y, z
   real*8, intent(out) :: res(3,3)
   real*8 :: dN(3,20)
   integer :: i

   do i=1,20
      call df(x, y, z, i, dN(1,i), dN(2,i), dN(3,i))
      !return df_i/dx, df_i/dy, df_i/dz in (x,y,z) in dN(1,:)
   end do
   res=matmul(dN, points_el)

end subroutine jacobian_3D
```

If $F = (f_1(\Pi), \ldots, f_q(\Pi))^T$, then the Jacobian matrix of the transformation, that will be useful for computing the integrals, is given by:

$$J(\boldsymbol{\xi}) = X \boldsymbol{\nabla} F(\boldsymbol{\xi})$$

Functions f_i also characterize the restriction of a base function on an element. Let $\mathcal{E}$ be the set of all elements, $\mathcal{V}$ be the set of vertices and $\mathcal{V}_i$ be the set of points on the i-th element $\mathcal{E}_i$. If an arbitrary point of the mesh $\boldsymbol{p}_j$ is the k^{th} point of $\mathcal{E}_i$ then

$$\phi_i|_{\mathcal{E}_i} = f_k(\boldsymbol{x})$$

else

$$\phi_i|_{\mathcal{E}_i} = 0$$

***Remark* C.1.1.** *We can check that the functions ϕ_i defined this way are continuous between two elements and are piecewise $\mathcal{C}^1$, so are in H^1*

Let's recall that the variational formulation is, on $\mathcal{H}_h$:

$$\forall i, \quad \int_\Omega \boldsymbol{\nabla} p \boldsymbol{\nabla} \phi_i^* - i\boldsymbol{k}.(\boldsymbol{\nabla} p \phi_i^* - \phi_i^* \boldsymbol{\nabla} p) + k^2 p \phi_i^* \, dV = \omega^2 \int_{S_f} p \phi_i^* \, dS \tag{C.1.1}$$

Writing $p = \Phi_i \phi_i(\boldsymbol{x})$, we can write (C.1.1) as

$$\left(M_\nabla - ik_x(M_x - M_x^T) - ik_y(M_y - M_y^T) + k^2 M\right) \Phi = \omega^2 M_{top} \Phi \tag{C.1.2}$$

Listing C.2: Computation of $E^i_{j,k}$.

```
subroutine quad_3D_df(points_el,res)

!points_el contains the coordinates of the nodal points
!res contains the jacobian matrix in (x,y,z)

implicit none
real*8, intent(in):: points_el(20,3)
real*8, intent(out) :: res(20,20)
real*8 :: pq(64,3), wq(64), gradfloc(3,20) , matJ(3,3), detJ, invJ(3,3), gradfglobal(3,20), test
integer :: i, j, q

!initialisation
do i=1,20
   do j=1,20
      res(i,j)=0D0
   end do
end do

call quad_3D(pq, wq) !returns the quadrature points and weights

do q=1,64
   do i=1,20
      call df(pq(q,1), pq(q,2), pq(q,3), i, gradfloc(1,i), gradfloc(2,i), gradfloc(3,i))
   end do
   call jacobian_3D(points_el,pq(q,1), pq(q,2), pq(q,3), matJ)
   call det(matJ,detJ)
   call inverse(matJ, invJ)
   gradfglobal=matmul(invJ,gradfloc)
   do i=1,20
      do j=1,20
         res(i,j)=res(i,j)+wq(q)*(gradfglobal(1,i)*gradfglobal(1,j)&
        +gradfglobal(2,i)*gradfglobal(2,j)&
        + gradfglobal(3,i)*gradfglobal(3,j))*abs(detJ)
      end do
   end do
end do

end subroutine quad_3D_df
```

In order to evaluate the coefficients of the matrices in the previous equation, the method is to go back to the reference elements: for example

$$\begin{aligned} M_{\nabla ij} &= \int_\Omega \nabla\phi_i \nabla\phi_j \, dV \\ &= \sum_{\mathcal{E}} \int_{\mathcal{E}_i} \nabla\phi_i \nabla\phi_j \, dV \\ &= \sum_{\mathcal{E}_i} \underbrace{\int_{\mathcal{E}_{ref}} \left(J^{-1}\nabla\phi_j(\boldsymbol{\xi})\right)\left(J^{-1}\nabla\phi_k(\boldsymbol{\xi})\right)|J| \, d\boldsymbol{\xi}}_{E^i_{j,k} \text{ for } P_j, P_k \in \mathcal{E}_i} \end{aligned}$$

As we know the expression of ϕ_i on an element in local coordinates we only have to perform the integration numerically. For this, I use Gauss Legendre quadrature with 64 points on the bricks and 28 points on the wedges (see Bathe (2006)). An example of routine to compute such an integral is given in Listing C.2

We finally want to impose that the functions are periodic. To do so, we can remove

the unnecessary degrees of freedom by writing

$$\Phi = S\Phi_{per}$$

where Φ_{per} contains only the degrees of freedom of the periodic problem. This way the eigenvalue problem is:

$$S^T \left(M_\nabla - ik_x(M_x - M_x^T) - ik_y(M_y - M_y^T) + k^2 M\right) S\Phi_{per} = S^T \omega^2 M_{top} S\Phi_{per} \tag{C.1.3}$$

We now have to solve this generalized eigenvalue problem.

In order to take advantage of the sparsity of the matrices (using full or banded matrices is not possible as it would require too much memory), we used the CSR format to store the matrices. The library SPARSKIT (Saad (2000)) provides routines in order to realize the usual operations. In order to solve the generalized eigenvalue problem, we used the library ARPACK (Sorensen et al. (2008)). It is based upon reverse communication, that is to say that the user has to provide a routine performing matrix vector products and another one solving linear systems. In order to do this last task, we used the Conjugate Gradient (CG) method with Jacobi pre-conditioner.

C.2 Validation of the simulation

In order to check the solution, we computed eigenvalues in a box (i.e. with no buoy) with different types of boundary conditions (periodicity, Neumann, free surface). We also computed band diagrams for the scattering by a cylinder, for which the problem can be solved using `FreeFEM++`. All these cases give good result.

The more critical point is the impact of the finite size of the buoy. Figure C-3(a) shows that the Finite Element solution is still accurate in this case. Note that using $\mathbb{P}_2$ elements, one could have expected a fourth order precision (See Babuska and Osborn (1990)), but we only have a third order scheme. This comes from the fact that our domain is singular.

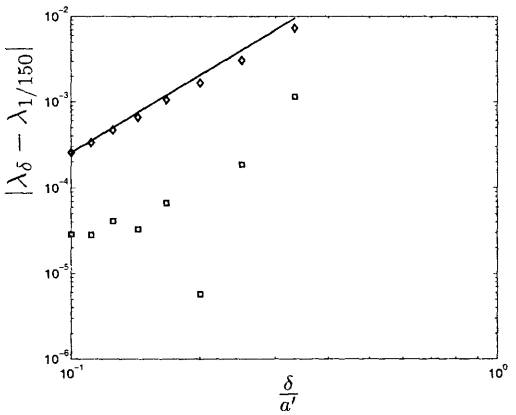

(a) Convergence of the first two eigenvalues with the mesh size δ. The line is proportional to δ^3. The squares correspond to the first eigenvalue and the diamonds to the second one. ($a' = 0.1$ and $d' = 1$)

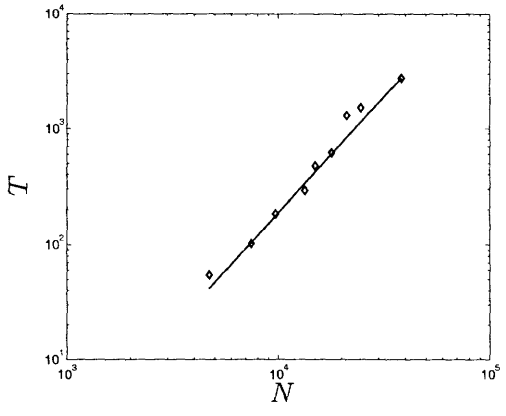

(b) Computation time T in seconds as a function of the number of degrees of freedom N. The line is proportional to N^2

Figure C-3: Numerical results for the Finite Element solution

C.3 Solution of the Boundary Value Problem in Chapter 2

The same steps can be followed in order to solve a Boundary Value problem. The only difference is that, once the matrices are built we only have to solve a linear system. This can be done efficiently using the CG method, as we do for the eigenvalue computation. One should however note that the value of the solution at one point should be imposed in order to make the stiffness matrix positive and definite, which is required for the uniqueness of the solution and for the convergence of the CG algorithm.

Figure C-4 shows the numerical solutions of equations (3.3.31) and (3.3.32). These confirm that solutions are localized near the buoy as expected.

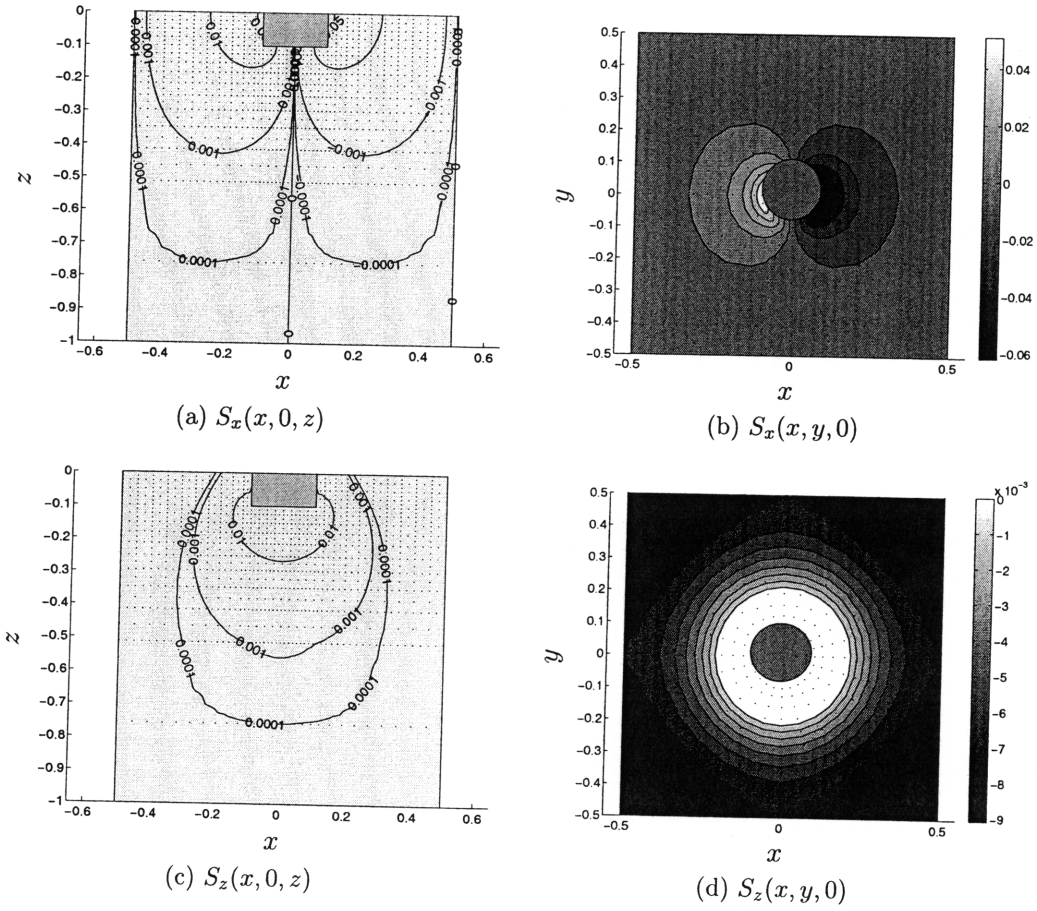

(a) $S_x(x, 0, z)$

(b) $S_x(x, y, 0)$

(c) $S_z(x, 0, z)$

(d) $S_z(x, y, 0)$

Figure C-4: Solutions of (3.3.31) and (3.3.32) for $a' = H' = 0.1$, $d = 1$ and $\mu = 1/10$

Appendix D

Bloch theorem

Bloch theorem is widely used in solid state physics, for which the governing equation is also an eigenvalue problem. A rigorous proof of this theorem would be very difficult, and is not given in most books. Let us follow a few steps to give some insight on the reasons for this theorem, and indicate the point where more mathematical work would be needed.

Let us take the example of the radiation problem expressed in (4.5.1). First of all, let us note that (4.5.1) does not have an unique solution as if ϕ solves it $\lambda\phi$ also does for any $\lambda \in \mathbb{C}$. This is related to the fact that we are considering an eigenvalue problem, as we showed in §4.5.

In order to get a first insight, let us first do the assumption that we have a simple eigenvalue, that is to say that if ϕ and φ are solutions for a given frequency, then $\exists\lambda \in \mathbb{C},\ \phi = \lambda\varphi$. As all boundary conditions are periodic, we can see that if ϕ is a solution then $\forall(n,m) \in \mathbb{Z}^2$

$$\phi(\boldsymbol{x}' + nd'\boldsymbol{e}_x + md'\boldsymbol{e}_y)$$

which is the initial solution translated of an arbitrary number of cells in the x' and y' directions, is also a solution. Therefore $\exists C_{n,m} \in \mathbb{C}$ so that

$$\phi(\boldsymbol{x} + nd\boldsymbol{e}_x + md\boldsymbol{e}_y) = C_{n,m}\phi(\boldsymbol{x})$$

We can also note that as the sum of two periods is another period, which gives

$$C_{n+n',m} = C_{n,m}C_{n',m}$$

so $\exists \boldsymbol{k}' = (k'_x, k'_y, 0)$ such that

$$C_{n,m} = \mathrm{e}^{\mathrm{i}(nk'_x + mk'_y)}$$

The vector $\boldsymbol{k}'$ should be real so that the solution is bounded.

Knowing $\boldsymbol{k}'$ and ϕ on an unit cell, we can know the value of the potential at any point, and

$$\widetilde{\phi} = \mathrm{e}^{-\mathrm{i}\boldsymbol{k}'\cdot\boldsymbol{x}'}\phi$$

is $d'-$periodic in both x'' and y'.

We can now try a more general reasoning. Indeed, one can note that the hypothesis that the eigenvalue is simple is not relevant, as for example in the case of a free surface with no buoy we know that solutions exist for any direction of the wave number, only its magnitude is given. Let $\mathcal{E}$ be the space of solutions of our problem, and let us assume that it has an Hermitian basis *(this is the point where the proof fails in general)*, $\mathcal{E} = \mathrm{Span}(\phi_1, ...)$. We now have that

$$\phi_i(x + d, y, z) = C'_{i,j}(d)\phi_j(x, y, z)$$

and similarly

$$[\phi_i(x + 2d, y, z)] = C'_{i,j}(d)C'_{j,k}(d)[\phi_k(x, y, z)]$$

and so on, so $C'(nd) = C'(d)^n$. Similarly, we find that

$$\phi_i(x + nd, y + md, z) = C'^n C''^m \phi_i(x, y, z)$$

We can now make use of the fact that C and C' commute and can be diagonalized *(this is also a critical point)*, so that they can be diagonalized simultaneously. Therefore

there would exist a set a functions φ_i

$$\varphi_i(x + nd, y + md, z) = \lambda_i^n \lambda_i^m \varphi_i(x, y, z)$$

Imposing that potentials should remain bounded gives us that there is a basis of functions (ψ_i) such that

$$\mathrm{e}^{-\mathrm{i}\boldsymbol{k}_i' \cdot \boldsymbol{x}'} \psi_i$$

is periodic in x' and y'.

Appendix E

Inner solution approximation for semi-spherical buoys

The objective in this part is to find an inner approximation to the flow around a small buoy for the scattering and radiation problems. The results that follow are derived for the approximation of the first order term of the multiple scale analysis and then modified for the flow around a single small buoy. Let us consider a semi-spherical buoy, and use spherical coordinates

$$\bar{r}, \theta, \varphi$$

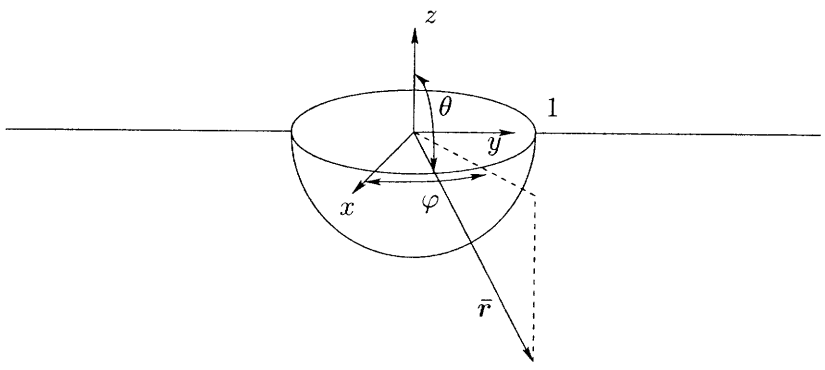

Figure E-1: Geommetry of the inner approximation

With these coordinates, the surface of the buoy is defined by

$$\bar{r} = 1 \qquad \theta \in \left[\frac{\pi}{2}, \pi\right] \qquad \phi \in [0, 2\pi]$$

E.1 Scattering

The first order solution for the scattering problem should compensate the mass flux inside the buoy due to the first order solution. Let us re-express this forcing term in spherical coordinates:

$$\begin{aligned}
\frac{\partial \phi_{S,1}}{\partial \bar{r}} &= -\frac{1}{\mu}\frac{\partial \alpha^+ Z(z)\mathrm{e}^{\mathrm{i}k'x'} + \alpha^- Z(z)\mathrm{e}^{-\mathrm{i}k'x'}}{\partial r'} \\
&= -\frac{1}{\mu}\left(\frac{\partial \alpha^+ Z(z)\mathrm{e}^{\mathrm{i}k'x'} + \alpha^- Z(z)\mathrm{e}^{-\mathrm{i}k'x'}}{\partial x'}\boldsymbol{e}_x.\boldsymbol{e}_r\right. \\
&\quad \left. + \frac{\partial \alpha^+ Z(z)\mathrm{e}^{\mathrm{i}k'x'} + \alpha^- Z(z)\mathrm{e}^{-\mathrm{i}k'x'}}{\partial z'}\boldsymbol{e}_x.\boldsymbol{e}_z\right) \\
&= -\frac{1}{\mathrm{i}\omega'\mu}\left(\mathrm{i}k'(\alpha^+ - \alpha^-)\sin(\theta)\cos(\varphi) + \omega'^2(\alpha^+ + \alpha^-)\cos(\theta)\right)
\end{aligned}$$

As we assumed that $\omega' \sim 1$ then

$$\frac{\partial \phi^{in}_{S,1}}{\partial \bar{z}} = \frac{1}{\mu}\frac{\partial \phi^{in}_{S,1}}{\partial z'} \gg \omega'^2 \phi^{in}_S$$

so the free surface condition for the inner approximation can be approximated by

$$\frac{\partial \phi^{in}_S}{\partial \bar{z}} = \bar{r}\frac{\partial \phi^{in}_S}{\partial \theta} = 0 \quad \text{for } \theta = \frac{\pi}{2},\ \bar{r} \geq \bar{1} \tag{E.1.1}$$

This condition is equivalent to assuming that the solution should be symmetric with respect to the (x, y) plane, i.e. $\theta = \pi/2$, so we are looking for ϕ^{in}_S so that $\forall\theta \in [0, \pi]$ and $\forall\varphi \in [0, 2\pi]$

$$\bar{\Delta}\phi^{in}_{S,1} = 0 \qquad \bar{r} \geq 1 \quad \text{(E.1.2)}$$

$$\frac{\partial \phi^{in}_{S,1}}{\partial \bar{r}} = -\frac{1}{\mathrm{i}\omega'\mu}\left(\mathrm{i}k'(\alpha^+ - \alpha^-)\sin(\theta)\cos(\varphi) + \omega'^2(\alpha^+ + \alpha^-)|\cos(\theta)|\right) \quad \bar{r} = 1 \quad \text{(E.1.3)}$$

Solving for the first term (E.1.3) takes a particularly simple form as

$$\frac{\mathrm{i}k'(\alpha^+ - \alpha^-)}{2\mathrm{i}\omega'\mu}\frac{\sin(\theta)\cos(\varphi)}{\bar{r}^2} \tag{E.1.4}$$

is a solution. Let us now focus on the second term: we look for ψ so that

$$\phi^{in}_{S,1} = -(\alpha^+ + \alpha^-)\frac{\omega'^2}{\mathrm{i}\omega'\mu}\psi + \frac{\mathrm{i}k'(\alpha^+ - \alpha^-)}{2\mathrm{i}\omega'\mu}\frac{\sin(\theta)\cos(\varphi)}{\bar{r}^2} \tag{E.1.5}$$

In order to solve the Laplace equation, ψ should be expandable using spherical harmonics (See Morse and Feshbach (1953), §10, or Weisstein (b) for further details. In particular we assumed there that the solution should tend to zero at infinity):

$$\psi = \sum_{l=0}^{\infty}\sum_{m=-l}^{l}\frac{f_{l,m}}{\bar{r}^{l+1}}Y_l^m(\theta,\varphi) \tag{E.1.6}$$

Using (E.1.6) in (E.1.3) we get that $\forall\theta,\varphi$

$$-\sum_{l=0}^{\infty}\sum_{m=-l}^{l}(l+1)f_{l,m}Y_l^m(\theta,\varphi) = |\cos(\theta)|$$

Using the orthogonality relations we get that

$$f_{l,m} = -\frac{1}{(l+1)}\int_0^{2\pi}\int_0^{\pi}\sin(\theta)|\cos(\theta)|Y_l^m(\theta,\varphi)^{\dagger}\,\mathrm{d}\theta\,\mathrm{d}\varphi$$

As

$$Y_l^m(\theta,\varphi) \equiv \sqrt{\frac{(2l+1)(l-m)!}{4\pi(l+m)!}}P_l^m(\cos(\theta))\mathrm{e}^{\mathrm{i}m\varphi}$$

we see that only the terms for $m = 0$ will be non zero, so we finally get (See Morse and Feshbach (1953), §5, or Weisstein (a))

$$\begin{aligned} f_l \equiv f_{l,0} &= -\frac{1}{(l+1)}\sqrt{\frac{2l+1}{4\pi}}\int_0^{\pi}\sin(\theta)|\cos(\theta)|P_l(\cos(\theta))\,\mathrm{d}\theta \\ &= \frac{1}{l+1}\sqrt{\frac{2l+1}{4\pi}}\int_{-1}^{1}|u|P_l(u)\,\mathrm{d}u \end{aligned}$$

with $P_l \equiv P_l^0$. Note first that as $P_l(u)$ is odd in u for l odd the integral will be zero in these cases. For l even, we have (See Byerly (1959), p. 172)

$$f_l = \frac{1}{l+1}\sqrt{\frac{2l+1}{4\pi}}\frac{(-1)^{l/2+1}l!}{2^{l-1}(l-1)(l+2)\left(\frac{l}{2}!\right)^2}$$

Using Stirling's formula, we see that $f_l \sim l^{-3}$, which makes the series absolutely convergent for $\bar{r} \geq 1$. We finally get that

$$\psi(\bar{r},\theta,\varphi) = \sum_{l=0}^{\infty} \frac{f_{2l}}{\bar{r}^{2l+1}}\sqrt{\frac{(4l+1)}{4\pi}}P_{2l}(\cos(\theta)) \tag{E.1.7}$$

so combining (E.1.4) and (E.1.7), we get that $\phi_{S,1}$ verifies

$$\phi_{S,1} \sim \frac{\mathrm{i}k'(\alpha^+ - \alpha^-)}{2\mathrm{i}\omega'\mu}\frac{\sin(\theta)\cos(\varphi)}{\bar{r}^2} - \frac{\omega'^2}{\mathrm{i}\omega'\mu}(\alpha^+ + \alpha^-)\sum_{l=0}^{\infty}\frac{f_{2l}}{\bar{r}^{2l+1}}\sqrt{\frac{(4l+1)}{4\pi}}P_{2l}(\cos(\theta)) \tag{E.1.8}$$

in the neighborhood of the buoy. Note that although the $\dfrac{\partial\phi_{S,1}}{\partial r'}$ is order μ^{-2} on the surface of the buoy, $\phi_{S,1}$ is only of order μ^{-1}, which is confirms our remark in §4.6.2. Let us now show that the same thing will be true for the radiation problem.

E.2 Radiation

The radiation problem is similar to the scattering problem, except this time the boundary condition in $\bar{r} = 1$ is

$$\frac{\partial\phi_{R,1}^{in}}{\partial\bar{r}} = -\frac{1}{\mathrm{i}\omega'\mu}\left(\mathrm{i}k'(\beta^+ - \beta^-)\sin(\theta)\cos(\varphi) + \omega'^2\left[\beta^+ + \beta^- - \zeta\right]|\cos(\theta)|\right) \tag{E.2.1}$$

and so

$$\phi_{R,1} \sim \frac{\mathrm{i}k'(\beta^+ - \beta^-)}{2\mathrm{i}\omega'\mu} \frac{\sin(\theta)\cos(\varphi)}{\bar{r}^2} - \frac{\omega'^2(\beta^+ + \beta^- - \zeta)}{\mathrm{i}\omega'\mu} \sum_{l=0}^{\infty} \frac{f_{2l}}{\bar{r}^{2l+1}} \sqrt{\frac{(4l+1)}{4\pi}} P_{2l}(\cos(\theta)) \quad \text{(E.2.2)}$$

This show us that the radiation potential is of the same order of magnitude as the scattering one.

E.3 Scattering and radiation by a small buoy

Let us consider a monochromatic incoming wave, and decompose the diffraction potential as

$$\phi = Z(z')\mathrm{e}^{\mathrm{i}k'x'} + \phi_S$$

Expressing that there should be no mass flux inside the buoy, we have

$$\frac{\partial \phi}{\partial \bar{r}} = \frac{\partial}{\partial \bar{r}} \left(Z(z')\mathrm{e}^{\mathrm{i}k'x'} \right) + \frac{\partial \phi_S}{\partial \bar{r}} = 0$$

Assuming that the buoy is located in $x' = 0$, it follows that

$$\frac{\partial \phi_S}{\partial \bar{r}} = -\mu Z(z') \frac{\partial \mathrm{e}^{\mathrm{i}k'x'}}{\partial r'}$$

which is very similar to the problem we just solved with $\alpha^+ = 1$ and $\alpha^- = 0$. The only difference is that we do not consider a perturbation expansion. The result is therefore

$$\phi_S \sim \frac{\mu}{\mathrm{i}\omega'} \left(\frac{\mathrm{i}k'}{2} \frac{\sin(\theta)\cos(\varphi)}{\bar{r}^2} - \omega'^2 \sum_{l=0}^{\infty} \frac{f_{2l}}{\bar{r}^{2l+1}} \sqrt{\frac{(4l+1)}{4\pi}} P_{2l}(\cos(\theta)) \right) \quad \text{(E.3.1)}$$

Similarly, the radiation potential can be approximated as

$$\phi_R \sim \mu\zeta \sum_{l=0}^{\infty} \frac{f_{2l}}{\bar{r}^{2l+1}} \sqrt{\frac{(4l+1)}{4\pi}} P_{2l}(\cos(\theta)) \quad \text{(E.3.2)}$$

What we see here is that even in the neighborhood of the buoy, the scattering and radiation potentials (and so the pressures) are of order μ compared to the potential due to the incoming wave. As a consequence, the only hydrodynamic forces applied to the buoy will be, to the leading order, a scattering force due to the incoming wave and forces due to hydrostatic pressure.

E.4 Application to the solvability condition

E.4.1 Scattering

Using the inner approximation derived earlier, we can use it in the solvability condition. The volume integral and the surface integral over S_f are computed in §4.6.2. Let us evaluate the integrals over the surface of the buoy. The first term is [1]

$$
\begin{aligned}
I_1 &\equiv \frac{1}{\mu^2}\int_{S_b} Z(z')\mathrm{e}^{\mp \mathrm{i}k'x'}\frac{\partial\left[\alpha^+ Z(z')\mathrm{e}^{\mathrm{i}k'x'}+\alpha^- Z(z')\mathrm{e}^{-\mathrm{i}k'x'}\right]}{\partial r}\,\mathrm{d}S' \\
&= \frac{1}{\mu^2}\alpha^+\int_{S_b} Z(z')\mathrm{e}^{\pm \mathrm{i}k'x'}\left(\mathrm{i}k'\boldsymbol{e}_r.\boldsymbol{e}_x\mathrm{e}^{\mathrm{i}k'x'}Z(z')+\boldsymbol{e}_r.\boldsymbol{e}_z\mathrm{e}^{\mathrm{i}k'x'}\frac{\mathrm{d}Z}{\mathrm{d}z'}\right)\mathrm{d}S' \\
&\quad + \frac{1}{\mu^2}\alpha^-\int_{S_b} Z(z')\mathrm{e}^{\pm \mathrm{i}k'x'}\left(-\mathrm{i}k'\boldsymbol{e}_r.\boldsymbol{e}_x\mathrm{e}^{-\mathrm{i}k'x'}Z(z')+\boldsymbol{e}_r.\boldsymbol{e}_z\mathrm{e}^{-\mathrm{i}k'x'}\frac{\mathrm{d}Z}{\mathrm{d}z'}\right)\mathrm{d}S' \\
&= -\frac{\alpha^+}{\omega'^2\mu^2}\int_{S_b}\left(\mathrm{i}k'\boldsymbol{e}_r.\boldsymbol{e}_x+\boldsymbol{e}_r.\boldsymbol{e}_z\omega'^2\right)\mathrm{d}S' \\
&\quad - \frac{\alpha^-}{\omega'^2\mu^2}\int_{S_b}\left(-\mathrm{i}k'\boldsymbol{e}_r.\boldsymbol{e}_x+\boldsymbol{e}_r.\boldsymbol{e}_z\omega'^2\right)\mathrm{d}S' \\
&= -\frac{\alpha^+}{\omega'^2}\int_0^{2\pi}\int_{\pi/2}^{\pi}\left(\mathrm{i}k'\sin(\theta)\cos(\varphi)+\cos(\theta)\omega'^2\right)\sin(\theta)\,\mathrm{d}\theta\,d\varphi \\
&\quad - \frac{\alpha^-}{\omega'^2}\int_0^{2\pi}\int_{\pi/2}^{\pi}\left(-\mathrm{i}k'\sin(\theta)\cos(\varphi)+\cos(\theta)\omega'^2\right)\sin(\theta)\,\mathrm{d}\theta\,d\varphi \\
&= -\pi\left(\alpha^+ + \alpha^-\right) + O(\mu)
\end{aligned}
$$

[1] S_b is the semi spherical surface of the buoy.

Equation (E.1.8) is needed in order to evaluate the last term:

$$
\begin{aligned}
I_2 &\equiv -\int_{S_b} \phi_1 \frac{\partial Z(z')\mathrm{e}^{\mp \mathrm{i}k'x'}}{\partial r}\,\mathrm{d}S' \\
&= -\int_{S_b} \frac{1}{\mathrm{i}\omega'}\left(\pm \mathrm{i}k' \boldsymbol{e}_r.\boldsymbol{e}_x + \boldsymbol{e}_r.\boldsymbol{e}_z\omega'^2\right)\phi_1^{in}\,\mathrm{d}S' \\
&= -\mu^2 \int_0^{2\pi}\int_{\pi/2}^{\pi} \frac{1}{\mathrm{i}\omega'}\left[\pm \mathrm{i}k'\sin(\theta)\cos(\varphi) + \cos(\theta)\omega'^2\right]\sin(\theta)\phi_1^{in}\,\mathrm{d}\theta\,\mathrm{d}\varphi \\
&= -\mu^2 \frac{\mathrm{i}k'(\alpha^+ - \alpha^-)}{2\mathrm{i}\omega'\mu}\int_0^{2\pi}\int_{\pi/2}^{\pi}\left(\pm \mathrm{i}k'\sin(\theta)\cos(\varphi) + \cos(\theta)\omega'^2\right) \\
&\qquad \times \sin^2(\theta)\cos(\varphi)\,\mathrm{d}\theta\,\mathrm{d}\varphi \\
&\quad + \mu^2 \frac{\omega'^2}{\mathrm{i}\omega'\mu}(\alpha^+ + \alpha^-)\int_0^{2\pi}\int_{\pi/2}^{\pi}\left(\pm \mathrm{i}k'\sin(\theta)\cos(\varphi) + \cos(\theta)\omega'^2\right) \\
&\qquad \times \sum_{l=0}^{\infty} f_{2l}\sqrt{\frac{(4l+1)}{4\pi}}P_{2l}(\cos(\theta))\sin(\theta)\,\mathrm{d}\theta\,\mathrm{d}\varphi \\
&= \frac{\mu}{\mathrm{i}\omega'}\left(\frac{k'^2(\alpha^+ - \alpha^-)\pi}{3} - \omega^4(\alpha^+ + \alpha^-)2\pi\sum_{l=0}^{\infty} f_{2l}\sqrt{\frac{(4l+1)}{4\pi}}\int_{-1}^{0} uP_{2l}(u)\,\mathrm{d}u\right)
\end{aligned}
$$

As we mentioned in §4.6.2, this term is of order μ compared to the previous one, and therefore should be neglected in the solvability condition. We finally get

$$
\frac{2d^2}{\mathrm{i}\omega'}\frac{\partial \alpha^{\pm}}{\partial t} \pm 2\mathrm{i}k'd^2\frac{\partial \alpha^{\pm}}{\partial x}\int_{-h}^{0} Z(z')^2\,\mathrm{d}z = -\pi\left(\alpha^+ + \alpha^-\right) + O(\mu)
$$

that is to say:

$$
\frac{\partial \alpha^{\pm}}{\partial t} \pm C_g'\frac{\partial \alpha^{\pm}}{\partial x} = -\mathrm{i}\Omega_0\left(\alpha^+ + \alpha^-\right) \tag{E.4.1}
$$

This is the same result as in the case of a cylindrical buoy, due to the fact that only the projection of the surface of the buoy onto the (x', y') plane matters.

E.4.2 Radiation

As we saw, the inner approximation for radiation is the same as that for scattering replacing $\alpha^+ + \alpha^-$ by $\beta^+ + \beta^- - \zeta$. This gives that the corresponding integrals in the solvability conditions are:

$$
I_1 = -\pi\left(\beta^+ + \beta^- - \zeta\right)
$$

and

$$I_2 = \mu\pi\left(\frac{k'^2(\beta^+ - \beta^-)}{3} - \omega'^4\left(\beta^+ + \beta^- - \zeta\right)\sum_{l=0}^{\infty} f_{2l}\sqrt{\frac{(4l+1)}{4\pi}}\int_{-1}^{0} uP_{2l}(u)\,\mathrm{d}u\right)$$

Once again, the result of the solvability condition is the same as for a cylindrical buoy, namely

$$\frac{\partial\beta^{\pm}}{\partial t} \pm C'_g\frac{\partial\beta^{\pm}}{\partial x} = -\mathrm{i}\Omega_0\left(\beta^+ + \beta^- - \zeta\right)$$

Appendix F

Solution of the radiation problem for the sparse array

F.1 Numerical solution

The system of equations (4.7.16) expresses a conservation law. A simple kind of scheme for this type of problem are the upwind schemes, that can be seen as Finite Differences schemes. The first step is therefore to divide the interval $[0, L]$ into N subintervals of length

$$\delta x = \frac{L}{N}$$

which gives $N + 1$ equi-spaced points

$$0 = x_0 \leq x_1 \leq \cdots \leq x_N = L$$

We do not need to solve for the scattering potentials, as we already have an analytical expression for them. Let us recall that we want to solve

$$-\mathrm{i}\Omega\widehat{\beta}^{+} + C_g' \frac{\partial \widehat{\beta}^{+}}{\partial x} = -\mathrm{i}\Omega_0 \left[(1 - \mathcal{G})(\widehat{\beta}^{+} + \widehat{\beta}^{-}) - \mathcal{G}(\widehat{\alpha}^{+} + \widehat{\alpha}^{-}) \right] \tag{F.1.1}$$

$$-\mathrm{i}\Omega\widehat{\beta}^{-} - C_g' \frac{\partial \widehat{\beta}^{-}}{\partial x} = -\mathrm{i}\Omega_0 \left[(1 - \mathcal{G})(\widehat{\beta}^{+} + \widehat{\beta}^{-}) - \mathcal{G}(\widehat{\alpha}^{+} + \widehat{\alpha}^{-}) \right] \tag{F.1.2}$$

so we have $2N$ degrees of freedom: the values of $\widehat{\beta}^+$ at $x_1, \ldots, x_N$ and the values of $\widehat{\beta}^-$ at $x_0, \ldots, x_{N-1}$. In order to discretize the differentiation operator, let us use the 2nd order finite difference formulas:

$$f'(x_j) = \frac{-3f(x_j) + 4f(x_{j+1}) - f(x_{j+2})}{2\delta x} + O(\delta x^2) \tag{F.1.3}$$

$$= \frac{f(x_{j-2}) - 4f(x_{j-1}) + 3f(x_j)}{2\delta x} + O(\delta x^2) \tag{F.1.4}$$

In (F.1.1), the information propagates from the left, so we use (F.1.4). On the contrary in (F.1.2) it goes from the right to the left, so we will use (F.1.3). At the end points, where we would need the values of $\widehat{\beta}^+(x_{-1})$ or $\widehat{\beta}^-(x_{N+1})$, we use centered finite differences

$$f'(x_j) = \frac{-f(x_{j-1}) + f(x_{j+1})}{2\delta x} + O(\delta x^2)$$

In matricial form, let us introduce the unknown

$$X = (\widehat{\beta}_1^+, \ldots, \widehat{\beta}_N^+, \widehat{\beta}_0^-, \ldots, \widehat{\beta}_{N-1}^-)^T$$

the forcing term

$$Y = (\widehat{\alpha}_1^+ + \widehat{\alpha}_1^-, \ldots, \widehat{\alpha}_N^+ + \widehat{\alpha}_N^-, \widehat{\alpha}_0^- + \widehat{\alpha}_0^-, \ldots, \widehat{\alpha}_{N-1}^- + \widehat{\alpha}_{N-1}^-)^T$$

and the matrices

$$R^+ = \begin{bmatrix} 0 & 1 & & \\ & \ddots & \ddots & \\ & & \ddots & 1 \\ & & & 0 \end{bmatrix} \qquad D^+ = \frac{1}{2\delta x} \begin{bmatrix} -3 & 4 & -1 & & \\ & \ddots & \ddots & \ddots & \\ & & \ddots & \ddots & -1 \\ & & & -3 & 4 \\ & & & -1 & 0 \end{bmatrix}$$

$$R^- = R^{+T} \qquad D^- = \frac{1}{2\delta x} \begin{bmatrix} 0 & 1 & & & \\ -4 & 3 & & & \\ 1 & \ddots & \ddots & & \\ & \ddots & \ddots & \ddots & \\ & & 1 & -4 & 3 \end{bmatrix}$$

This allows us to express the discrete problem as

$$\left[\begin{array}{c|c} (-\mathrm{i}(\Omega - \Omega_0\mathcal{G})\mathrm{Id} + C_g' D^- & \mathrm{i}\Omega_0\mathcal{G}R^+ \\ \hline \mathrm{i}\Omega_0\mathcal{G}R^- & -\mathrm{i}(\Omega - \Omega_0\mathcal{G})\mathrm{Id} - C_g' D^+ \end{array}\right] X = \mathrm{i}\Omega_0\mathcal{G}Y \qquad \text{(F.1.5)}$$

where Id is the identity matrix. We can check numerically that this scheme is second order accurate, as it is shown in figure F-1

F.2 Analytical solution

F.2.1 General case

The forcing term, $\widehat{\alpha}^+ + \widehat{\alpha}^-$, can be written of the form

$$\widehat{\alpha}^+ + \widehat{\alpha}^- = \mathcal{A}^+ \mathrm{e}^{\mathrm{i}K_S x} + \mathcal{A}^- \mathrm{e}^{-\mathrm{i}K_S x}$$

where $\mathcal{A}^\pm$ are known from (4.6.22). In order to simplify the algebra let us solve separately for each of the complex exponential above. Let us first consider the auxiliary

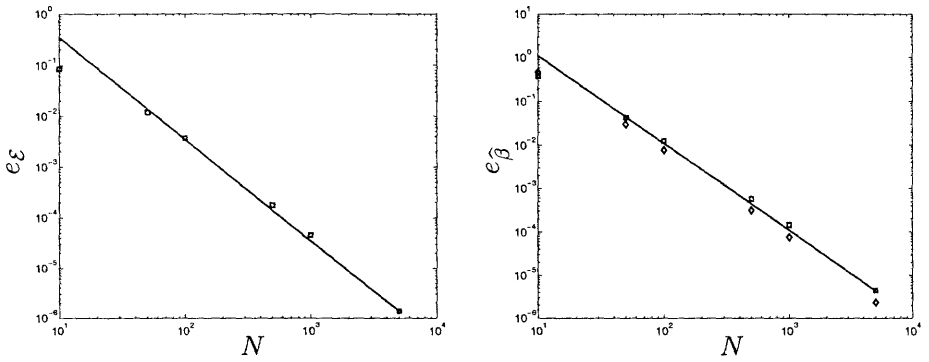

(a) $\Omega = \Omega_0$

(b) $\Omega = \Omega_0$

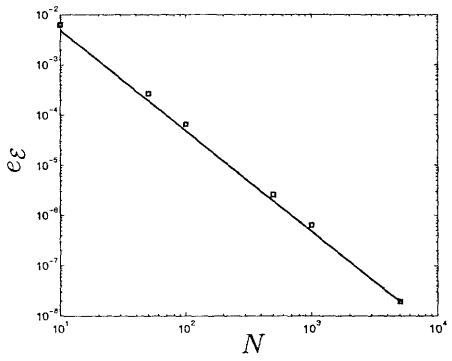

(c) $\Omega = 0$

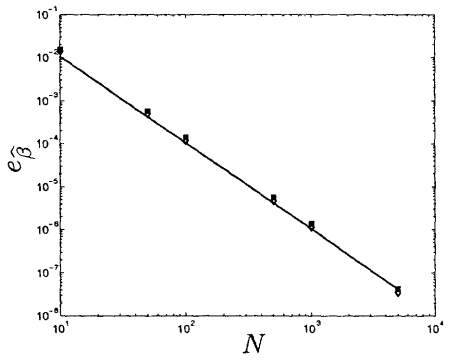

(d) $\Omega = 0$

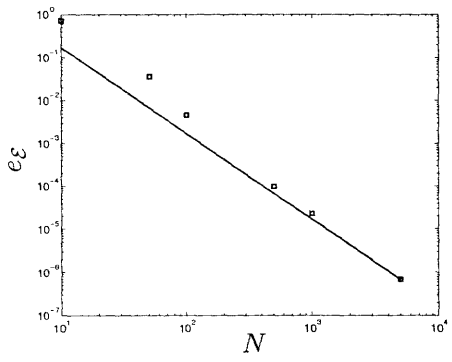

(e) $\Omega = -\Omega_0$

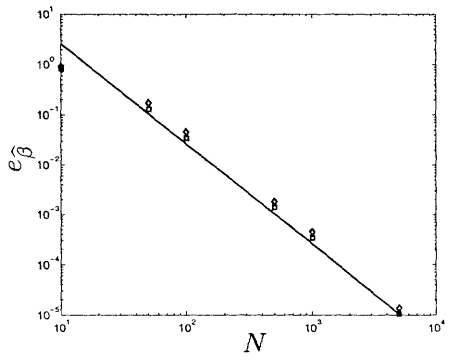

(f) $\Omega = -\Omega_0$

Figure F-1: Convergence of the numerical solution in terms of $e_{\mathcal{E}} = \frac{|\mathcal{E}_N - \mathcal{E}_{N_0}|}{\mathcal{E}_{N_0}}$ and $e_{\widehat{\beta}^{\pm}} = \frac{\left\|\widehat{\beta}^{\pm}_N - \widehat{\beta}^{\pm}_{N_0}\right\|_{L^2}}{\left\|\widehat{\beta}^{\pm}_{N_0}\right\|_{L^2}}$. The squares represent $e_{\widehat{\beta}^+}$ and the diamonds $e_{\widehat{\beta}^-}$. ($\lambda_g = 1$, $L = 1$ and $N_0 = 10^4$)

problem

$$-\mathrm{i}K\widehat{\beta}_1^+ + \frac{\partial\widehat{\beta}_1^+}{\partial x} = -\mathrm{i}K_\lambda(\widehat{\beta}_1^+ + \widehat{\beta}_1^-) + \mathrm{e}^{\mathrm{i}K_S x} \tag{F.2.1a}$$

$$-\mathrm{i}K\widehat{\beta}_1^- - \frac{\partial\widehat{\beta}_1^-}{\partial x} = -\mathrm{i}K_\lambda(\widehat{\beta}_1^+ + \widehat{\beta}_1^-) + \mathrm{e}^{\mathrm{i}K_S x} \tag{F.2.1b}$$

with

$$K_\lambda = (1-\mathcal{G})\Omega_0/C_g'$$

It is possible to decouple these two equations by differentiating (F.2.1). We get

$$\frac{\mathrm{d}^2\widehat{\beta}_1^+}{\mathrm{d}x^2} + K_R^2\widehat{\beta}_1^+ = \mathrm{i}\,(K+K_S)\,\mathrm{e}^{\mathrm{i}K_S x}$$
$$\frac{\mathrm{d}^2\widehat{\beta}_1^-}{\mathrm{d}x^2} + K_R^2\widehat{\beta}_1^- = \mathrm{i}\,(K-K_S)\,\mathrm{e}^{\mathrm{i}K_S x}$$

with

$$K_R \equiv \sqrt{K\,(K-2K_\lambda)}$$

Recall that

$$K = \Omega/C_g'$$

K_R is the natural wave number of the radiated wave. As $\mathcal{G}$ is complex for any non zero λ_g, K_R will be too. This means that for any detuning the wave amplitude will be attenuated. This is consistent with the fact that this problem takes into account the energy extraction. One can also see that this natural frequency differs from K_S, which means that no resonance is to be expected.

Note that we traded two first order coupled equations for two second order decoupled equations. We will therefore have to re-express the coupling later. It is easy to see that

$$\widehat{\beta}_1^+ = C_1^1\mathrm{e}^{\mathrm{i}K_R x} + C_1^2\mathrm{e}^{-\mathrm{i}K_R x} + \mathrm{i}\frac{K+K_S}{K_R^2-K_S^2}\mathrm{e}^{\mathrm{i}K_S x}$$
$$\widehat{\beta}_1^- = C_1^3\mathrm{e}^{\mathrm{i}K_R x} + C_1^4\mathrm{e}^{-\mathrm{i}K_R x} + \mathrm{i}\frac{K-K_S}{K_R^2-K_S^2}\mathrm{e}^{\mathrm{i}K_S x}$$

Let us introduce

$$A_1^+ = \frac{K + K_S}{K_R^2 - K_S^2} \qquad A_1^- = \frac{K - K_S}{K_R^2 - K_S^2}$$

We should now express the boundary conditions

$$C_1^1 + C_1^2 = -\mathrm{i}A_1^+ \tag{F.2.2a}$$

$$C_1^3 \mathrm{e}^{\mathrm{i}K_R L} + C_1^4 \mathrm{e}^{-\mathrm{i}K_R L} = -\mathrm{i}A_1^- \mathrm{e}^{\mathrm{i}K_S L} \tag{F.2.2b}$$

and the coupling between the two equations, for example at $x = 0$

$$\mathrm{i}K_R(C_1^1 - C_1^2) + \mathrm{i}A^+\mathrm{i}K_S + \mathrm{i}\Omega_0 \left(C_1^3 + C_1^4 + \mathrm{i}A_1^-\right) = 1 \tag{F.2.2c}$$

$$-\mathrm{i}(\Omega - \Omega_0) \left(C_1^3 + C_1^4 + \mathrm{i}A^-\right) - \mathrm{i}K_R(C_1^3 - C_1^4) - \mathrm{i}A_1^+\mathrm{i}K_S + = 1 \tag{F.2.2d}$$

This gives us a system of 4 equations and 4 unknown. Note however that (F.2.2b) and (F.2.2d) can be solved first and then the result can be inserted in the two other equations. In any case, the system can be solved analytically, and the result is given in (F.2.3) on page 182.

Correctness of the expression has been checked with numerical solution of (F.2.2). We can similarly treat the problem where the forcing is $\exp(-\mathrm{i}K_S x)$. This is exactly the same thing replacing K_S by $-K_S$. Let us introduce

$$\widehat{\beta}_2^+ = C_2^1 \mathrm{e}^{\mathrm{i}K_R x} + C_2^2 \mathrm{e}^{-\mathrm{i}K_R x} + \mathrm{i}\frac{K - K_S}{K_R^2 - K_S^2} \mathrm{e}^{\mathrm{i}K_S x}$$

$$\widehat{\beta}_2^- = C_2^3 \mathrm{e}^{\mathrm{i}K_R x} + C_2^4 \mathrm{e}^{-\mathrm{i}K_R x} + \mathrm{i}\frac{K + K_S}{K_R^2 - K_S^2} \mathrm{e}^{\mathrm{i}K_S x}$$

As we did before, we can express the coupling and boundary condition. The result is given (F.2.3) on page 182.

Let us now write

$$\widehat{\alpha}^+ + \widehat{\alpha}^- = C_g' \left(\mathcal{A}^+ \mathrm{e}^{\mathrm{i}K_S x} + \mathcal{A}^- \mathrm{e}^{-\mathrm{i}K_S x}\right)$$

Using (4.6.22), we find

$$\mathcal{A}^+ = \mathrm{e}^{-\mathrm{i}K_S L}\frac{K_S + K}{2\left(-\mathrm{i}(\Omega - \Omega_0)\sin(K_S L) + \Omega_1\cos(K_S L)\right)}$$
$$\mathcal{A}^- = \mathrm{e}^{\mathrm{i}K_S L}\frac{K_S - K}{2\left(-\mathrm{i}(\Omega - \Omega_0)\sin(K_S L) + \Omega_1\cos(K_S L)\right)}$$

It is now easy to see that

$$\widehat{\beta}^+ = \mathrm{i}\Omega_0\mathcal{G}\left(\mathcal{A}^+\widehat{\beta}_1^+ + \mathcal{A}^-\widehat{\beta}_2^+\right)$$
$$\widehat{\beta}^- = \mathrm{i}\Omega_0\mathcal{G}\left(\mathcal{A}^+\widehat{\beta}_1^- + \mathcal{A}^-\widehat{\beta}_2^-\right)$$

are the solutions of the radiation problem, as they solve (F.1.1) and (F.1.2) as well as the boundary conditions (4.7.21). The numerical results obtained with these formulas are consistent with those obtained by the Finite Volume method.

$$C_1^1 = -\mathrm{i}\frac{K_R\left(A_1^+(K_R+K_S)+A_1^-K_\lambda+1\right)\cos(K_RL)-A_1^-K_\lambda K_R\mathrm{e}^{\mathrm{i}K_SL}+\mathrm{i}\left(-A_1^+(K-K_\lambda)(K_R+K_S)+A_1^-K_\lambda K_S-K\right)\sin(}{2K_R\left(K_R\cos(K_RL)-\mathrm{i}(K-K_\lambda)\sin(K_RL)\right)} \tag{F}$$

$$C_1^2 = \mathrm{i}\frac{K_R\left(A_1^+(K_S-K_R)+A_1^-K_\lambda+1\right)\cos(K_RL)-A_1^-K_\lambda K_R\mathrm{e}^{\mathrm{i}K_SL}+\mathrm{i}\left(-A_1^+(K-K_\lambda)(-K_R+K_S)+A_1^-K_\lambda K_S-K\right)\sin(}{2K_R\left(K_R\cos(K_RL)-\mathrm{i}(K-K_\lambda)\sin(K_RL)\right)} \tag{F.}$$

$$C_1^3 = -\mathrm{i}\frac{A_1^-\left((K_R-K+K_\lambda)\mathrm{e}^{\mathrm{i}K_SL}+(K_S+K-K_\lambda)\mathrm{e}^{-\mathrm{i}K_RL}\right)-\mathrm{e}^{-\mathrm{i}K_RL}}{2\left(K_R\cos(K_RL)-\mathrm{i}(K-K_\lambda)\sin(K_RL)\right)} \tag{F}$$

$$C_1^4 = \mathrm{i}\frac{-A_1^-\left((K_R+K-K_\lambda)\mathrm{e}^{\mathrm{i}K_SL}-(K_S+K-K_\lambda)\mathrm{e}^{\mathrm{i}K_RL}\right)-\mathrm{e}^{\mathrm{i}K_RL}}{2\left(K_R\cos(K_RL)-\mathrm{i}(K-K_\lambda)\sin(K_RL)\right)} \tag{F.}$$

$$C_2^1 = -\mathrm{i}\frac{K_R\left(A_2^+(K_R-K_S)+A_2^-K_\lambda+1\right)\cos(K_RL)-A_2^-K_\lambda K_R\mathrm{e}^{-\mathrm{i}K_SL}-\mathrm{i}\left(A_2^+(K-K_\lambda)(K_R-K_S)+A_2^-K_\lambda K_S+K\right)\sin(}{2K_R\left(K_R\cos(K_RL)-\mathrm{i}(K-K_\lambda)\sin(K_RL)\right)} \tag{F}$$

$$C_2^2 = \mathrm{i}\frac{K_R\left(-A_2^+(K_R+K_S)+A_2^-K_\lambda+1\right)\cos(K_RL)-A_2^-K_\lambda K_R\mathrm{e}^{\mathrm{i}K_SL}+\mathrm{i}\left(A_2^+(K-K_\lambda)(K_R+K_S)+A_2^-K_\lambda K_S-K\right)\sin(K}{2K_R\left(K_R\cos(K_RL)-\mathrm{i}(K-K_\lambda)\sin(K_RL)\right)} \tag{F}$$

$$C_2^3 = -\mathrm{i}\frac{A_2^-\left((K_R-K+K_\lambda)\mathrm{e}^{-\mathrm{i}K_SL}+(-K_S+K-K_\lambda)\mathrm{e}^{-\mathrm{i}K_RL}\right)-\mathrm{e}^{-\mathrm{i}K_RL}}{2\left(K_R\cos(K_RL)-\mathrm{i}(K-K_\lambda)\sin(K_RL)\right)} \tag{F.}$$

$$C_2^4 = \mathrm{i}\frac{-A_2^-\left((K_R+K-K_\lambda)\mathrm{e}^{-\mathrm{i}K_SL}-(-K_S+K-K_\lambda)\mathrm{e}^{\mathrm{i}K_RL}\right)-\mathrm{e}^{\mathrm{i}K_RL}}{2\left(K_R\cos(K_RL)-\mathrm{i}(K-K_\lambda)\sin(K_RL)\right)} \tag{F.}$$

Appendix G

Energy extraction from a sparse array

In order to prove that the two measures of the energy extracted given in §4.7.3 are equivalent, let us recall that the potentials are coupled by

$$C_g' \frac{\partial \alpha^+}{\partial x} = -\mathrm{i}\Omega_0 \left(\alpha^+ + \alpha^-\right) + \mathrm{i}\Omega\alpha^+ \tag{G.0.1a}$$

$$-C_g' \frac{\partial \alpha^-}{\partial x} = -\mathrm{i}\Omega_0 \left(\alpha^+ + \alpha^-\right) + \mathrm{i}\Omega\alpha^- \tag{G.0.1b}$$

$$C_g' \frac{\partial \beta^+}{\partial x} = -\mathrm{i}\Omega_0 \left[(1-\mathcal{G})(\beta^+ + \beta^-) - \mathcal{G}(\alpha^+ + \alpha^-)\right] + \mathrm{i}\Omega\beta^+ \tag{G.0.1c}$$

$$-C_g' \frac{\partial \beta^-}{\partial x} = -\mathrm{i}\Omega_0 \left[(1-\mathcal{G})(\beta^+ + \beta^-) - \mathcal{G}(\alpha^+ + \alpha^-)\right] + \mathrm{i}\Omega\beta^- \tag{G.0.1d}$$

and the the buoy displacement is given by:

$$\zeta = \mathcal{G}\left[\left(\alpha^+ + \alpha^-\right) + \left(\beta^+ + \beta^-\right)\right] \tag{G.0.2}$$

Let us introduce

$$\xi = \mathcal{G}\left[\left(\alpha^+ + \beta^+\right) - \left(\alpha^- + \beta^-\right)\right]$$

Taking (G.0.1a) − (G.0.1b) + (G.0.1c) − (G.0.1d), we find that

$$C_g' \frac{\mathrm{d}\zeta}{\mathrm{d}x} = \mathrm{i}\Omega\xi$$

Taking (G.0.1a) + (G.0.1b) + (G.0.1c) + (G.0.1d), we get

$$C'_g \frac{\mathrm{d}\xi}{\mathrm{d}x} = -\mathrm{i}\left(2\Omega_0\left(1-\mathcal{G}\right)-\Omega\right)\zeta$$

so we can evaluate

$$C'_g \frac{\mathrm{d}\zeta^\dagger\xi}{\mathrm{d}x} = -\mathrm{i}\left(2\Omega_0\left(1-\mathcal{G}\right)-\Omega\right)|\zeta|^2 - \mathrm{i}\Omega|\xi^2|$$

and

$$C'_g \frac{\mathrm{d}\zeta\xi^\dagger}{\mathrm{d}x} = \mathrm{i}\left(2\Omega_0\left(1-\mathcal{G}^\dagger\right)-\Omega\right)|\zeta|^2 + \mathrm{i}\Omega|\xi^2|$$

which gives us

$$C'_g \frac{\mathrm{d}\left(\zeta^\dagger\xi+\zeta\xi^\dagger\right)}{\mathrm{d}x} = 2\mathrm{i}\Omega_0\left(\mathcal{G}-\mathcal{G}^\dagger\right)|\zeta|^2$$

Recall that

$$\mathcal{G} = \frac{1}{1-\mathrm{i}\omega'\lambda_g}$$

so

$$\mathcal{G}-\mathcal{G}^\dagger = \frac{2\mathrm{i}\omega'\lambda_g}{1+\omega'^2\lambda_g^2}$$

and note that

$$\zeta^\dagger\xi+\zeta\xi^\dagger = -2|\mathcal{G}|^2\left(\left|\alpha^- + \beta^-\right|^2 - \left|\alpha^+ + \beta^+\right|^2\right)$$

so we finally get

$$\frac{\mathrm{d}}{\mathrm{d}x}\left[\left|\alpha^- + \beta^-\right|^2 - \left|\alpha^+ + \beta^+\right|^2\right] = 2\Omega_0\lambda_g\omega'|\zeta|^2$$

which allows us to prove that $\mathcal{E} = \mathcal{E}'$ writing

$$\begin{aligned}
\mathcal{E} &= \frac{2\Omega_0\lambda_g\omega'}{C'_g}\int_0^L |\zeta|^2\,\mathrm{d}x \\
&= \Omega_0\left[\left|\alpha^- + \beta^-\right|^2 - \left|\alpha^+ + \beta^+\right|^2\right]_0^L \\
&= \mathcal{E}'
\end{aligned}$$

The boundary conditions (4.6.20) and (4.7.21) have been used in the last line.

Bibliography

ABAQUS. *ABAQUS Theory Manual.* Hibbitt, Karlsson and Sorensen Inc.

ABB Power Systems Inc. URL `http://www02.abb.com/global/gad/gad02077.nsf/lupLongContent/D74F5739AAE738F6C12571D800305007`.

M. Abramowitz and I.A. Stegun. *Handbook of mathematical functions.* Dover Publications., 1964.

J.A. Aranha, C.C. Mei, and D.K.P. Yue. Some properties of a hybrid element method for water waves. *International Journal for Numerical Methods in Engineering*, 14 (11):1627–1641, 1979.

I. Babuska and J. Osborn. *Handbook of Numerical Analysis, Volume II: Finite Element Method (Part 1)*, chapter Eigenvalue Problems, pages 640–787. North-Holland, 1990.

K.J. Bathe. *Finite element procedures.* Prentice Hall, 2006.

J.L. Black, C.C. Mei, and M.C.G. Bray. Radiation and scattering of water waves by rigid bodies. *Journal of Fluid Mechanics*, 46(1):151–164, 1971.

K. Budal and J. Falnes. A resonant point absorber of ocean-wave power. *Nature*, 256 (5517):478–479, August 1975.

W.E. Byerly. *An Elementary Treatise on Fourier's Series, and Spherical, Cylindrical, and Ellipsoidal Harmonics, with Applications to Problems in Mathematical Physics.* Dover, 1959.

P.G. Chamberlain. Water wave scattering by finite arrays of circular structures. *IMA J Appl Math*, 72(1):52–66, 2007.

L.S. Chen, C.H. Kuo, Z. Ye, and X. Sun. Band gaps in the propagation and scattering of surface water waves over cylindrical steps. *Phys. Rev. E*, 69(6):066308–, June 2004.

T. Chou. Band structure of surface flexural gravity waves along periodic interfaces. *Journal of Fluid Mechanics*, 369(-1):333–350, 2000.

P.G. Ciarlet and J.L. Lions, editors. *Handbook of Numerical Analysis.* North-Holland, 1990.

D. Cioranescu and P. Donato. *An introduction to homogenization.* Oxford University Press, 1999.

J. Cruz. *Ocean Wave Energy.* Springer, 2008.

M. Eriksson, J. Isberg, and M. Leijon. Hydrodynamic modelling of a direct drive wave energy converter. *International Journal of Engineering Science*, 43(17-18): 1377 – 1387, 2005. ISSN 0020-7225.

D.V. Evans. Power from water waves. *Annual Review of Fluid Mechanics*, 13(1): 157–187, 1981.

António F. de O. Falcão. Phase control through load control of oscillating-body wave energy converters with hydraulic pto system. *Ocean Engineering*, 35(3-4):358–366, March 2008. ISSN 0029-8018. URL `http://www.sciencedirect.com/science/article/B6V4F-4PXM6KB-1/2/6c0c0c83e8f3dd0a6b54c58482749d71`.

J. Falnes. *Ocean Waves and Oscillating Systems.* Cambridge University Press, 2002a.

J. Falnes. A review of wave-energy extraction. *Marine Structures*, 20:185–201, 2007.

J. Falnes. Optimum control of oscillation of wave-energy converters. *International Journal of Offshore and Polar Engineering*, 12:147–155, 2002b.

Johannes Falnes. Radiation impedance matrix and optimum power absorption for interacting oscillators in surface waves. *Applied Ocean Research*, 2(2):75–80, April 1980. ISSN 0141-1187.

Johannes Falnes. Wave-power absorption by an array of attenuators oscillating with unconstrained amplitudes. *Applied Ocean Research*, 6(1):16–22, 1984.

Johannes Falnes and Kjell Budal. Wave-power absorption by parallel rows of interacting oscillating bodies. *Applied Ocean Research*, 4(4):194–207, 1982.

C.J.R. Garrett. Wave forces on a circular dock. *Journal of Fluid Mechanics*, 46(1): 129–139, 1971.

F. Hecht, O. Pironneau, A. Le Hyaric, and K. Ohtsuka. *FreeFEM++.* http://www.freefem.org/ff++.

P. Huerre. *Mécanique des fluides.* Cours de l'Ecole Polytechnique, 1998.

J.D. Joannopoulos, S.G. Johnson R.D.Meade, and J.N. Winn. *Photonic cristals, Molding the flow of light.* Princeton University Press, 2008.

H. Kagemoto and D.K.P. Yue. Interactions among multiple three-dimensional bodies in water waves: an exact algebraic method. *Journal of Fluid Mechanics*, 166(-1): 189–209, 1986.

Y. Li and C.C. Mei. Multiple resonant scattering of water waves by a two-dimensional array of vertical cylinders: Linear aspects. *Phys. Rev. E*, 76(016302), 2007a.

Y. Li and C.C. Mei. Bragg scattering by a line array of small cylinders in a waveguide. part 1. linear aspects. *Journal of Fluid Mechanics*, 583(-1):161–187, 2007b.

C.M. Linton and D.V. Evans. The radiation and scattering of surface waves by a vertical circular cylinder in a channel. *Philosophical Transactions: Physical Sciences and Engineering*, 338(1650):325–357, 1992.

C.M. Linton and R. McIver. The scattering of water waves by an array of circular cylinders in a channel. *Journal of Engineering Mathematics*, 30(-1):661–682, 1996.

S. A. Mavrakos and P. McIver. Comparison of methods for computing hydrodynamic characteristics of arrays of wave power devices. *Applied Ocean Research*, 19(5-6): 283–291, 1997.

M.E. McCormick. *Ocean Wave Energy Conversion*. New York, Wiley-Interscience, 1981.

P. McIver. Wave interaction with arrays of structures. *Applied Ocean Research*, 24 (3):121–126, 2002.

C.C. Mei. Resonant reflection of surface water waves by periodic sandbars. *Journal of Fluid Mechanics*, 152(-1):315–335, 1985.

C.C. Mei, M. Stiassnie, and D.K.P Yue. *Theory and application of ocean surface waves*. World Scientific, 2005.

P.M. Morse and H. Feshbach. *Methods of Theoretical Physics*. McGraw-Hill, 1953.

A.E. Mynett, D.D. Serman, and C.C. Mei. Characteristics of salter's cam for extracting energy from ocean waves. *Applied Ocean Research*, 1:13–20, 1979.

M. Naciri and C.C. Mei. Bragg scattering of water waves by a doubly periodic seabed. *Journal of Fluid Mechanics*, 192(-1):51–74, 1988.

J.N. Newman. Absorption of wave energy by elongated bodies. *Applied Ocean Research*, (1):189–196., 1979.

Ocean Power Technologies Inc. URL `http://www.oceanpowertechnologies.com/`.

Oregon State University. Wallace energy systems and renewables facility. URL `http://eecs.oregonstate.edu/wesrf/`.

M. A. Peter, M.H. Meylan, and C. M. Linton. Water-wave scattering by a periodic array of arbitrary bodies. *Journal of Fluid Mechanics*, 548(-1):237–256, 2006.

M.A. Peter and M.H. Meylan. Water-wave scattering by a semi-infinite periodic array of arbitrary bodies. *Journal of Fluid Mechanics*, 575(-1):473–494, 2007.

R. Porter and D.V. Evans. Complementary approximations to wave scattering by vertical barriers. *Journal of Fluid Mechanics*, 294(-1):155–180, 1995.

Y. Saad. *SPARSKIT*, 2000. URL `http://www-users.cs.umn.edu/~saad/software/SPARSKIT/sparskit.html/`.

D.C. Sorensen, R.B. Lehoucq, and and K. Maschhoff. C. Yang. *ARPACK*, 2008. URL `http://www.caam.rice.edu/software/ARPACK/`.

T. Utsunomiya and E. Watanabe. Fast multipole method for wave diffraction/radiation problems and its applications to vlfs. *International Journal of Offshore and Polar Engineering*, 16:253–260, 2006.

E.W. Weisstein. Legendre polynomial. From MathWorld–A Wolfram Web Resource., a. URL `http://mathworld.wolfram.com/LegendrePolynomial.html`.

E.W. Weisstein. Spherical harmonic. From MathWorld–A Wolfram Web Resource., b. URL `http://mathworld.wolfram.com/SphericalHarmonic.html`.